

PA 751

Copy No.

4

~~RESTRICTED~~

RM No. L7D11a

STATUS

~~CONFIDENTIAL~~

Activity



authority of NACA let. to *Helms*, 9-23-49,  
C.H. Helms, TTN/ds, *for info* note to *LaS*  
dated 3-6-52. *By H.R. 4-7-52*

# RESEARCH MEMORANDUM

PERFORMANCE OF COMPRESSOR BLADE CASCADES

AT HIGH MACH NUMBERS

By Seymour M. Bogdonoff

Langley Memorial Aeronautical Laboratory  
Langley Field, Va.

CLASSIFIED DOCUMENT

This document contains classified information affecting the National Defense of the United States within the meaning of the Espionage Act, USC 5011 and 5012. Its transmission or the revelation of its contents in any manner to an unauthorized person is prohibited by law. Information so classified may be imparted only to persons in the military and naval services of the United States, appropriate civilian officers and employees of the Federal Government who have a legitimate interest therein, and to United States citizens of known loyalty and discretion who of necessity must be informed thereof.

## NATIONAL ADVISORY COMMITTEE FOR AERONAUTICS

WASHINGTON

June 12, 1947

DATA LIBRARY  
NATIONAL ADVISORY COMMITTEE FOR AERONAUTICS  
WASHINGTON, D.C.

~~RESTRICTED~~

## NATIONAL ADVISORY COMMITTEE FOR AERONAUTICS

## RESEARCH MEMORANDUM

## PERFORMANCE OF COMPRESSOR BLADE CASCADES

## AT HIGH MACH NUMBERS

By Seymour M. Bogdonoff

## SUMMARY

Three 10-percent-thick and two 6-percent-thick blower blades were investigated in a high Mach number two-dimensional cascade tunnel in several configurations for a range of Mach number. Pressure distributions, schlieren photographs, turning angles, and pressure rises were obtained to evaluate the effects of Mach number on the basic cascade and compressor design parameters.

The turning angles and design angles of attack found from low-speed cascade studies may be used directly in high-speed designs since no significant changes were found to occur at high Mach numbers.

The Mach numbers for critical speed are 4 to 5 percent greater than that predicted by the von Kármán-Tsien extrapolation applied to the low-speed pressure distribution. The Mach numbers for force break are 16 percent higher than the predicted critical Mach number for a solidity of 1.5 and 13 percent higher for a solidity of 1.0.

The extrapolation of low-speed rotor tests to a compressor stage operating below the Mach number for force break with an efficiency of 90 percent indicates that pressure ratios of the order of 1.4 per stage should be obtainable.

Significant increases in compressor performance can be made by the use of 6-percent-thick tip sections since their limiting Mach number is 3 to 4 percent greater than that of the 10-percent-thick blades.

## INTRODUCTION

In an effort to increase the pressure rise and efficiency which can be obtained with axial-flow compressors, the National Advisory Committee for Aeronautics is conducting an investigation to develop

high-performance compressor blades. The first phase of this investigation, which was conducted at the Langley Memorial Aeronautical Laboratory, is a study of blade sections in a low-speed two-dimensional cascade tunnel and is given in references 1 and 2. This work was extended to low-speed tests of rotating blades with very high loadings which were also conducted at the Langley Laboratory (reference 3). The results have shown that the cascade data can be used to design highly loaded rotating blades with very high efficiencies.

The present paper extends the low-speed cascade studies to the high Mach numbers at which modern axial-flow compressors need to operate. It also presents the limiting Mach numbers at which large losses make compressor operation impracticable. The effects of compressibility are evaluated for the basic design parameters of references 1 to 3; namely, turning angle, shape of the pressure distribution, and design angle of attack. The investigation was made in a high Mach number two-dimensional cascade tunnel at the Langley Laboratory.

#### SYMBOLS

- a velocity of sound, feet per second
- $c_p$  specific heat of air at constant pressure, foot-pounds per slug per °F
- M Mach number entering the cascade ( $W_1/a_1$ )
- P pressure coefficient  $\left( \frac{P_2 - P_1}{q_1} \right)$
- $P_{cr}$  pressure coefficient for sonic velocity at given entering Mach number
- p static pressure, pounds per square foot
- q dynamic pressure, pounds per square foot
- T temperature, °F absolute
- U rotational speed of rotor element, feet per second
- W velocity relative to rotor and to cascade simulating rotor, feet per second
- $\alpha$  angle of attack, degrees (angle between entering air and chord line of blade)

- $\beta$  stagger angle, degrees (angle between perpendicular to cascade and entering air)
- $\gamma$  ratio of specific heats of air
- $\sigma$  solidity (chord of blade divided by gap between blades; see fig. 3)
- $\theta$  angle through which air is turned by blades, degrees

## Subscripts:

- 1 ahead of cascade or rotor
- 2 behind cascade or rotor
- d design conditions
- l local

## APPARATUS

## High Mach Number Cascade Tunnel

The two-dimensional cascade tunnel used in the present investigation is shown schematically in figure 1. The tunnel is similar to that used in references 1 and 2 except that, because of the large powers required, no control of the wall boundary layer ahead of the cascade was attempted. In addition, the width of the test section was only 4 inches. The tunnel was driven by compressed air from a large tank at pressures from 60 to 300 pounds per square inch. The air flowed past a motorized control valve to the settling chamber; through three sets of 40-mesh screens, the converging entrance section, and the test cascade; and to the atmosphere. Static-pressure orifices were installed in the settling chamber and along a line  $1/3$  chord ahead of the cascade. From  $1/2$  chord ahead of the blades to approximately  $1/4$  chord behind the blades the top and bottom walls consisted of adjustable flexible plates. The angle of attack of the blades could be varied, but changes in stagger and solidity necessitated a complete change of tunnel walls. Walls were provided for the following test conditions:  $\beta = 45^\circ$ ,  $\sigma = 1.5$ ;  $\beta = 60^\circ$ ,  $\sigma = 1.5$ ; and  $\beta = 60^\circ$ ,  $\sigma = 1.0$ .

### Description of Blades

The blades tested consisted of three 10-percent-thick blades, the same as those of references 1 and 2, and two 6-percent-thick blades derived from NACA 65,2-006 airfoils with the trailing edge thickened as in reference 1. The thick sections were cambered for free-air lift coefficients of 0.8, 1.2, and 1.8; the thin section, for lift coefficients of 0.8 and 1.2. For the pressure-distribution tests, the test cascade consisted of four solid blades and a master blade provided with pressure orifices. For the schlieren studies, the master blade was replaced by a fifth solid blade. The blades have a 4-inch span and a 5-inch chord. Ordinates for these blade sections are given in tables 1 to 5 and cross sections are shown in figure 2.

### Schlieren Setup

The schlieren system used to photograph the high-speed flow through the cascade consisted of a high-intensity spark, two 16-inch parabolic mirrors of 90-inch focal length, and associated equipment. The knife edge of the schlieren system was set parallel to the stagger line for all tests. Two or three of the set of five blades were mounted between  $\frac{3}{4}$ -inch glass plates (measuring approximately 5 by 7 inches) which replaced sections of the tunnel walls. The blades were held in place by short pins fitted into holes drilled in the glass.

### TESTING METHODS

The blades were installed in the cascade tunnel at the desired conditions of stagger, solidity, and angle of attack with the pressure blade in the center of the cascade (fig. 1). At a Mach number of approximately 0.2, the flexible walls were adjusted until the static pressure ahead of the cascade was uniform. The speed was then raised until further increases showed no increase in the static-pressure rise across the cascade. At intervals during this process, photographs of a mercury manometer were taken to record the settling-chamber pressure, static pressures ahead of the blades, pressures on the blade surface, and atmospheric pressure. This procedure was repeated for the five blade sections at the various conditions of stagger, solidity, and angle of attack. Schlieren photographs were then taken at speeds from below the critical speed to above the speed for maximum pressure rise for the various test conditions. Photographs of the mercury manometer were taken simultaneously with the schlieren photographs to record the chamber pressure, static pressure ahead of the blades, and atmospheric pressure.

The variation of turning angle with Mach number was first obtained by making yaw surveys behind the airfoils with a claw-type yaw tube. Photographs of a tuft in the air stream behind the blade and the use of a vernier protractor to measure the angles were found to give results which agreed with results obtained with the yaw tube to within  $\pm 1^\circ$ . All other yaw surveys were then made by use of a tuft because of the ease in making these measurements.

#### PRESENTATION OF DATA AND DISCUSSION

The data presented herein are based on entrance conditions instead of mean conditions as in references 1 and 2. This base was chosen primarily to simplify the use of the data and to permit direct application to high-speed-compressor design for which the blade entrance conditions are usually known or fixed. The tests cover a range of Mach number from approximately 0.30 to 0.95 and corresponding Reynolds numbers, based on the blade chord, of 700,000 to 1,800,000.

The entrance Mach number was calculated from the pressures measured by the static-pressure orifices in the settling chamber and ahead of the cascade. Stagnation temperature was assumed to be room temperature ( $520^\circ$  F absolute) since the deviations from this value were not significant. The inflection in the pressure-ratio curve is designated force break and corresponds to blade stall.

As the Mach number entering the cascade increased, the pressure ratio across the cascade, and therefore the density ratio, also increased. From the continuity relations, the exiting axial velocity component would be expected to be smaller than entering axial velocity since the axial-flow area is constant. For this particular test setup, however, the boundary layers on the walls were found to modify the exit area so that the axial velocity entering and leaving the cascade was the same for all tests (fig. 3). The results presented are, therefore, directly applicable only to the case of blading with constant axial velocity and not to blading with constant axial-flow area.

#### Pressure-Distribution Measurements

In figures 4 to 30, the pressure distributions over the central airfoil of the cascade are presented for a range of Mach number. The pressures are plotted in the form of pressure coefficients  $P$  and the critical pressure coefficient (pressure coefficient at which sonic velocity is reached at that stream Mach number) is noted on

each plot. The low-speed pressure distributions are very similar to those of reference 1, and in figure 5 the pressure distribution from reference 1 is included for comparison. The blower blades show characteristics very similar to those of the isolated airfoil as the Mach number varies. Any pressure peaks on the top or bottom surfaces increase rapidly as the Mach number increases. Shortly after the critical pressure coefficient is exceeded on the airfoil a break in the pressure-coefficient curve at that point is noticeable as the supersonic velocities return to subsonic velocities through a shock wave.

For angles below the design angle (the angle at which the pressure distribution is essentially uniform or without peaks, reference 1), the pressure peak on the lower surface usually is the first part of the blade to reach critical speed, but no stalling is noticeable. (See figs. 7, 10, 11, and 23.) This angle would seem to be a good operating condition, but data presented in the section of the present paper entitled "Schlieren Photographs" show that large losses occur shortly after the critical speed is reached. These losses are caused by the strong shock waves which extend completely across the blade passage.

Blade stall is defined as the condition at which no pressure is recovered over the rear part of the airfoil upper surface and which indicates separation. This stalling is indicated by a flat region on the pressure-distribution curves and a point of inflection on the pressure-ratio curve discussed in the section entitled "Pressure Ratio across the Cascade." For high angles of attack, at which a pressure peak occurs on the upper surface, the blade stall may be divided into two categories: blades which are loaded very highly stall because of the increase in Mach number even before critical speed is reached (figs. 9, 17, 18, 19, 22, 28, 29, and 30), and blades loaded more moderately stall at or slightly above the critical speed. From these pressure distributions, it is obvious that the least losses at very high Mach numbers will be obtained with a uniform-load pressure distribution; that is, one with no velocity peaks on either the upper or lower surface. This conclusion is verified by a study of the pressure distribution at or near the design angle of attack (table 6) at which there appears to be no stalling until Mach numbers from 0.05 to 0.10 above the critical speed have been reached.

It is interesting to note that the occurrence of a shock on the lower surface where the boundary layer is very thin is noticeable on the pressure distribution as a sharp break. On the top surface, however, where the boundary layers are thick, the pressure rise across the shock is distributed over a noticeable length of the blade surface.

### Schlieren Photographs

In figures 31 to 50, schlieren photographs of the flow through the cascade are shown. A complete study was made for a stagger of  $45^\circ$  and a solidity of 1.5, and a few photographs were taken at the other conditions to show any changes which might exist. The black dots near the rear of the blades are the holes drilled in the glass to provide a means of changing the angle of attack. The thick blade boundary layer which is noticed in the first photographs actually occurs only at the blade-wall intersection. A study of the pressure distributions shows no stalling at these Mach numbers. An increase in speed above the critical speed is immediately noticeable because very small shocks appear on the airfoil. As the Mach number is further increased, the shock waves grow much stronger until finally the flow behind these waves separates from the airfoil. As the blade angle of attack is varied, noticeable changes in these shock patterns are seen.

In figure 31, in which the angle of attack is much less than the design angle, small shock waves are first noticeable just behind the 50-percent-chord station on the top surface. As soon as the Mach number is increased to the point at which the waves extend entirely across the passage between the blades, separation is noticeable and any additional increase in chamber pressure causes increased shock strength and separation. Once sonic velocities extend entirely across the passage, an increase in Mach number is not possible. A few schlieren tests show an apparent increase in Mach number above this point, probably due to flow around the ends of the cascade which are not yet choked. Photographs which show such a phenomenon are therefore noted with a question mark. At an angle of attack close to the design angle (fig. 32), the shock waves appear farther forward on the airfoil and separation is not apparent until a Mach number of approximately 0.03 above the previous case is reached (table 6). If the angle of attack is increased further, the peak pressures move closer to the nose and the separation caused by the shock waves (fig. 33) starts at approximately the same Mach number as in the first case. At still higher angles of attack (fig. 34) separation occurs at a much lower Mach number. In this case, the shock waves never are confined by the blades but extend out into the stream, the wave from one airfoil becoming the bow-wave of the neighboring airfoil. These phenomena are repeated in the schlieren photographs for the other configurations with only slight variations in the shock-wave structure.

### Turning Angle

For the 6-percent-thick sections, turning angles obtained from the tuft surveys at low Mach numbers have been included in table 6,

since no such data were available from previous low-speed cascade investigations. The variation of turning angle with Mach number is shown for two cases in figure 51. The first curve (NACA 65-(12)06 blower blade,  $\beta = 45^\circ$ , and  $\sigma = 1.5$ ) shows a typical variation; the second curve (NACA 65-(12)10 blower blade,  $\beta = 60^\circ$ , and  $\sigma = 1.0$ ) shows the maximum variation which was obtained ( $1^\circ$ ). These results were obtained by photographing a tuft placed in the air leaving the cascade. For both configurations, a slight increase in the turning angle with Mach number occurs up to the force break, above which there is an abrupt drop. Turning angles were obtained for all the other blade sections and configurations for the range of Mach number investigated. In all cases, from Mach numbers of 0.30 to force break, the increase in turning angle was less than  $1^\circ$ . The turning angles predicted from the low-speed cascade studies of references 1 and 2 are, therefore, sufficiently accurate for the design of high-speed blades.

#### Pressure Ratio across the Cascade

In reference 1, it was shown that the incompressible theoretical static-pressure rise across the cascade could be expressed as a function of the turning and stagger angles of the cascade. The corresponding static-pressure-rise expression for high Mach numbers can be derived. From Bernoulli's equation of compressible flows (see vector diagram, fig. 3)

$$\frac{W_1^2}{2} + c_p T_1 = \frac{W_2^2}{2} + c_p T_2$$

or

$$\frac{T_2}{T_1} = \frac{W_1^2 - W_2^2}{2c_p T_1} + 1$$

Since the velocity of sound of the entering flow is

$$a_1 = \sqrt{(\gamma - 1)c_p T_1}$$

and the entering Mach number is

$$M_1 = \frac{W_1}{a_1}$$

the temperature ratio across the cascade is

$$\frac{T_2}{T_1} = \frac{\gamma - 1}{2} M_1^2 \left[ 1 - \left( \frac{W_2}{W_1} \right)^2 \right] + 1$$

The velocity ratio  $W_2/W_1$  can be expressed as

$$\frac{W_2}{W_1} = \frac{\cos \beta}{\cos (\beta - \theta)}$$

if it is assumed that the axial velocity is constant through the cascade. If it is further assumed that no losses occur, the isentropic relationship of temperature and pressures may be used to obtain the following relation for the theoretical static-pressure rise across the cascade:

$$\frac{P_2}{P_1} = \left( \frac{\gamma - 1}{2} M_1^2 \left\{ 1 - \left[ \frac{\cos \beta}{\cos (\beta - \theta)} \right]^2 \right\} + 1 \right)^{\frac{\gamma}{\gamma - 1}}$$

In figures 52 to 62, curves of the variation of measured static-pressure ratio with Mach number are presented for the angle of attack closest to the design point of the blade for each test condition. Included on each figure is the theoretical curve obtained from equation (1) with the use of the turning angles predicted from references 1 and 2 for the 10-percent-thick sections and angles measured at low Mach numbers for the 6-percent-thick sections. Measured values of pressure ratio should not be used in the calculation of compressor-blade performance since these values include the losses due to the boundary layer on the walls and are very susceptible to settings of the flexible floors. The curves, however, give a good indication of where the blade losses start to increase sharply (a reversal in curve direction). An examination of these curves shows that no significant change in blade losses occurs until the critical speed has been exceeded by approximately 12 percent to 16 percent. Once force break occurs, further increases in Mach number yield little or no increases in pressure rise, the added power being dissipated in shock-wave losses and severe separation.

#### Critical Speed and Force Break

The Mach numbers for critical speed and force break are summarized in table 6. For the blades which were tested at more

than three angles of attack, the variation of Mach number for critical speed and force break with angle of attack are shown in figures 63 to 69. These curves show that the design point chosen from the low-speed cascade tests of references 1 and 2 correspond very closely to the high-speed design point. The design points fall very close to the maximum Mach number for critical speed and force break. From the pressure distributions and pressure-ratio curves, it appears that critical speed, in itself, is not an important parameter since no change in performance is noticeable until force break occurs.

Several theories exist which predict the critical speed of isolated airfoils from the low-speed pressure distributions, but no such theory is yet available for blades in cascade. In the absence of any theory, the experimental results were compared with those which would be obtained if the von Kármán-Tsien extrapolation were applied to the low-speed pressure distribution of the blade in cascade based on entrance velocity. The critical Mach number predicted by this method was consistently 4 to 5 percent below the measured value for all the 10-percent-thick blades tested. Since no low-speed tests of the 6-percent-thick blower blades are yet available, the data on these blades are simply presented and no attempt at analysis is made. It appears, however, that the decrease in airfoil thickness from 10 percent to 6 percent allows an increase in Mach number of about 3 to 4 percent for both critical speed and force break.

The Mach numbers for force break are approximately 16 percent higher than the critical Mach number predicted by von Kármán and Tsien for the tests at a solidity of 1.5 and approximately 13 percent higher for tests at a solidity of 1.0. These empirical relations were applied to the pressure distributions of reference 1 to obtain the Mach number for critical speed and force break for all the sections tested. The results are presented with the design turning angle of the blade section in figure 70. For any desired turning angle, stagger, and solidity, the blade section and angle of attack can be obtained from the design charts of references 1 and 2. Figure 70 then may be used to predict both the Mach number for critical speed and force break. These results are directly applicable only to NACA 65-series blower blades in the Reynolds number range tested. Extensive German tests (reference 4) have shown that changes in Reynolds number greater than 150,000 have small effect on the efficiencies and pressure rise. It seems likely, therefore, that the results presented herein are applicable to blades in the whole Reynolds number range above 150,000. The extrapolation of the low-speed rotor tests of reference 3 to a compressor stage operating below the Mach number for force break with an efficiency of 90 percent indicates that pressure ratios of the order of 1.4 per stage should be obtainable.

It is recommended that further research be carried out to cover the range of Reynolds number below 150,000 and to check the values of Mach number for force break in high-speed rotor tests

### CONCLUSIONS

From the investigation of NACA 65-series blower blades in a high Mach number two-dimensional cascade tunnel, the following conclusions have been reached:

1. The turning angles and design angles of attack found from low-speed cascade studies may be used directly in high-speed designs since no significant changes were found at high Mach numbers.

2. The Mach numbers for critical speed are 4 to 5 percent greater than that predicted by the von Kármán-Tsien extrapolation applied to the low-speed pressure distribution. The Mach numbers for force break are 16 percent higher than the predicted critical Mach number for a solidity of 1.5 and 13 percent higher for a solidity of 1.0.

3. The extrapolation of low-speed rotor tests to a compressor stage operating below the Mach number for force break with an efficiency of 90 percent indicates that pressure ratios of the order of 1.4 per stage should be obtainable.

4. Significant increases in compressor performance can be made by the use of 6-percent-thick tip sections since their allowable operating Mach number is 3 to 4 percent greater than the 10-percent-thick blades.

Langley Memorial Aeronautical Laboratory  
National Advisory Committee for Aeronautics  
Langley Field, Va.

## REFERENCES

1. Bogdonoff, Seymour M., and Bogdonoff, Harriet E.: Blade Design Data for Axial-Flow Fans and Compressors. NACA ACR No. L5F07a, 1945.
2. Bogdonoff, Seymour M., and Hess, Eugene E.: Axial-Flow Fan and Compressor Blade Design Data at  $52.5^\circ$  Stagger and Further Verification of Cascade Data by Rotor Tests. NACA TN No. 1271, 1947.
3. Bogdonoff, Seymour M., and Herrig, L. Joseph: Performance of Axial-Flow Fan and Compressor Blades Designed for High Loadings. NACA TN No. 1201, 1946.
4. Eckert, B.: Summary of the Results of Research on Axial Flow Compressors at the Stuttgart Research Institute for Automobiles and Engines. Vol. 3, part A, BuShips 338, May 1946. (W.A.C. Eng. Translation No. 22.)

TABLE I.- ORDINATES FOR NACA 65-810 BLOWER BLADE

Upper surface		Lower surface	
x (percent chord)	y (percent chord)	x (percent chord)	y (percent chord)
0	0	0	0
.260	.913	.740	-.513
.486	1.130	1.014	-.570
.949	1.510	1.551	-.654
2.143	2.274	2.857	-.786
4.591	3.448	5.409	-.920
7.072	4.371	7.928	-.979
9.569	5.149	10.431	-1.013
14.589	6.415	15.411	-1.031
19.629	7.386	20.371	-1.018
24.681	8.139	25.319	-.979
29.740	8.705	30.260	-.929
34.804	9.098	35.196	-.858
39.870	9.339	40.130	-.771
44.936	9.409	45.064	-.649
50.000	9.282	50.000	-.458
55.058	8.950	54.942	-.190
60.107	8.434	59.893	.134
65.143	7.744	64.857	.496
70.164	6.922	69.836	.854
75.171	6.025	74.829	1.135
80.162	5.024	79.838	1.344
85.137	3.935	84.863	1.449
90.104	2.810	89.896	1.326
95.065	1.612	94.935	.916
100.048	.142	99.952	-.142

L.E. radius: 0.666 percent chord

TABLE II.- ORDINATES FOR NACA 65-806 BLOWER BLADE

Upper surface		Lower surface	
x (percent chord)	y (percent chord)	x (percent chord)	y (percent chord)
0	0	0	0
.348	.652	.652	-.252
.579	.829	.921	-.269
1.057	1.121	1.443	-.265
2.282	1.679	2.718	-.191
4.757	2.559	5.243	-.031
7.247	3.276	7.753	.116
9.745	3.889	10.255	.247
14.756	4.899	15.244	.485
19.779	5.686	20.221	.682
24.809	6.308	25.191	.852
29.844	6.781	30.156	.995
34.882	7.123	35.118	1.117
39.921	7.341	40.079	1.227
44.961	7.431	45.039	1.329
50.000	7.387	50.000	1.437
55.036	7.204	54.964	1.556
60.057	6.891	59.933	1.677
65.092	6.462	64.908	1.778
70.110	5.925	69.890	1.851
75.119	5.283	74.881	1.877
80.119	4.532	79.881	1.836
85.109	3.679	84.891	1.705
90.089	2.707	89.911	1.429
95.052	1.596	94.938	.932
100.048	.142	99.952	-.142

L.E. radius: 0.256 percent chord

TABLE III.— ORDINATES FOR NACA 65(12)10 BLOWER BLADE

Upper surface		Lower surface	
x (percent chord)	y (percent chord)	x (percent chord)	y (percent chord)
0	0	0	0
.161	.971	.839	-.371
.374	1.227	1.126	-.387
.817	1.679	1.683	-.395
1.981	2.599	3.019	-.367
4.399	4.035	5.601	-.243
6.868	5.178	8.132	-.090
9.361	6.147	10.639	.057
14.388	7.734	15.612	.342
19.477	8.958	20.553	.594
24.523	9.915	25.477	.825
29.611	10.640	30.389	1.024
34.706	11.153	35.294	1.207
39.804	11.479	40.196	1.373
44.904	11.598	45.096	1.542
50.000	11.488	50.000	1.748
55.087	11.139	54.913	2.001
60.161	10.574	59.839	2.278
65.214	9.801	64.786	2.559
70.245	8.860	69.755	2.804
75.256	7.808	74.744	2.932
80.242	6.607	79.758	2.945
85.204	5.272	84.796	2.804
90.154	3.835	89.846	2.369
95.096	2.237	94.904	1.555
100.068	.134	99.932	-.134

L.E. radius: 0.666 percent chord

TABLE IV.- ORDINATES FOR NACA 65-(12)06 BLOWER BLADE

Upper surface		Lower surface	
x (percent chord)	y (percent chord)	x (percent chord)	y (percent chord)
0	0	0	0
.285	.726	.715	-.126
.507	.941	.993	-.101
.973	1.306	1.527	-.022
2.183	2.022	2.817	.210
4.643	3.165	5.357	.627
7.127	4.100	7.873	.988
9.622	4.902	10.378	1.302
14.637	6.228	15.363	1.848
19.670	7.266	20.330	2.286
24.715	8.090	25.285	2.650
29.766	8.720	30.234	2.944
34.823	9.180	35.177	3.180
39.882	9.482	40.118	3.370
44.942	9.620	45.058	3.520
50.000	9.593	50.000	3.643
55.054	9.343	54.946	3.747
60.101	9.032	59.899	3.820
65.138	8.520	64.862	3.840
70.165	7.865	69.835	3.799
75.178	7.058	74.822	3.672
80.178	6.117	79.822	3.435
85.162	5.018	84.838	3.058
90.132	3.733	89.868	2.471
95.091	2.221	94.909	1.571
100.068	.134	99.932	-.134

L.E. radius: 0.256 percent chord

TABLE V.- ORDINATES FOR NACA 65-(18)10 BLOWER BLADE

Upper surface		Lower surface	
x (percent chord)	y (percent chord)	x (percent chord)	y (percent chord)
0	0	0	0
.046	1.049	.954	-.149
.240	1.359	1.260	-.099
.654	1.916	1.846	.010
1.770	3.065	3.230	.283
4.137	4.891	5.863	.797
6.583	6.365	8.417	1.267
9.066	7.620	10.934	1.686
14.097	9.692	15.903	2.422
19.179	11.301	20.821	3.027
24.289	12.569	25.711	3.541
29.419	13.537	30.581	3.959
34.560	14.233	35.440	4.307
39.707	14.688	40.293	4.590
44.856	14.882	45.144	4.828
50.000	14.797	50.000	5.057
55.131	14.423	54.869	5.287
60.241	13.783	59.759	5.495
65.320	12.883	64.680	5.657
70.366	11.764	69.634	5.732
75.381	10.476	74.619	5.634
80.360	8.976	79.640	5.352
85.302	7.271	84.698	4.843
90.225	5.367	89.775	3.939
95.138	3.170	94.862	2.518
100.091	.120	99.909	-.120

L.E. radius: 0.666 percent chord

TABLE VI.- SUMMARY OF HIGH MACH NUMBER TESTS OF  
NACA 65-SERIES BLOWER BLADES

$\alpha$	$M_{cr}$	$M_{Pb}$	Figure		
			Pressure distribution	Schlieren photographs	$P_2/P_1$
NACA 65-810 blower blade					
$\beta = 45^\circ$ ; $\sigma = 1.5$ ; $\alpha_d = 12.9^\circ$ ; $\theta_d = 18.0^\circ$					
10.6	.76	.81	--	31	--
11.6	.75	.82	4	--	52
12.5	.76	.84	--	32	--
15.6	.72	.82	--	33	--
20.6	.69	.77	--	34	--
$\beta = 60^\circ$ ; $\sigma = 1.5$ ; $\alpha_d = 12.0^\circ$ ; $\theta_d = 15.8^\circ$					
10.0	.76	.82	5	--	53
16.6	.64	.75	6	--	--
$\beta = 60^\circ$ ; $\sigma = 1.0$ ; $\alpha_d = 10.5^\circ$ ; $\theta_d = 12.5^\circ$					
6.7	.76	.80	7	--	--
10.3	.74	.84	8	--	54
10.5	.72	.83	--	35	--
12.6	<sup>a</sup> .76	<sup>a</sup> .80	9	--	--
15.5	<sup>a</sup> .63	<sup>a</sup> .73	--	36	--
NACA 65-806 blower blade					
$\beta = 45^\circ$ ; $\sigma = 1.5$ ; $\alpha_d = 11.5(\text{approx.})$ ; $\theta_d = 18.5(\text{approx.})$					
5.3	.63	.71	10	--	--
9.5	.75	.82	11	--	--
11.5	.76	.89	--	37	--
13.3	.71	.83	12	--	55
16.5	.70	.85	--	38	--

<sup>a</sup>Blade stalled before critical speed was reached.

TABLE VI.- SUMMARY OF HIGH MACH NUMBER TESTS OF  
NACA 65-SERIES BLOWER BLADES - Continued

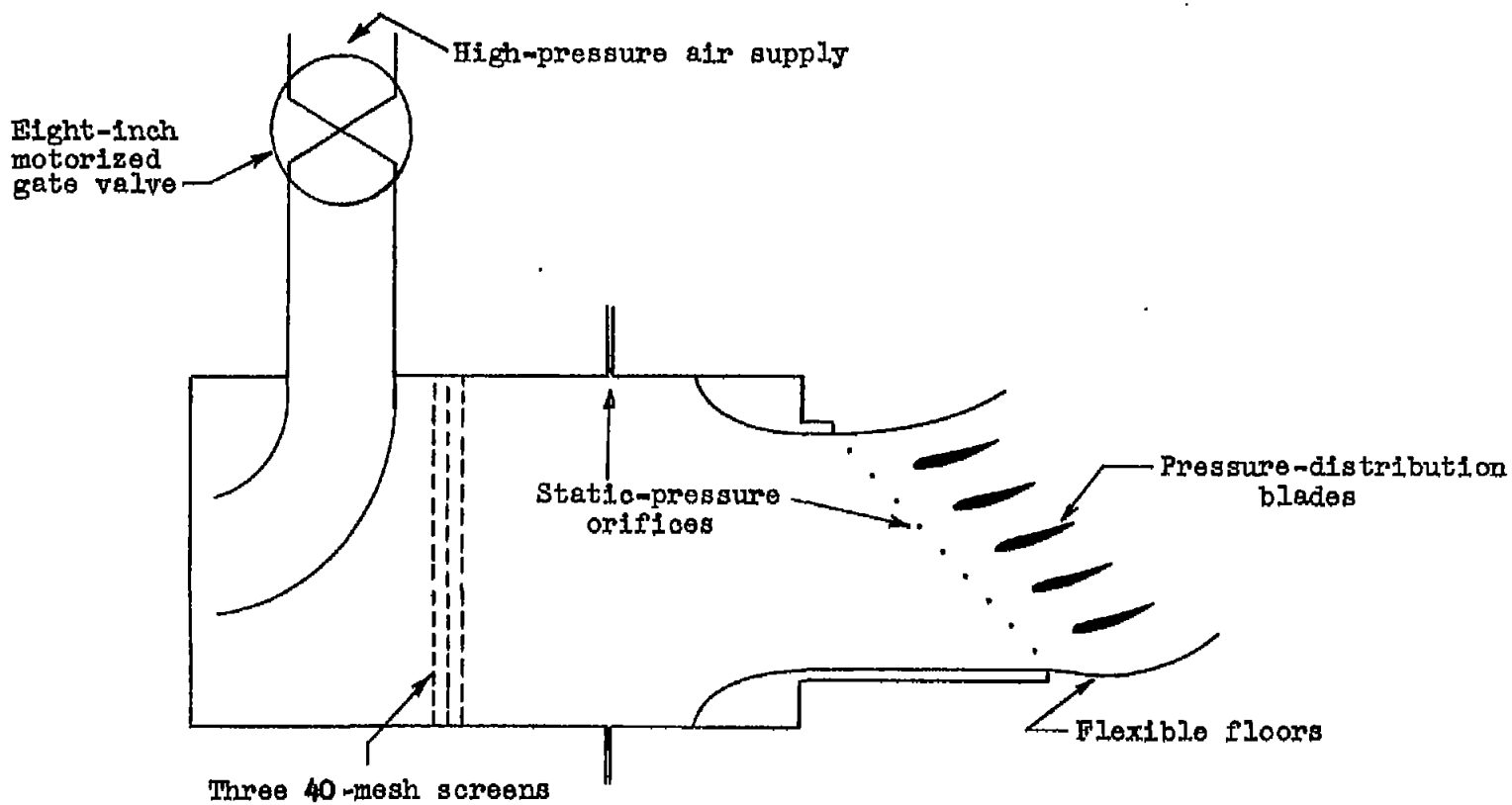
$\alpha$	$M_{cr}$	$M_{fb}$	Figure		
			Pressure distribution	Schlieren photographs	$p_2/p_1$
NACA 65-806 blower blade					
$\beta = 60^\circ$ ; $\sigma = 1.0$ ; $\alpha_d = 10.0$ (approx.); $\theta_d = 12.5$ (approx.)					
7.5	.80	.89	13	--	--
10.0	.77	.88	14	--	56
12.5	.67	.84	15	--	--
NACA 65-(12)10 blower blade					
$\beta = 45^\circ$ ; $\sigma = 1.5$ ; $\alpha_d = 16.9^\circ$ ; $\theta_d = 25.7^\circ$					
12.0	.73	.74	--	39	--
14.5	.73	.81	--	40	--
14.9	.72	.77	16	--	57
17.0	.73	.79	--	41	--
18.9	<sup>a</sup> .71	.76	17	--	--
22.0	<sup>a</sup> .69	.76	--	42	--
$\beta = 60^\circ$ ; $\sigma = 1.5$ ; $\alpha_d = 16.2^\circ$ ; $\theta_d = 22.7^\circ$					
14.2	.74	.82	18	--	58
15.2	.70	.80	--	43	--
19.2	<sup>a</sup> .64	.73	19	--	--
$\beta = 60^\circ$ ; $\sigma = 1.0$ ; $\alpha_d = 14.0^\circ$ ; $\theta_d = 18.5^\circ$					
9.0	.73	.82	20	--	--
11.5	.75	.82	21	--	--
14.0	<sup>a</sup> .75	.80	22	--	59

<sup>a</sup>Blade stalled before critical speed was reached.

TABLE VI.- SUMMARY OF HIGH MACH NUMBER TESTS OF  
NACA 65-SERIES BLOWER BLADES - Concluded

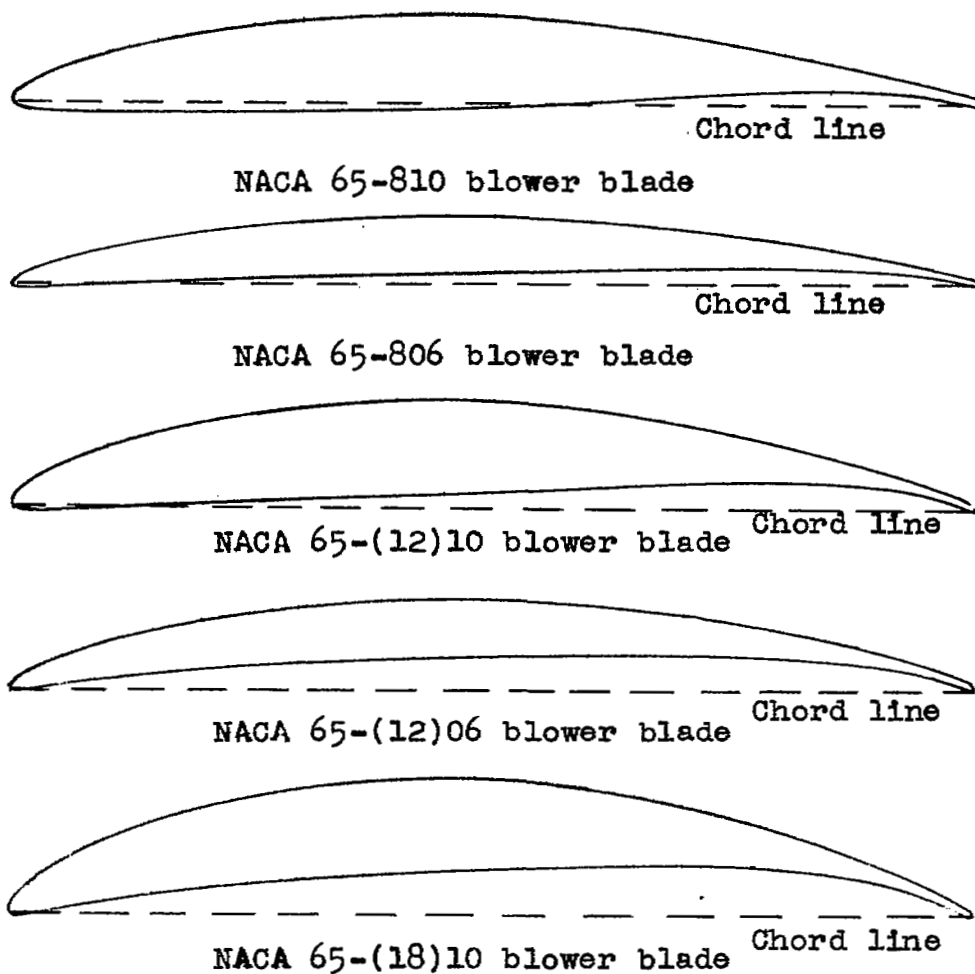
$\alpha$	$M_{cr}$	$M_{Tb}$	Figure		
			Pressure distribution	Schlieren photographs	$P_2/P_1$
NACA 65-(12)06 blower blade					
$\beta = 45^\circ$ ; $\sigma = 1.5$ ; $\alpha_d = 15.3^\circ$ (approx.); $\theta_d = 25.0^\circ$ (approx.)					
10.0	.71	.77	23	--	--
12.5	.78	.84	--	44	--
15.0	.76	.83	24	45	60
17.5	.76	.82	--	46	--
22.5	.66	.78	--	47	--
$\beta = 60^\circ$ ; $\sigma = 1.0$ ; $\alpha_d = 13.5^\circ$ (approx.); $\theta_d = 19.0^\circ$ (approx.)					
9.0	.76	.82	25	--	--
11.5	.74	.82	26	--	--
14.0	.73	.80	27	--	61
16.5	<sup>a</sup> .69	.77	28	--	--
NACA 65-(18)10 blower blade					
$\beta = 45^\circ$ ; $\sigma = 1.5$ ; $\alpha_d = 22.5^\circ$ ; $\theta_d = 34.3^\circ$					
18.3	.70	.75	--	48	--
20.8	.69	.77	--	49	--
21.5	.69	.77	29	--	--
23.3	<sup>a</sup> .71	.76	--	50	62
26.5	<sup>a</sup> .62	.72	30	--	--

<sup>a</sup>Blade stalled before critical speed was reached.



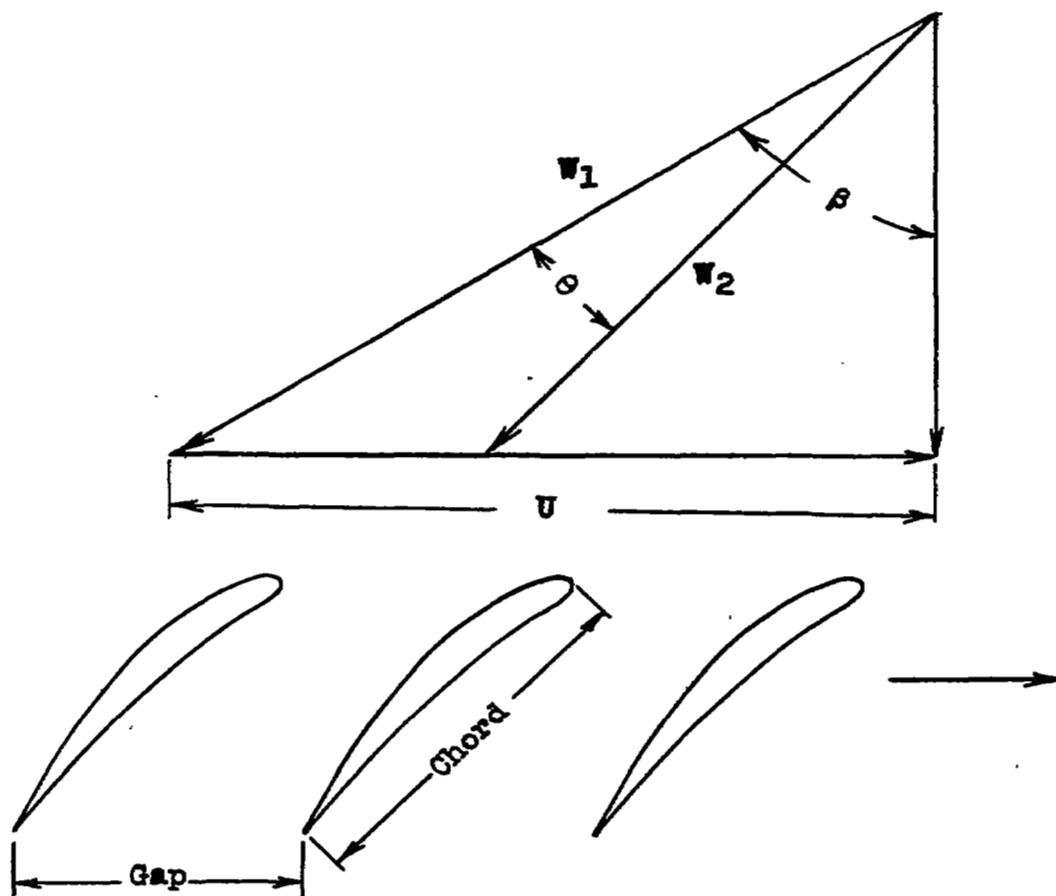
NATIONAL ADVISORY  
COMMITTEE FOR AERONAUTICS

Figure 1 .- Schematic diagram of high Mach number two-dimensional cascade tunnel.



NATIONAL ADVISORY  
COMMITTEE FOR AERONAUTICS

Figure 2.- NACA 65-series blower blades tested at high Mach numbers.



NATIONAL ADVISORY  
COMMITTEE FOR AERONAUTICS

Figure 3.- Typical vector diagram of flow through a compressor rotor.

Fig. 4

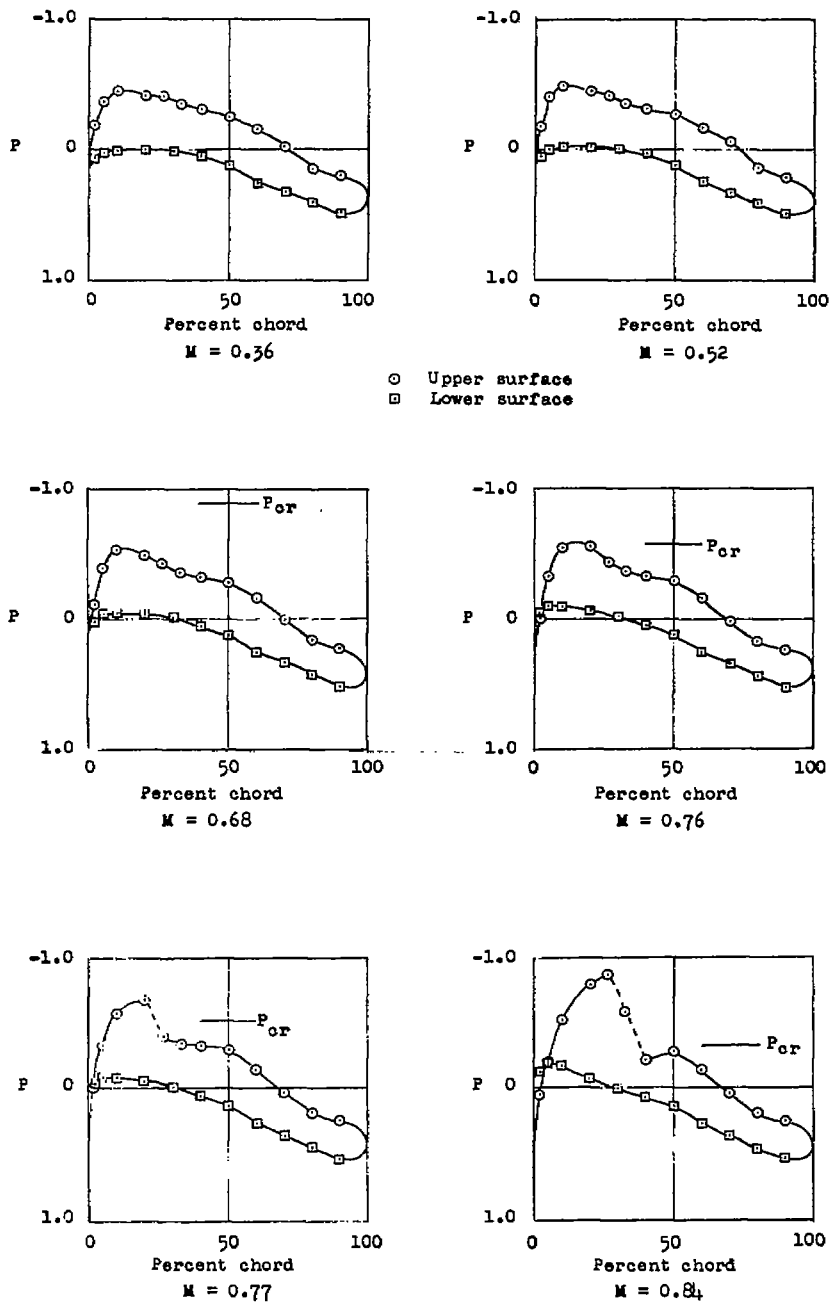


Figure 4.- Section pressure distribution for a range of Mach numbers. Cascade of NACA 65-810 blower blades;  $\alpha = 11.6^\circ$ ;  $\beta = 45^\circ$ ;  $\sigma = 1.5$ .

NATIONAL ADVISORY  
 COMMITTEE FOR AERONAUTICS

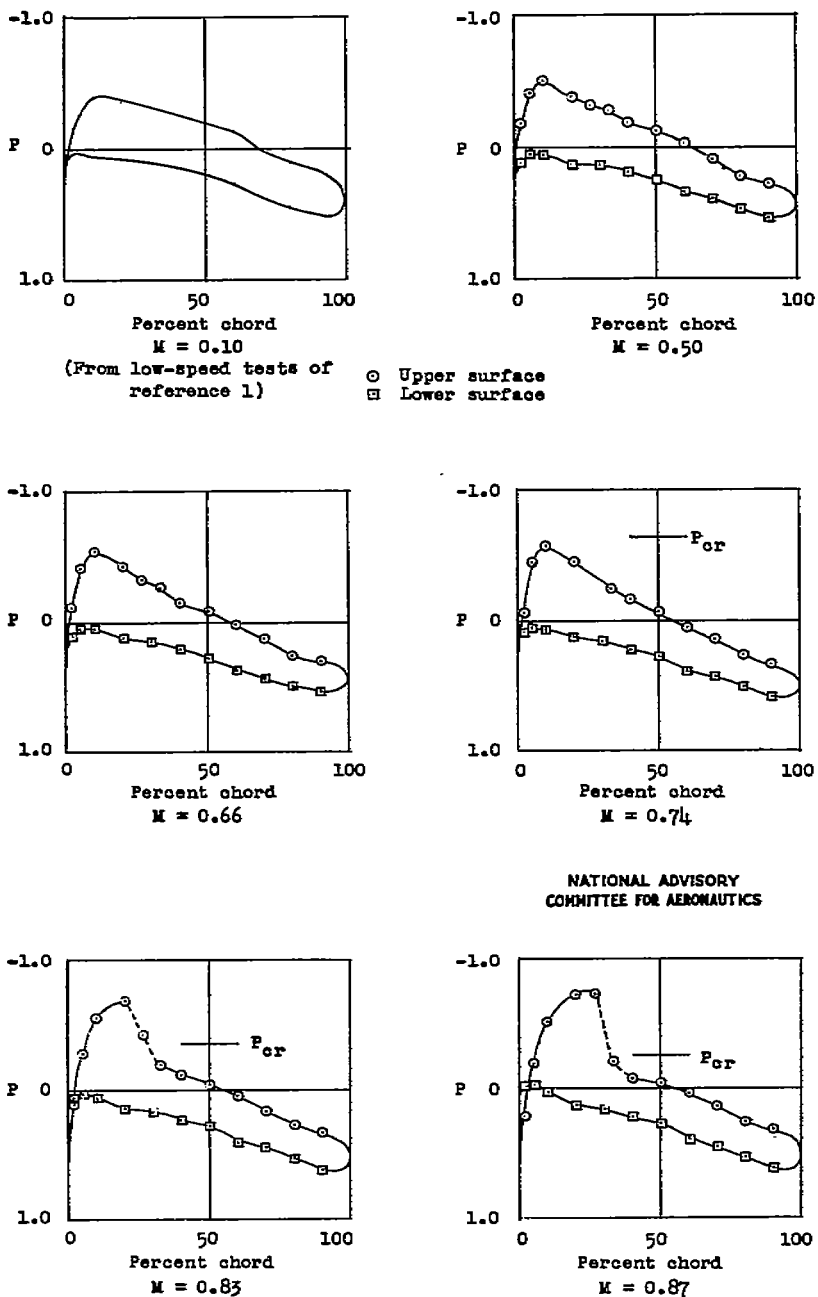


Figure 5.- Section pressure distributions for a range of Mach numbers. Cascade of NACA 65-810 blower blades;  $\alpha = 10.0^\circ$ ;  $\beta = 60^\circ$ ;  $\sigma = 1.5$ .

Fig. 6

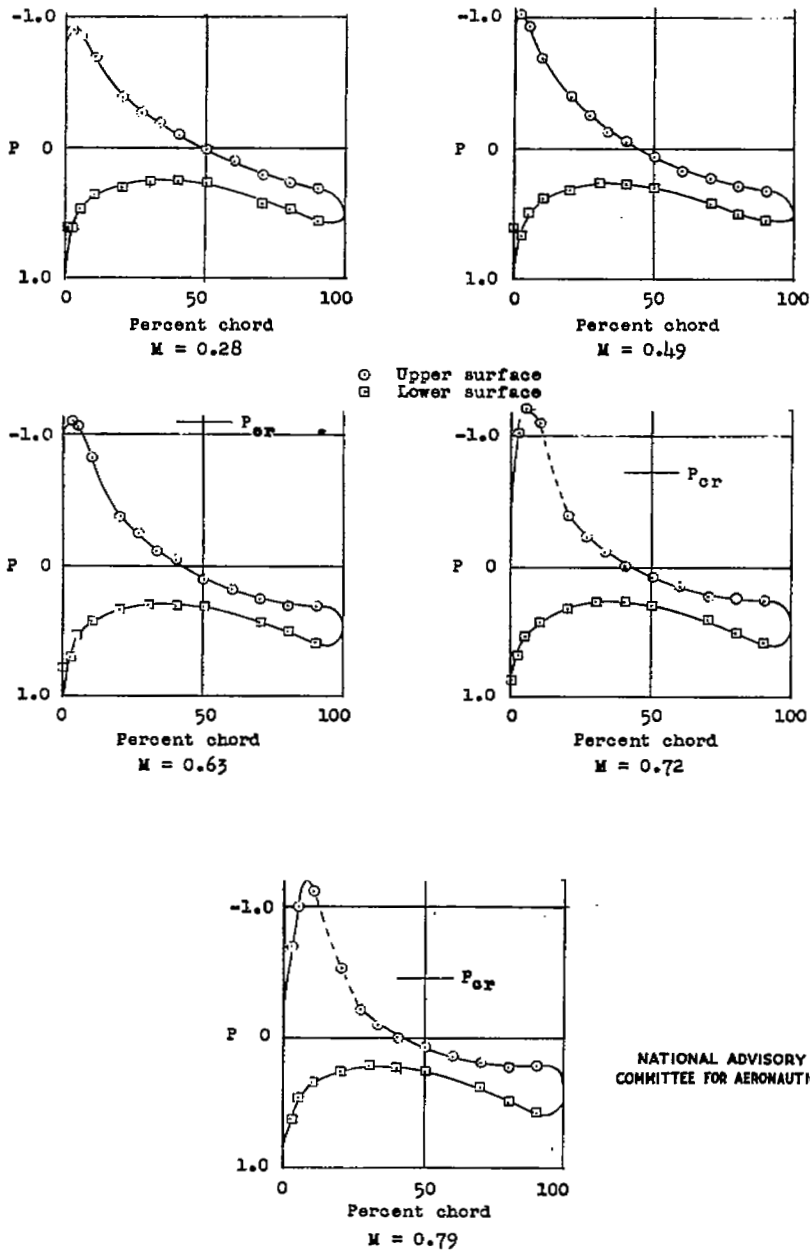


Figure 6.- Section pressure distributions for a range of Mach numbers. Cascade of NACA 65-810 blower blades;  $\alpha = 16.6^\circ$ ;  $\beta = 60^\circ$ ;  $\sigma = 1.5$ .

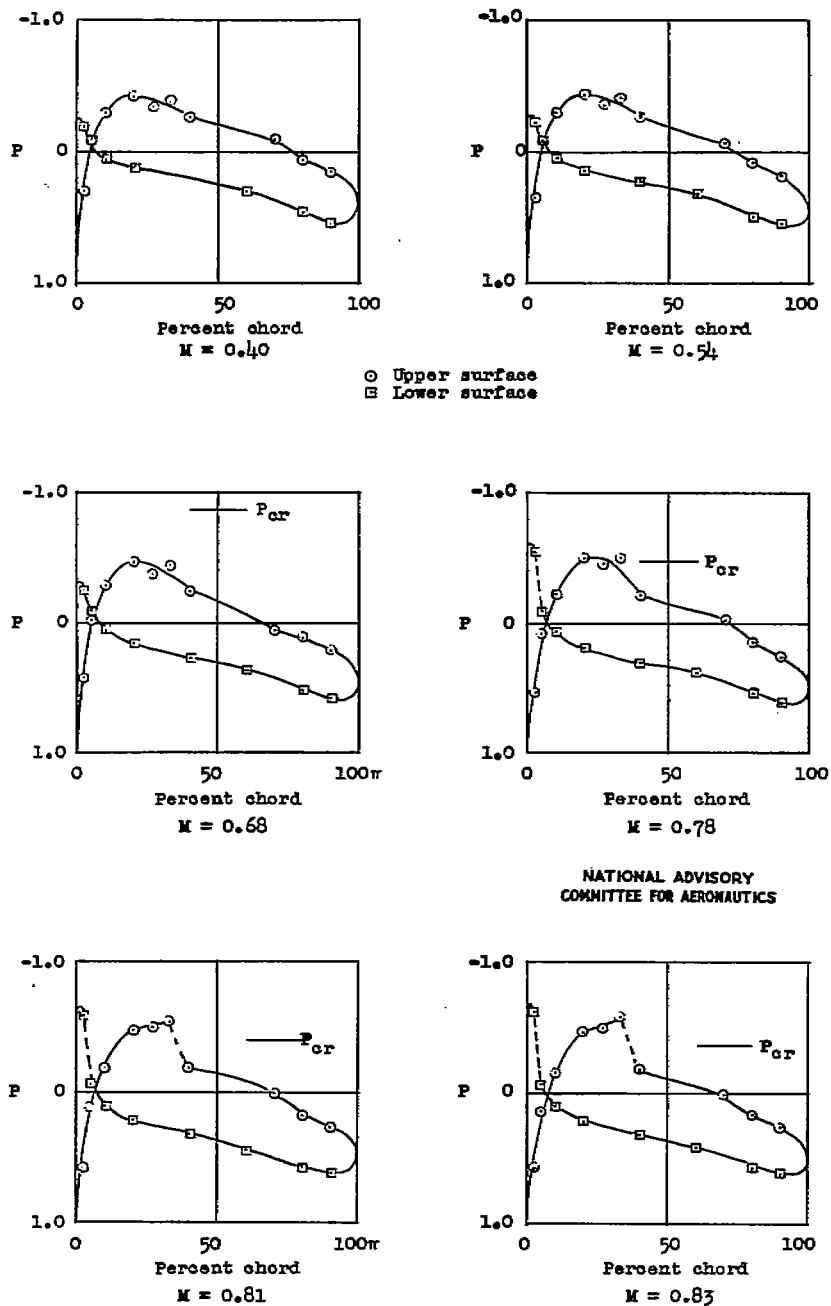


Figure 7.- Section pressure distributions for a range of Mach numbers. Cascade of NACA 65-810 blower blades;  $\alpha = 6.7^\circ$ ;  $\beta = 60^\circ$ ;  $\sigma = 1.0$ .

Fig. 8

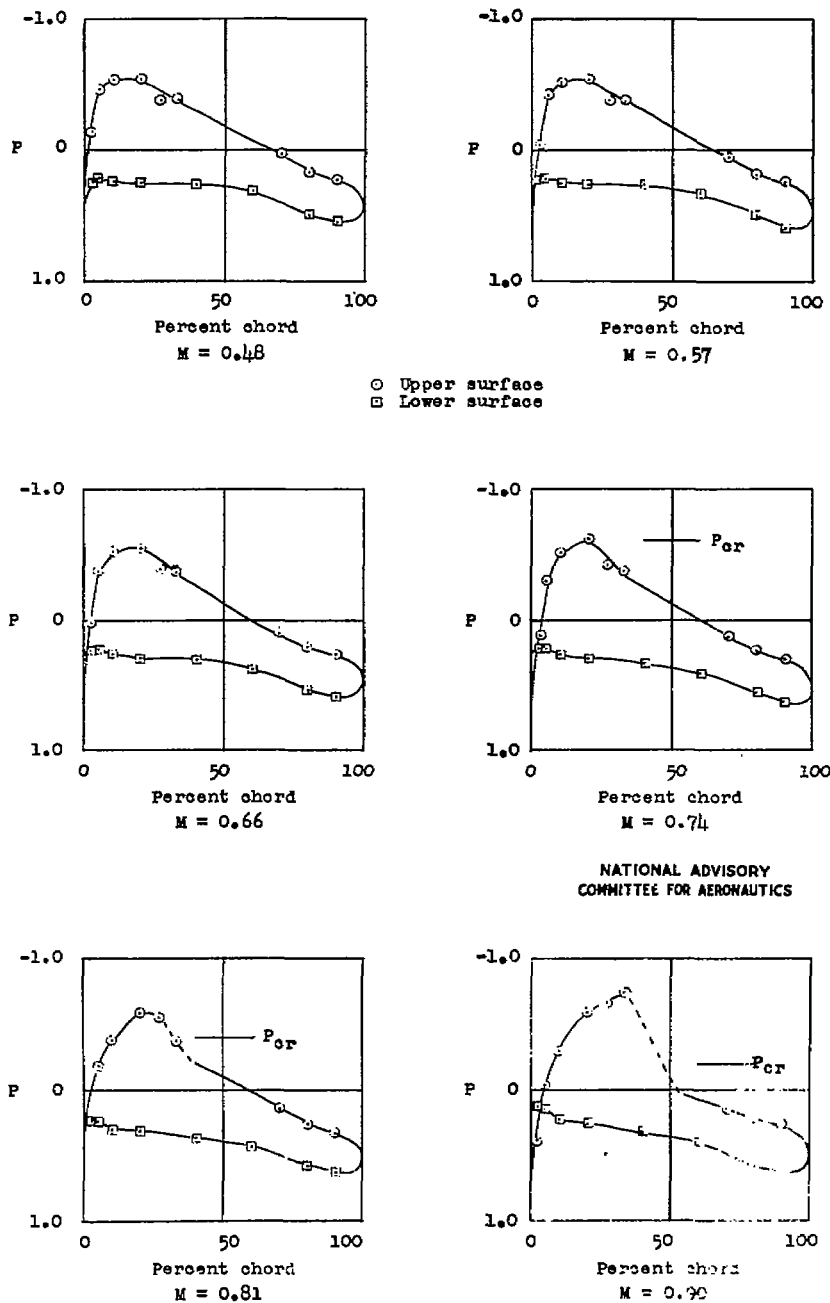


Figure 8.- Section pressure distributions for a range of Mach numbers. Cascade of NACA 65-310 blower blades;  $\alpha = 10.3^\circ$ ;  $\beta = 60^\circ$ ;  $\sigma = 1.0$ .

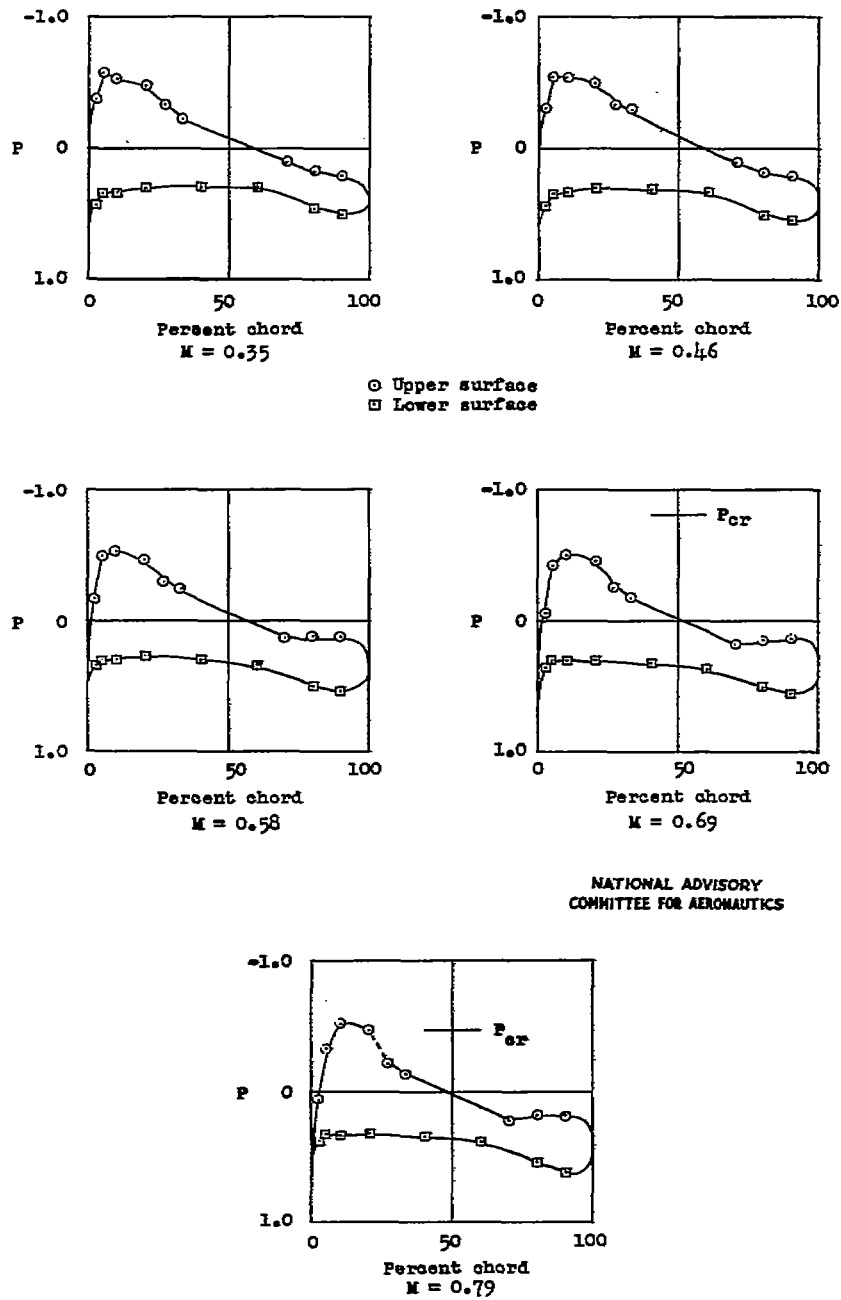


Figure 9.- Section pressure distributions for a range of Mach numbers. Cascade of NACA 65-810 blower blades;  $\alpha = 12.6^\circ$ ;  $\beta = 60^\circ$ ;  $\sigma = 1.0$ .

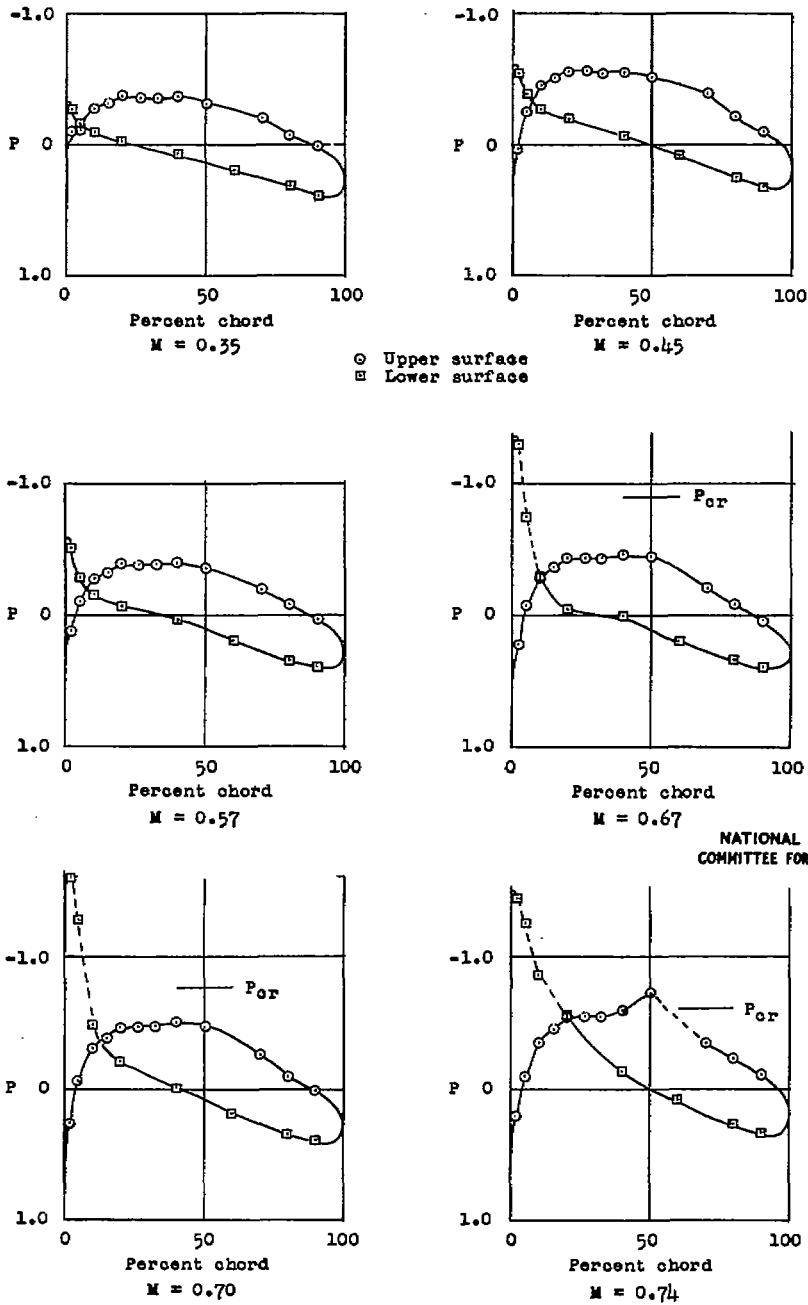


Figure 10.- Section pressure distributions for a range of Mach numbers. Cascade of NACA 65-806 blower blades;  $\alpha = 5.3^\circ$ ;  $\beta = 45^\circ$ ;  $\sigma = 1.5$ .

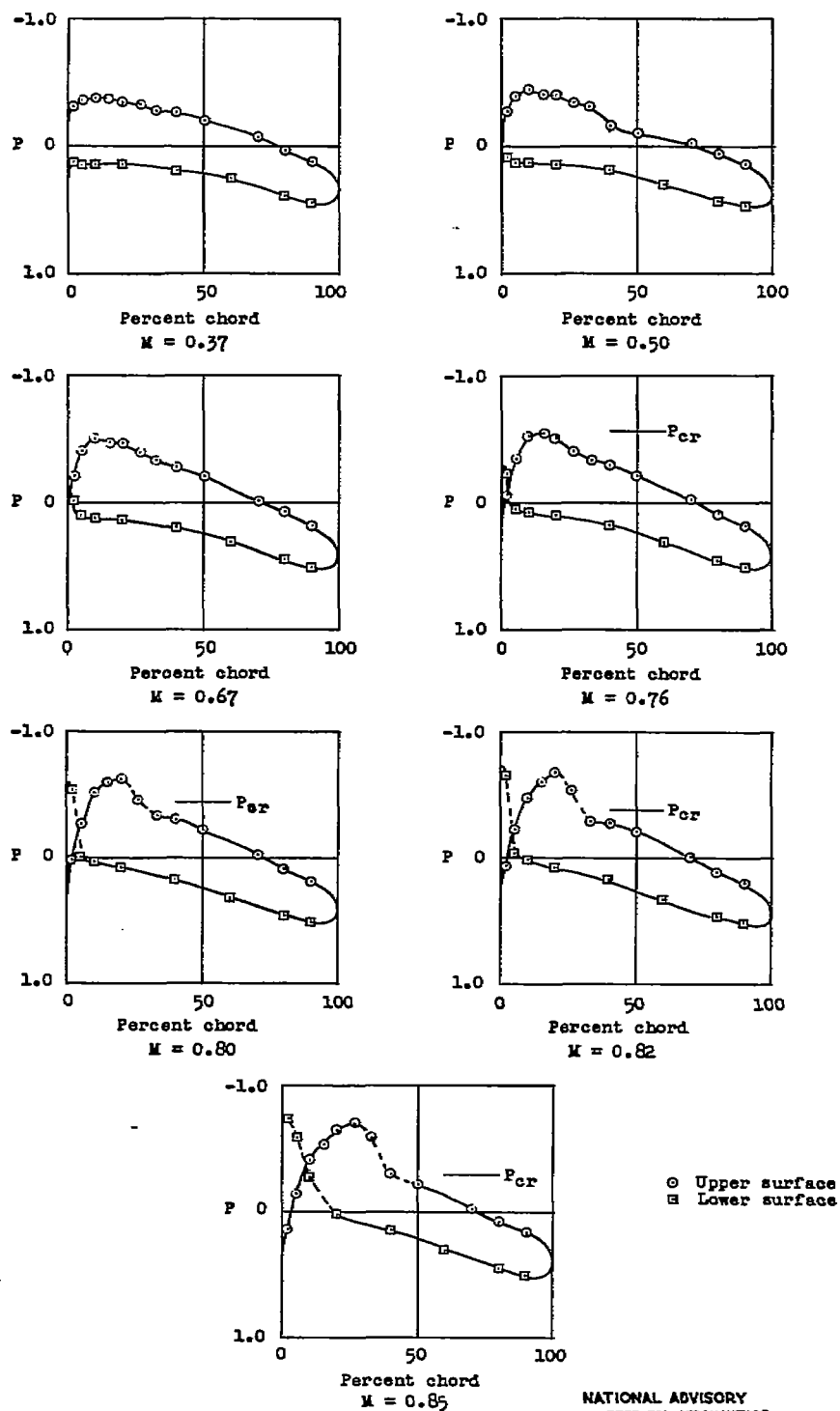


Figure 11.- Section pressure distributions for a range of Mach numbers. Cascade of NACA 65-806 blower blades;  $\alpha = 9.5^\circ$ ;  $\beta = 45^\circ$ ;  $\sigma = 1.5$ .

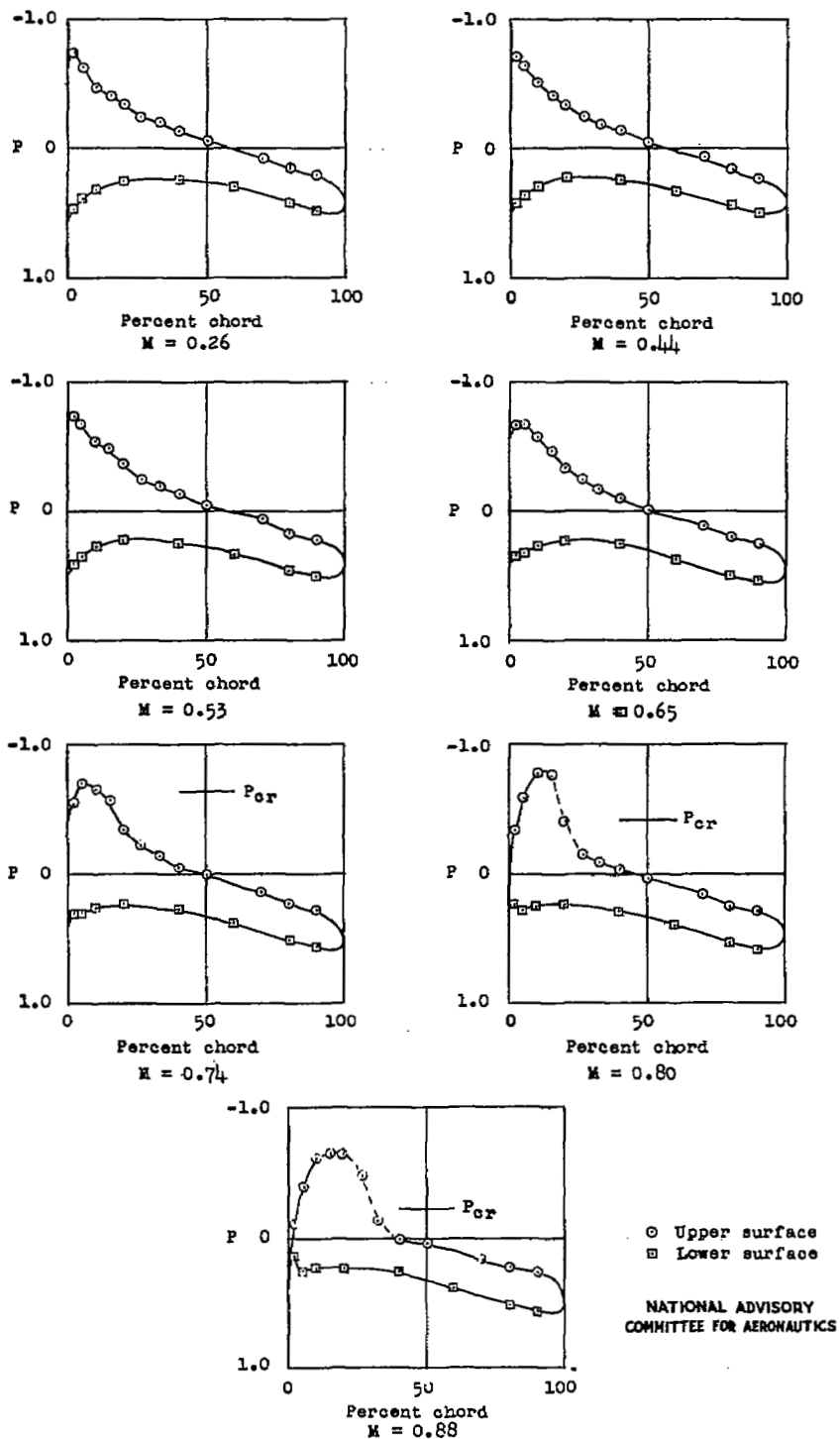


Figure 12.- Section pressure distributions for a range of Mach numbers. Cascade of NACA 65-806 blower blades;  $\alpha = 13.5^\circ$ ;  $\beta = 45^\circ$ ;  $\sigma = 1.5$ .

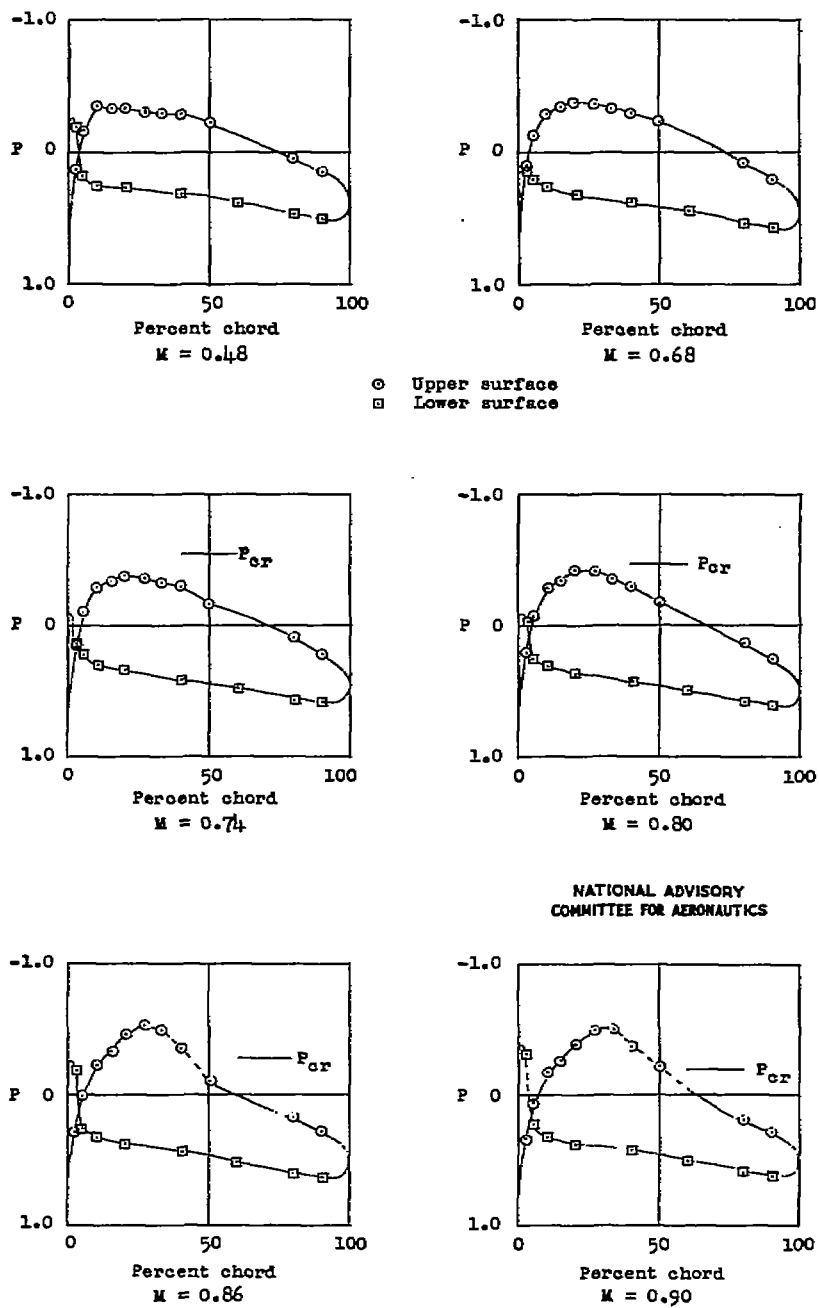


Figure 13.- Section pressure distributions for a range of Mach numbers. Cascade of NACA 65-806 blower blades;  $\alpha = 7.5^\circ$ ;  $\beta = 60^\circ$ ;  $\sigma = 1.0$ .

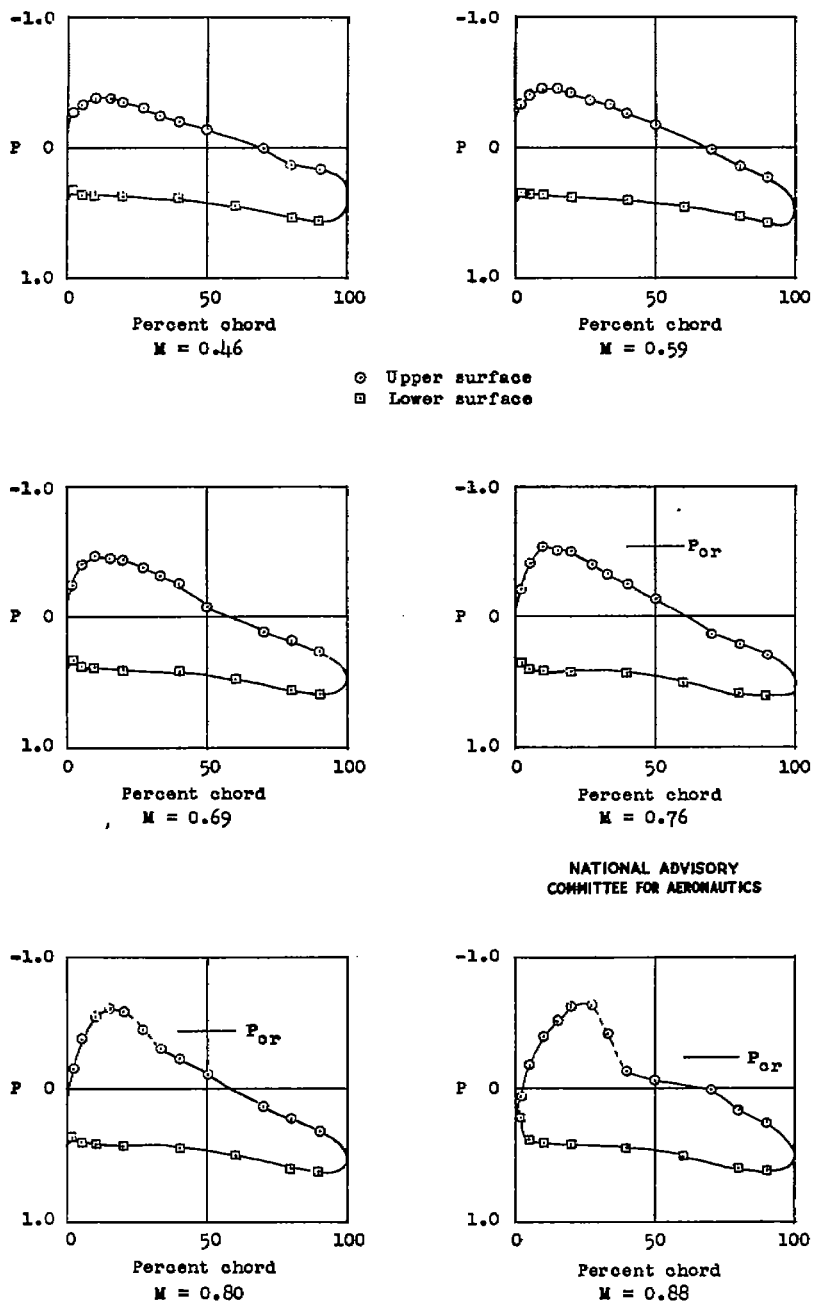


Figure 14.- Section pressure distributions for a range of Mach numbers. Cascade of NACA 65-806 blower blades;  $\alpha = 10^\circ$ ;  $\beta = 60^\circ$ ;  $\sigma = 1.0$ .

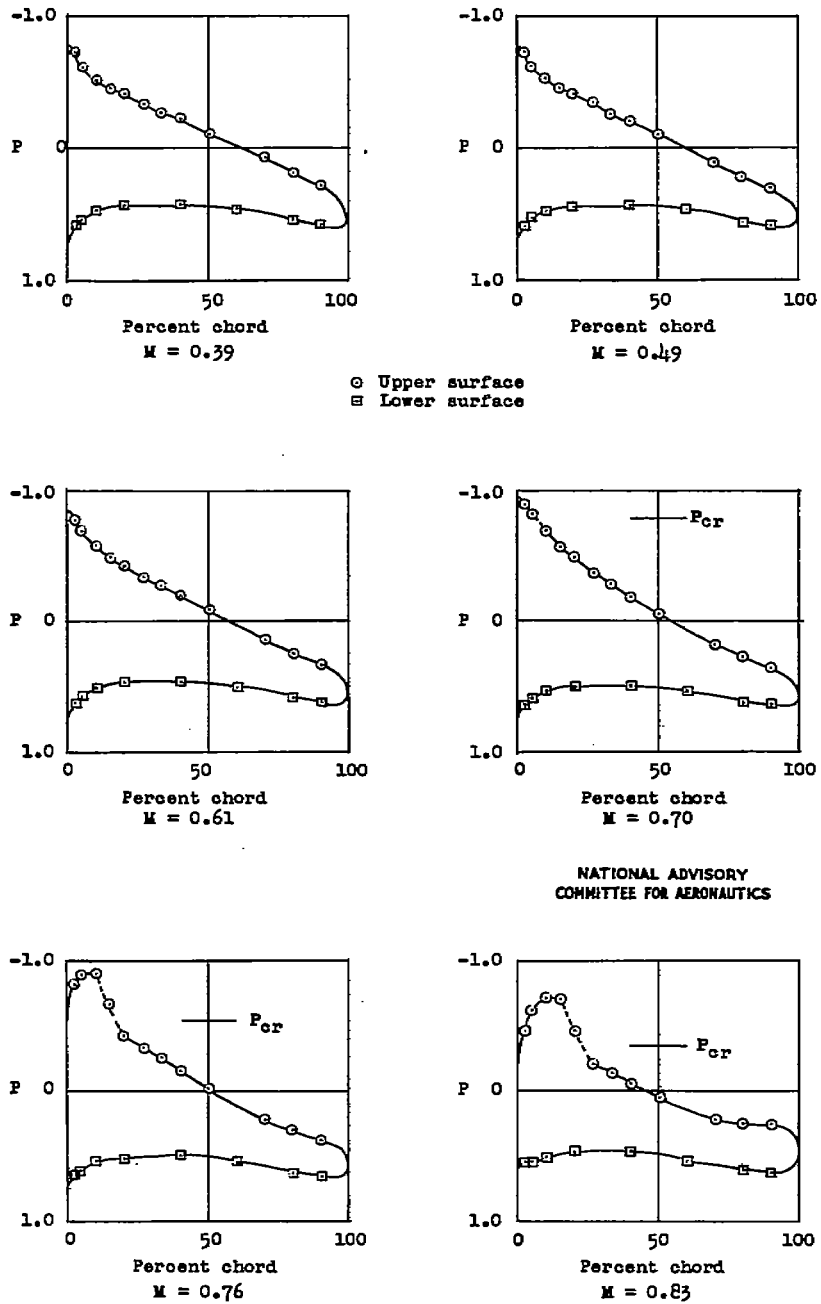


Figure 15.- Section pressure distributions for a range of Mach numbers. Cascade of NACA 65-806 blower blades;  $\alpha = 12.5^\circ$ ;  $\beta = 60^\circ$ ;  $\sigma = 1.0$ .

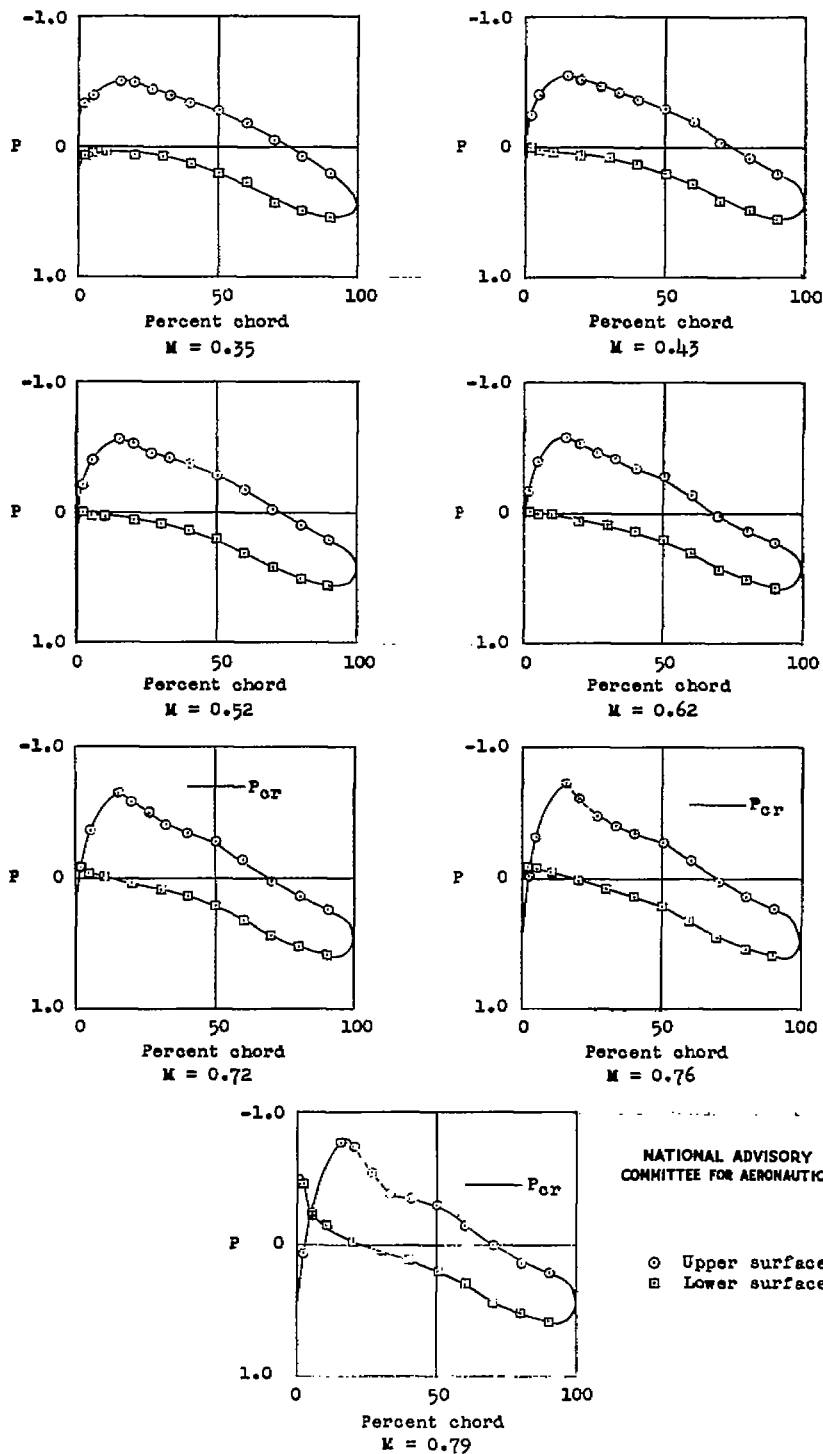


Figure 16.- Section pressure distributions for a range of Mach numbers. Cascade of NACA 65-(12)10 blower blades;  $\alpha = 14.9^\circ$ ;  $\beta = 45^\circ$ ;  $\sigma = 1.5$ .

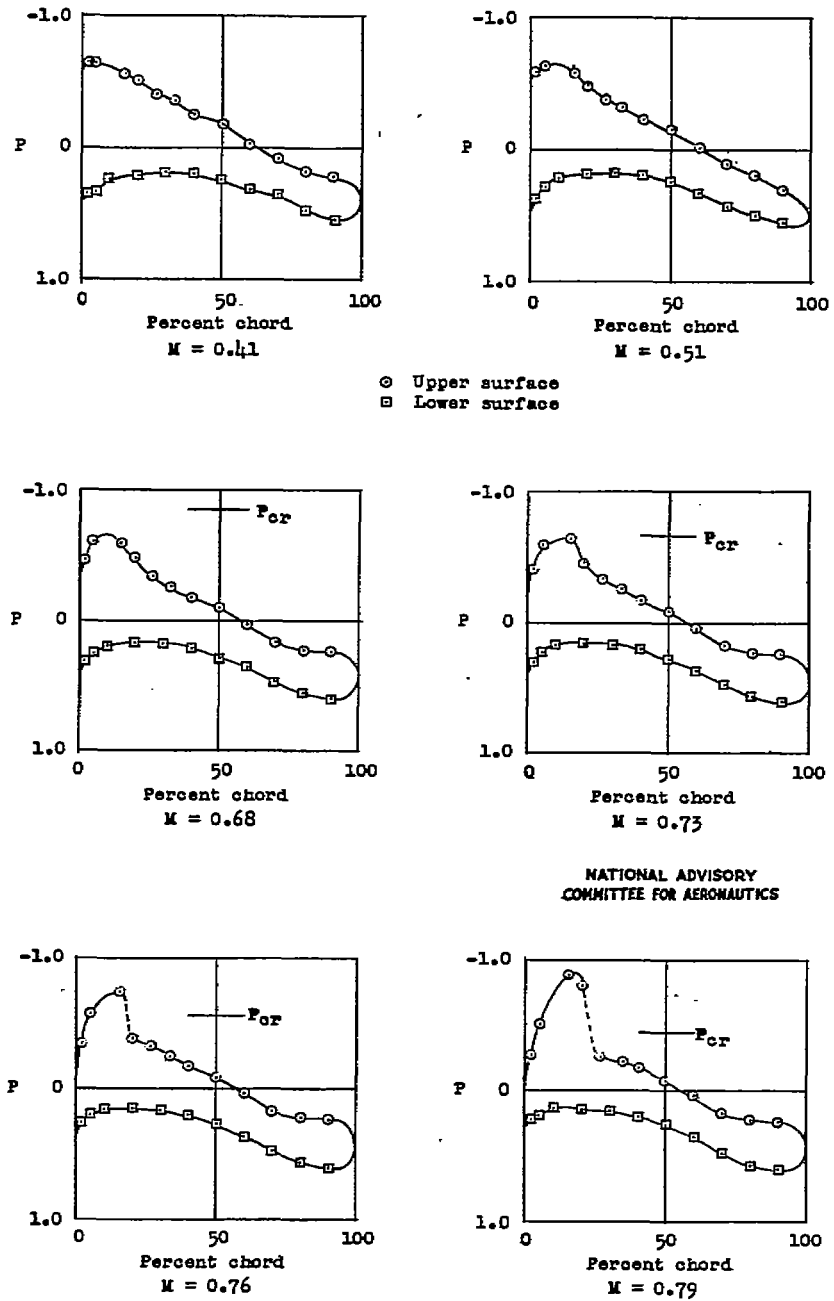


Figure 17.- Section pressure distributions for a range of Mach numbers. Cascade of NACA 65-(12)10 blower blades;  $\alpha = 18.9^\circ$ ;  $\beta = 45^\circ$ ;  $\sigma = 1.5$ .

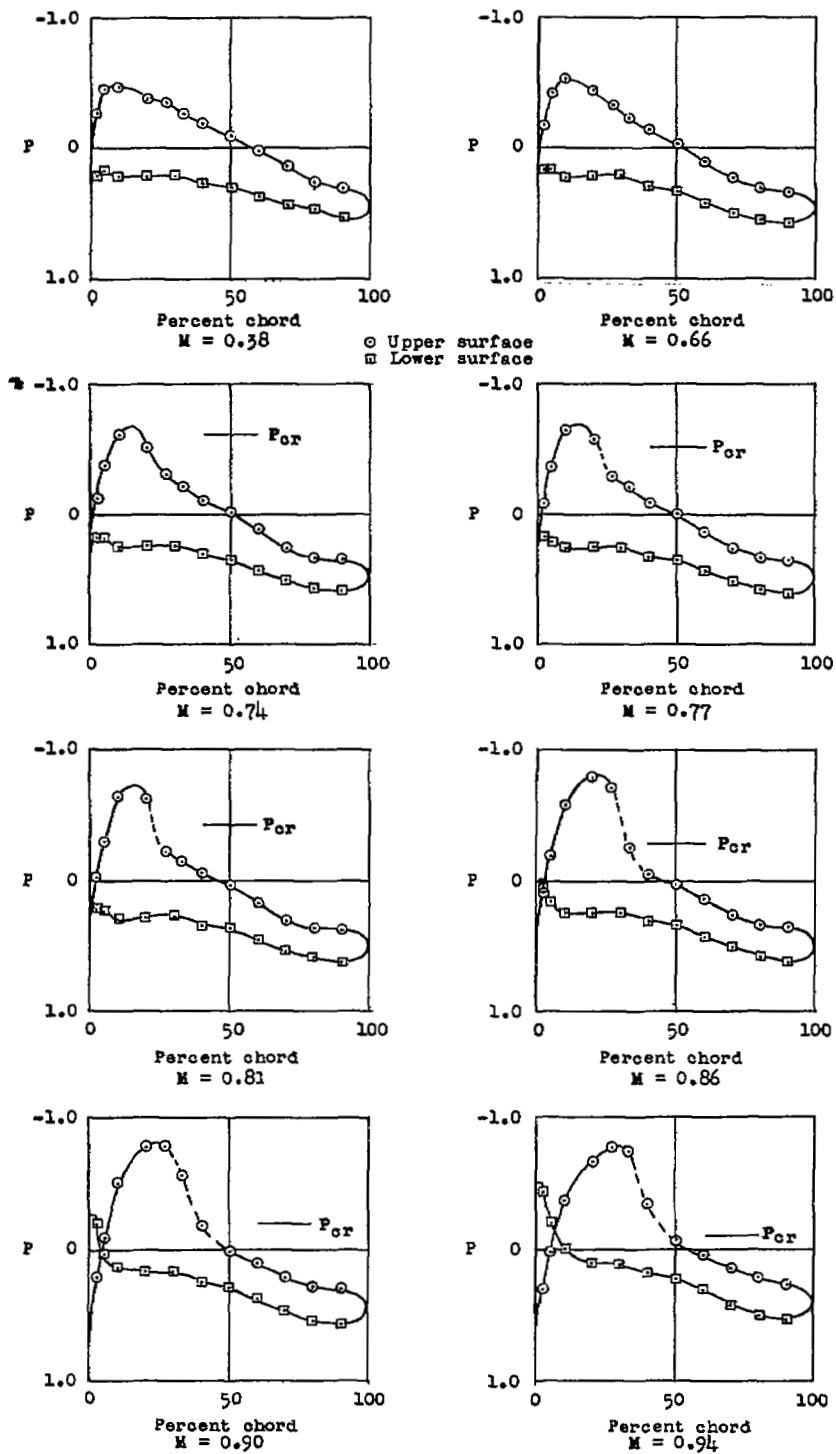


Figure 18.- Section pressure distributions for a range of Mach numbers. Cascade of NACA 65-(12)10 blower blades;  $\alpha = 14.2^\circ$ ;  $\beta = 60^\circ$ ;  $\sigma = 1.5$ . NATIONAL ADVISORY COMMITTEE FOR AERONAUTICS

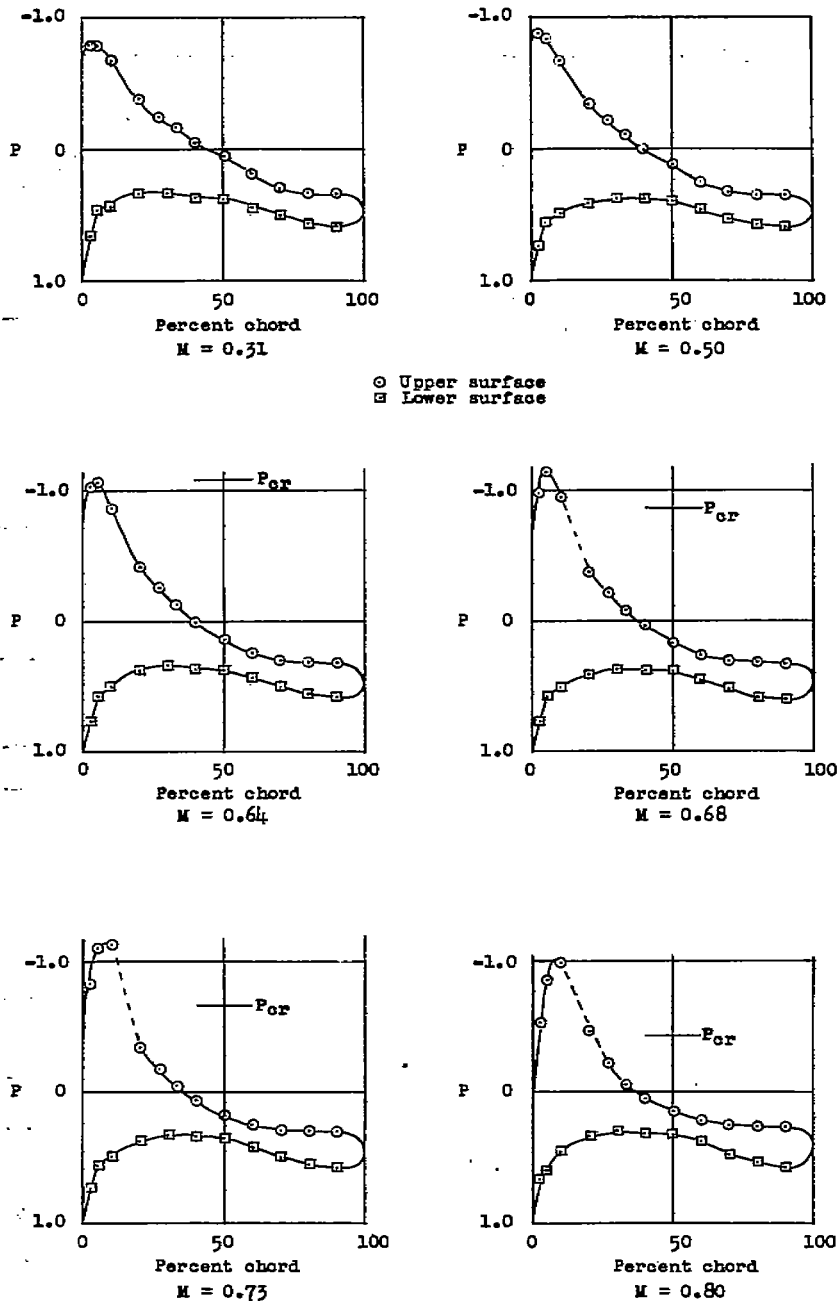


Figure 19.- Section pressure distributions for a range of Mach numbers. Cascade of NACA 65-(12)10 blower blades;  $\alpha = 19.2^\circ$ ;  $\beta = 60^\circ$ ;  $\sigma = 1.5$ .

NATIONAL ADVISORY  
COMMITTEE FOR AERONAUTICS

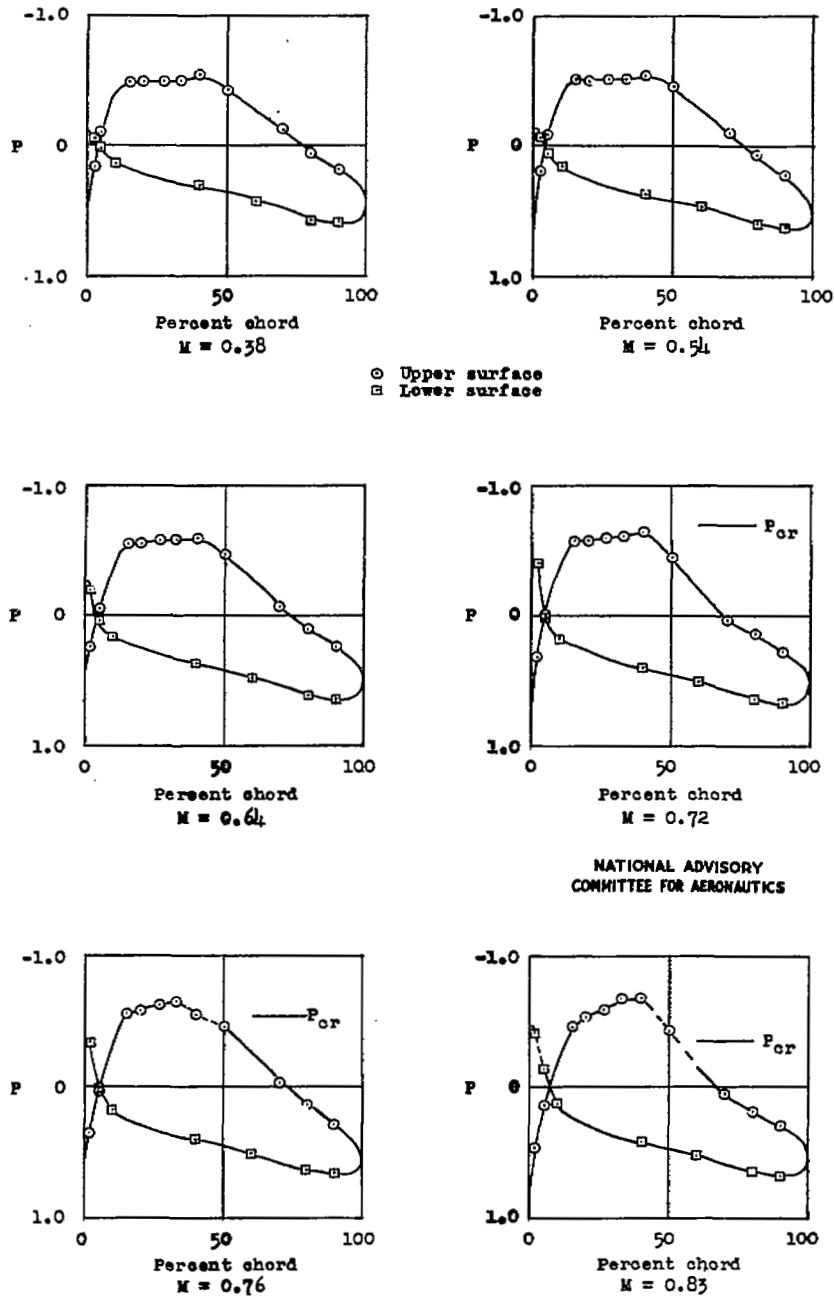


Figure 20.- Section pressure distributions for a range of Mach numbers. Cascade of NACA 65-(12)10 blower blades;  $\alpha = 9^\circ$ ;  $\beta = 60^\circ$ ;  $\sigma = 1.0$ .

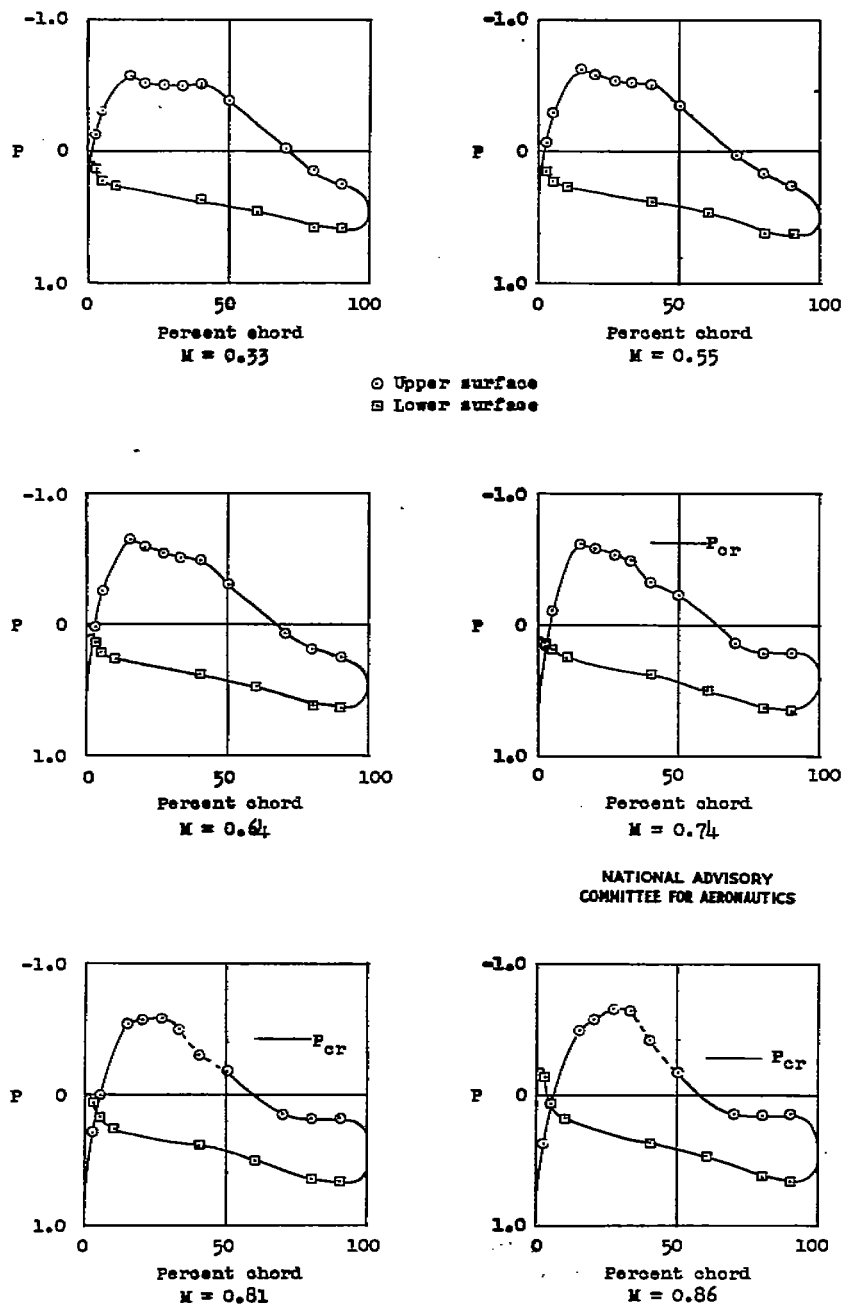


Figure 21.- Section pressure distributions for a range of Mach numbers. Cascade of NACA 65-(12)10 blower blades;  $\alpha = 11.5^\circ$ ;  $\beta = 60^\circ$ ;  $\sigma = 1.0$ .

Fig. 22

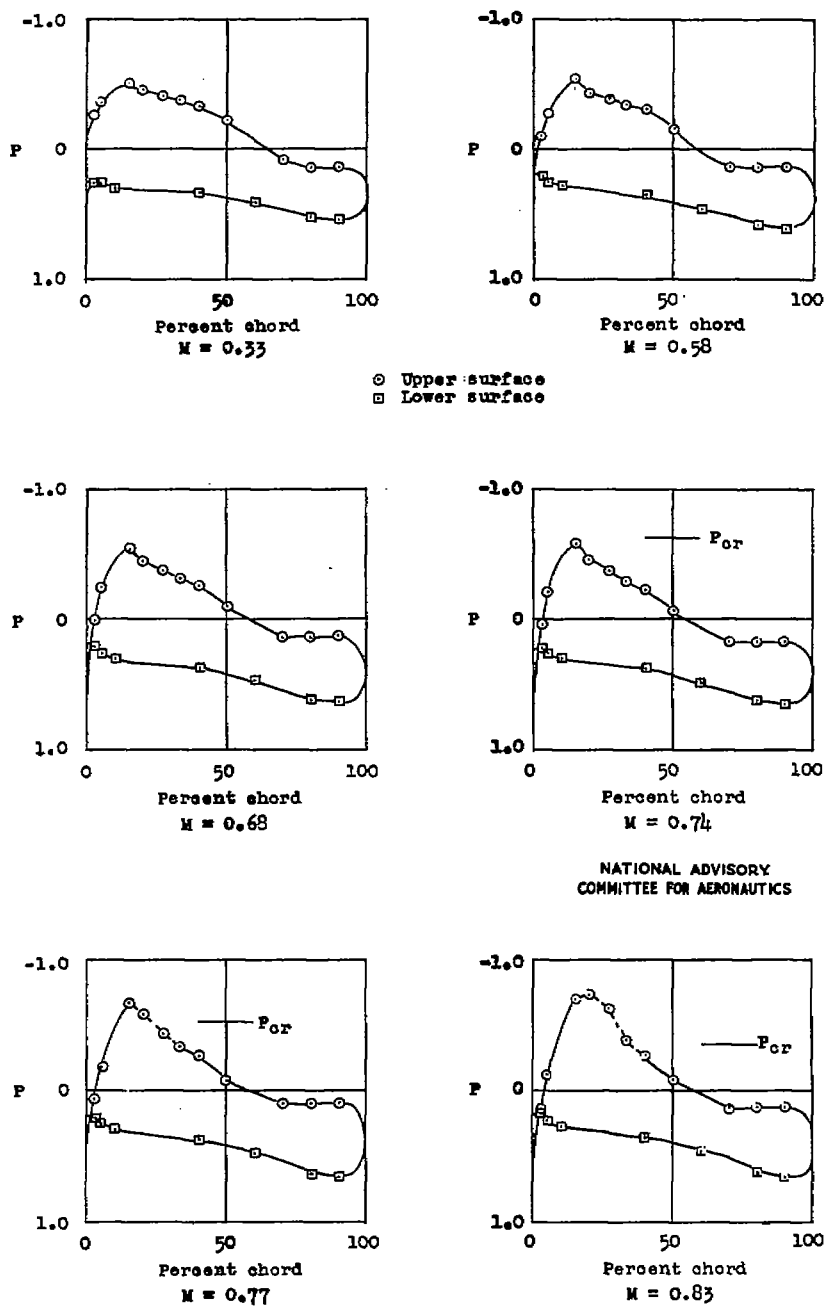


Figure 22.- Section pressure distributions for a range of Mach numbers. Cascade of NACA 65-(12)10 blower blades;  $\alpha = 14^\circ$ ;  $\beta = 60^\circ$ ;  $\sigma = 1.0$ .

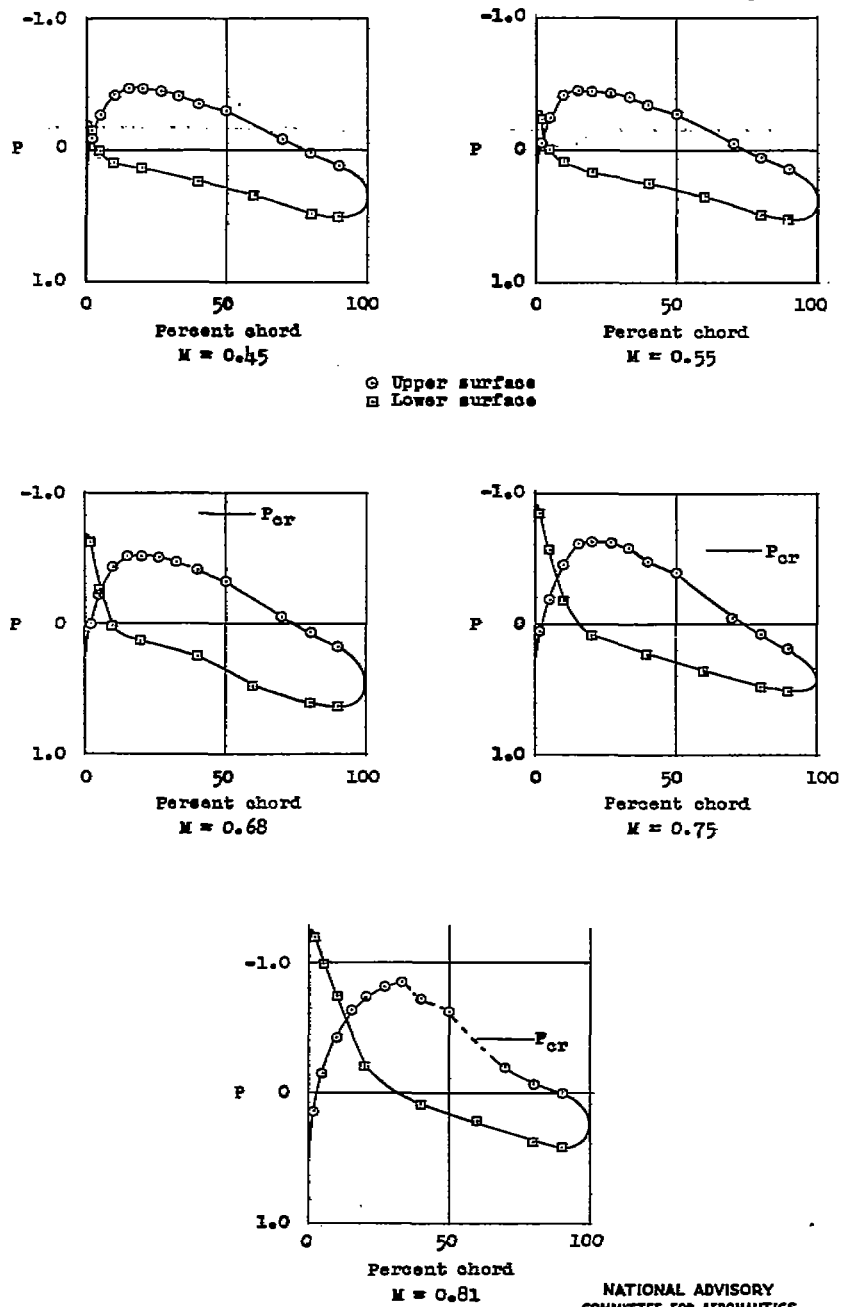


Figure 23.- Section pressure distributions for a range of Mach numbers. Cascade of NACA 65-(12)06 blower blades;  $\alpha = 10^\circ$ ;  $\beta = 45^\circ$ ;  $\sigma = 1.5$ .

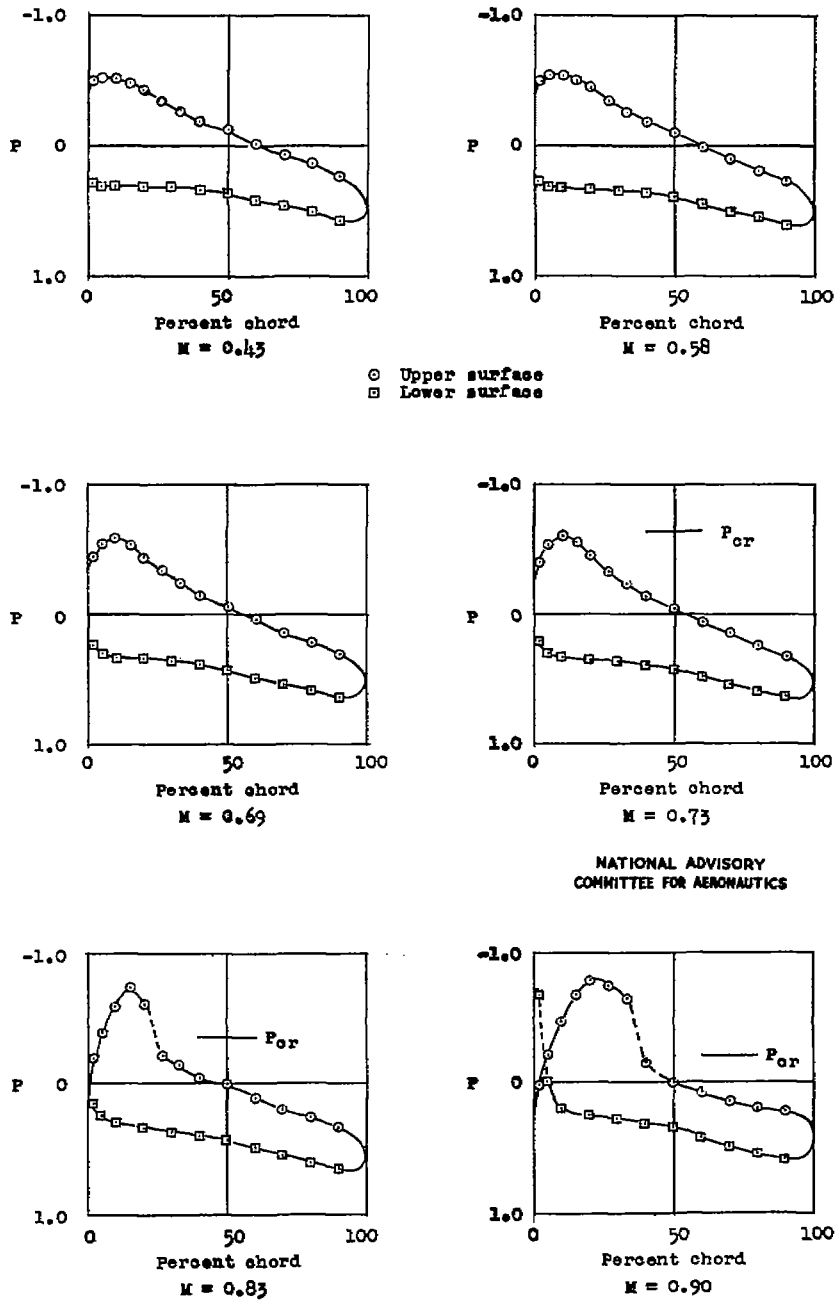


Figure 24.- Section pressure distributions for a range of Mach numbers. Cascade of NACA 65-(12)06 blower blades;  $\alpha = 15^\circ$ ;  $\beta = 45^\circ$ ;  $\sigma = 1.5$ .

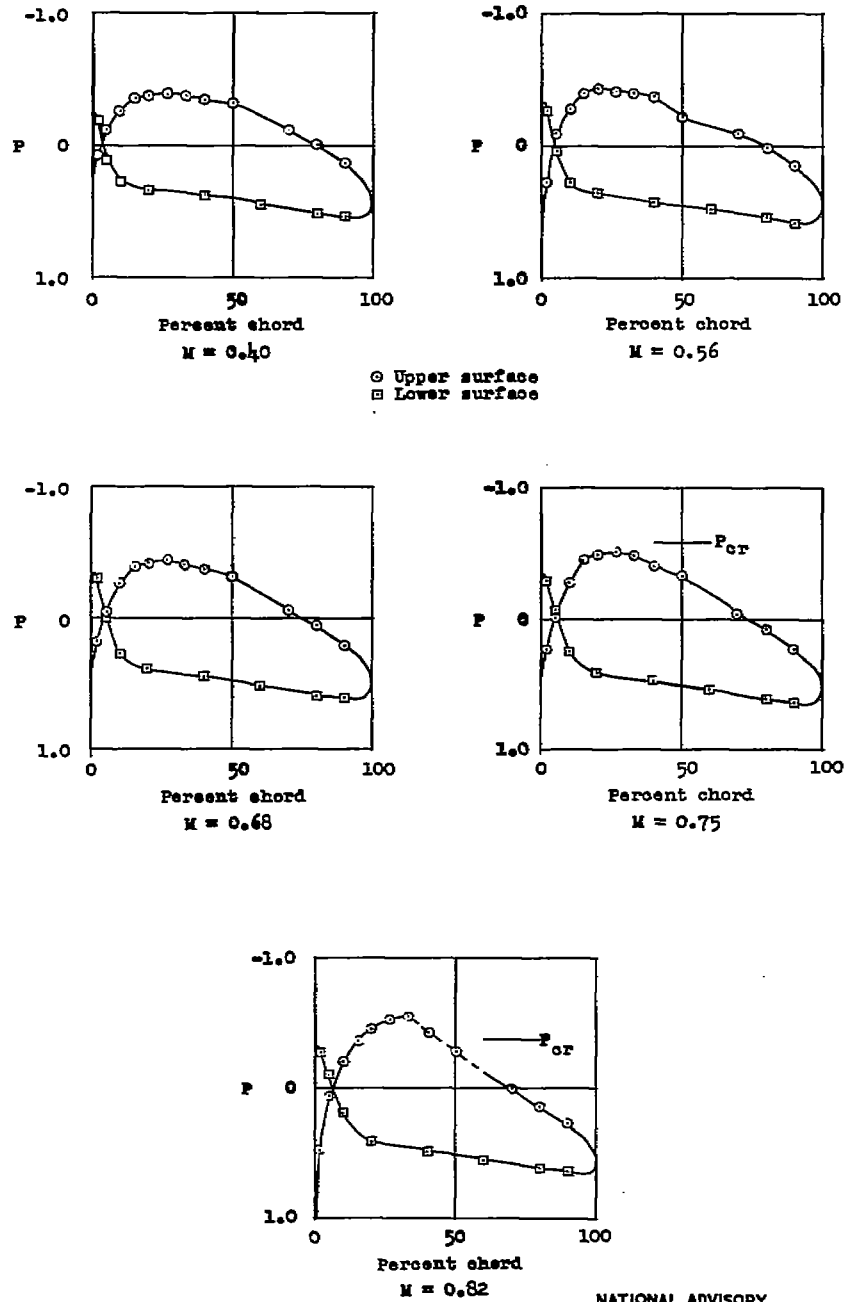


Figure 25.- Section pressure distributions for a range of Mach numbers. Cascade of NACA 65-(12)06 blower blades;  $\alpha = 9^\circ$ ;  $\beta = 60^\circ$ ;  $\sigma = 1.0$ .

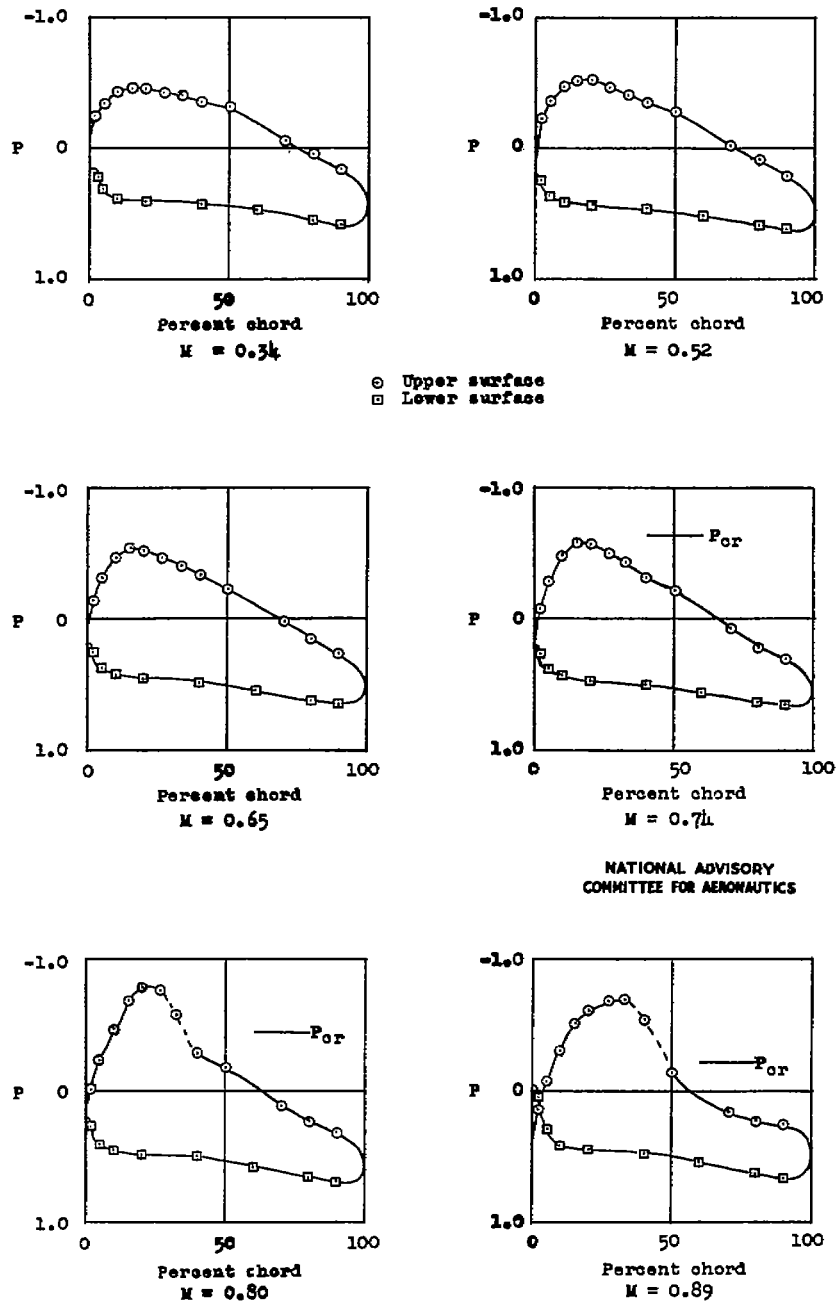


Figure 26.- Section pressure distributions for a range of Mach numbers. Cascade of NACA 65-(12)06 blower blades;  $\alpha = 11.5^\circ$ ;  $\beta = 60^\circ$ ;  $\sigma = 1.0$ .

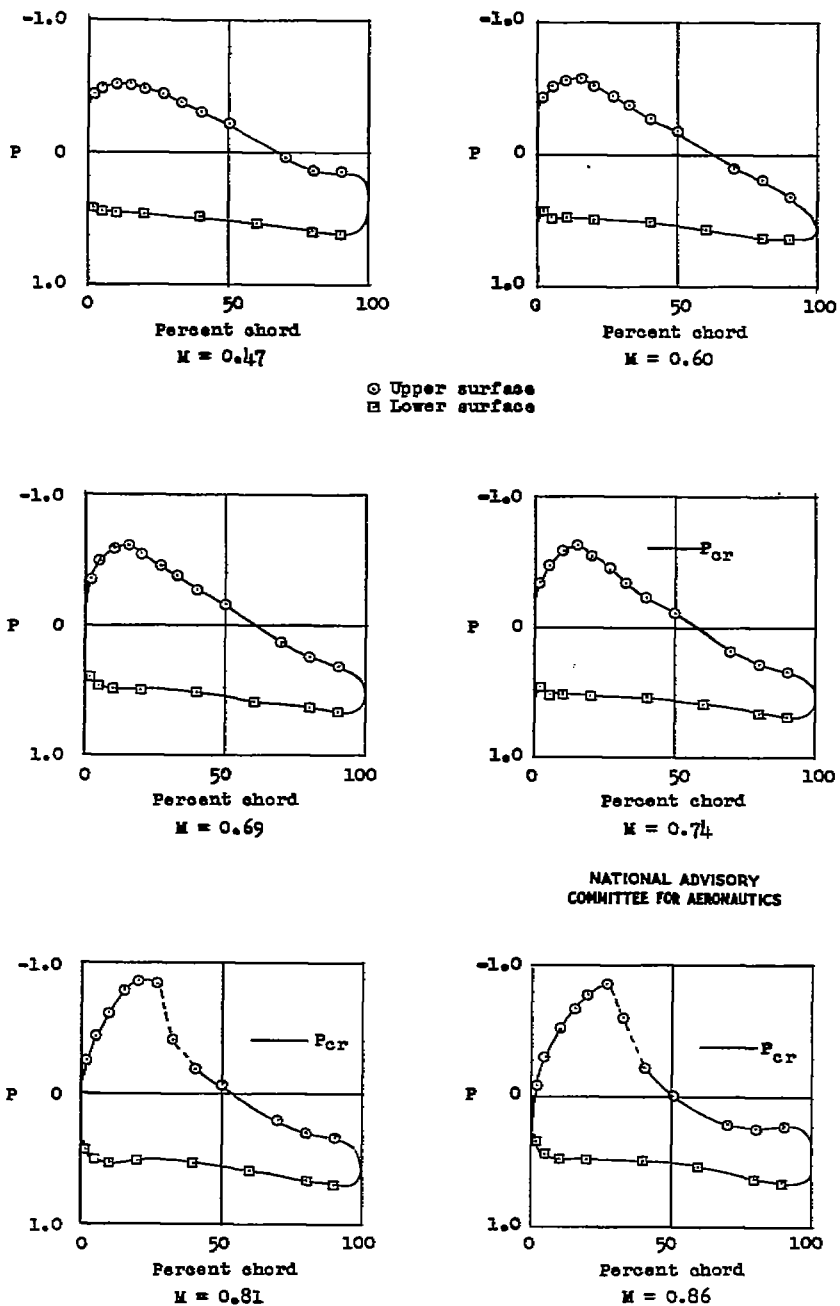


Figure 27.- Section pressure distributions for a range of Mach numbers. Cascade of NACA 65-(12)06 blower blades;  $\alpha = 14^\circ$ ;  $\beta = 60^\circ$ ;  $\sigma = 1.0$ .

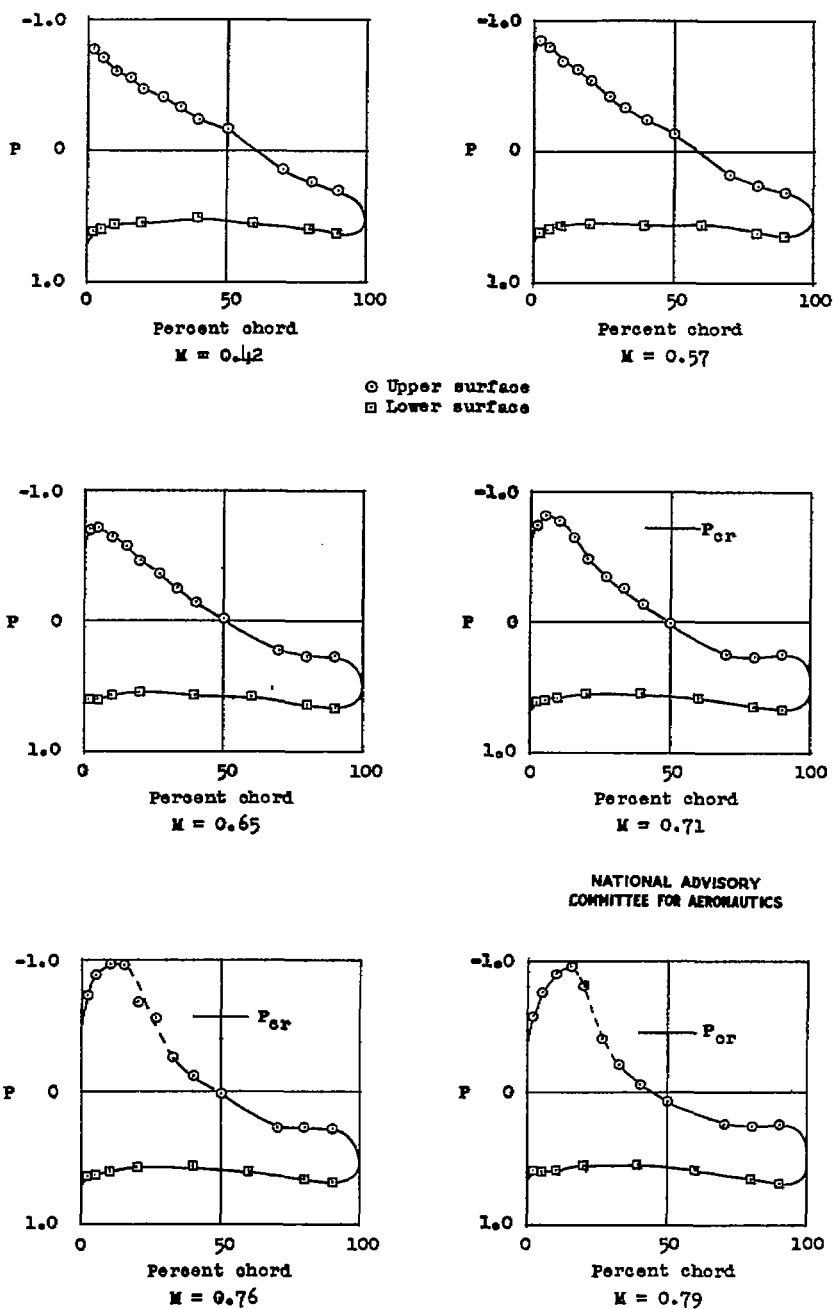


Figure 28.- Section pressure distributions for a range of Mach numbers. Cascade of NACA 65-(12)06 blower blades;  $\alpha = 16.5^\circ$ ;  $\beta = 60^\circ$ ;  $\sigma = 1.0$ .

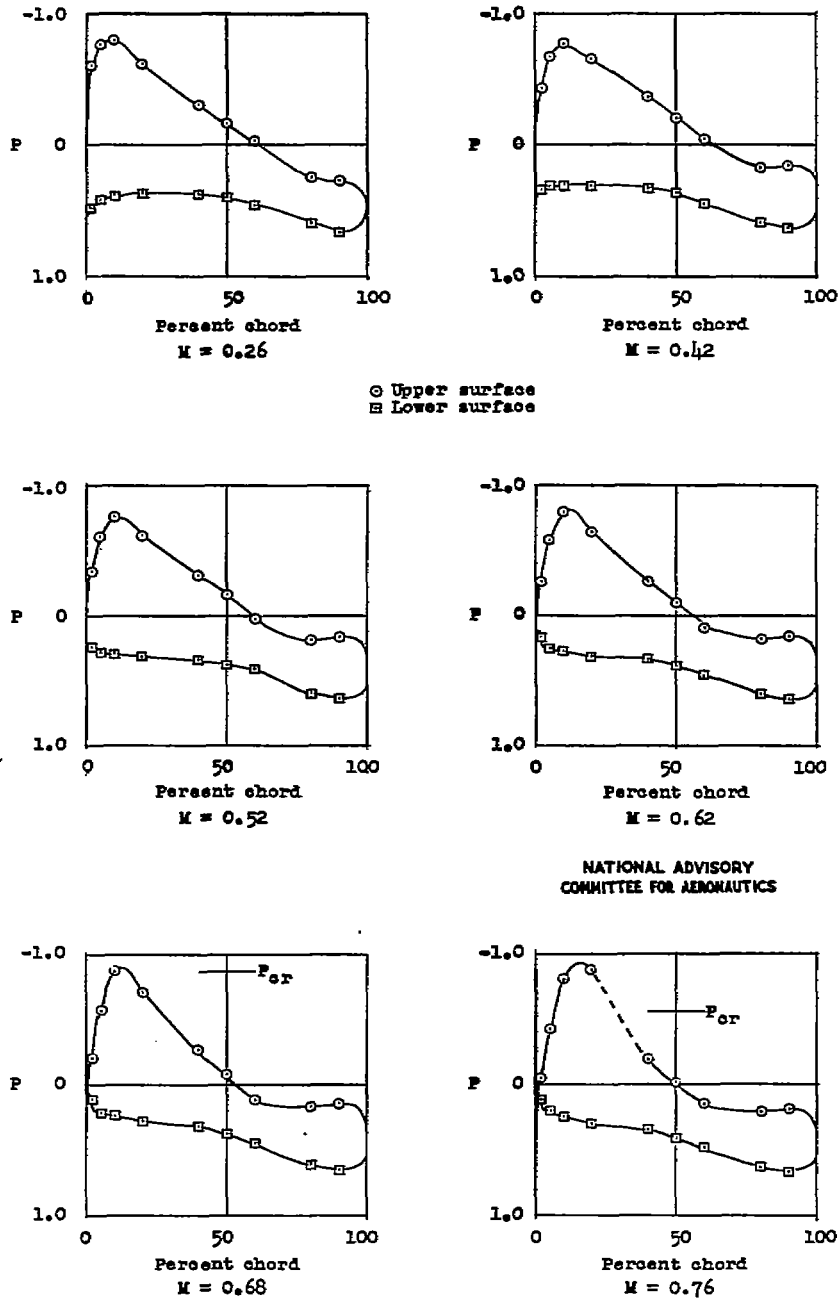


Figure 29.- Section pressure distributions for a range of Mach numbers. Cascade of NACA 65-(18)10 blower blades;  $\alpha = 21.5^\circ$ ;  $\beta = 4.5^\circ$ ;  $\sigma = 1.5$ .

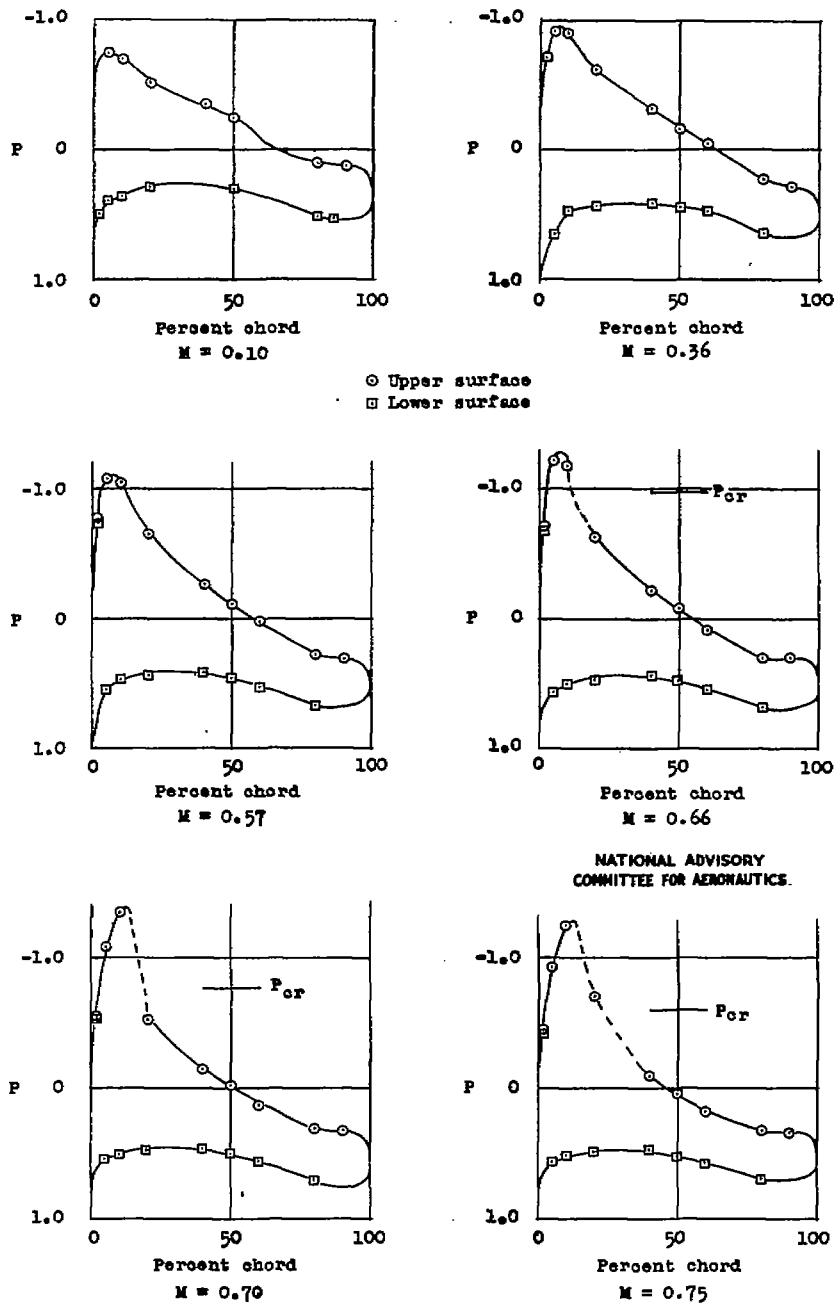


Figure 30.- Section pressure distributions for a range of Mach numbers. Cascade of NACA 65-(18)10 blower blades;  $\alpha = 26.5^\circ$ ;  $\beta = 45^\circ$ ;  $\sigma = 1.5$ .

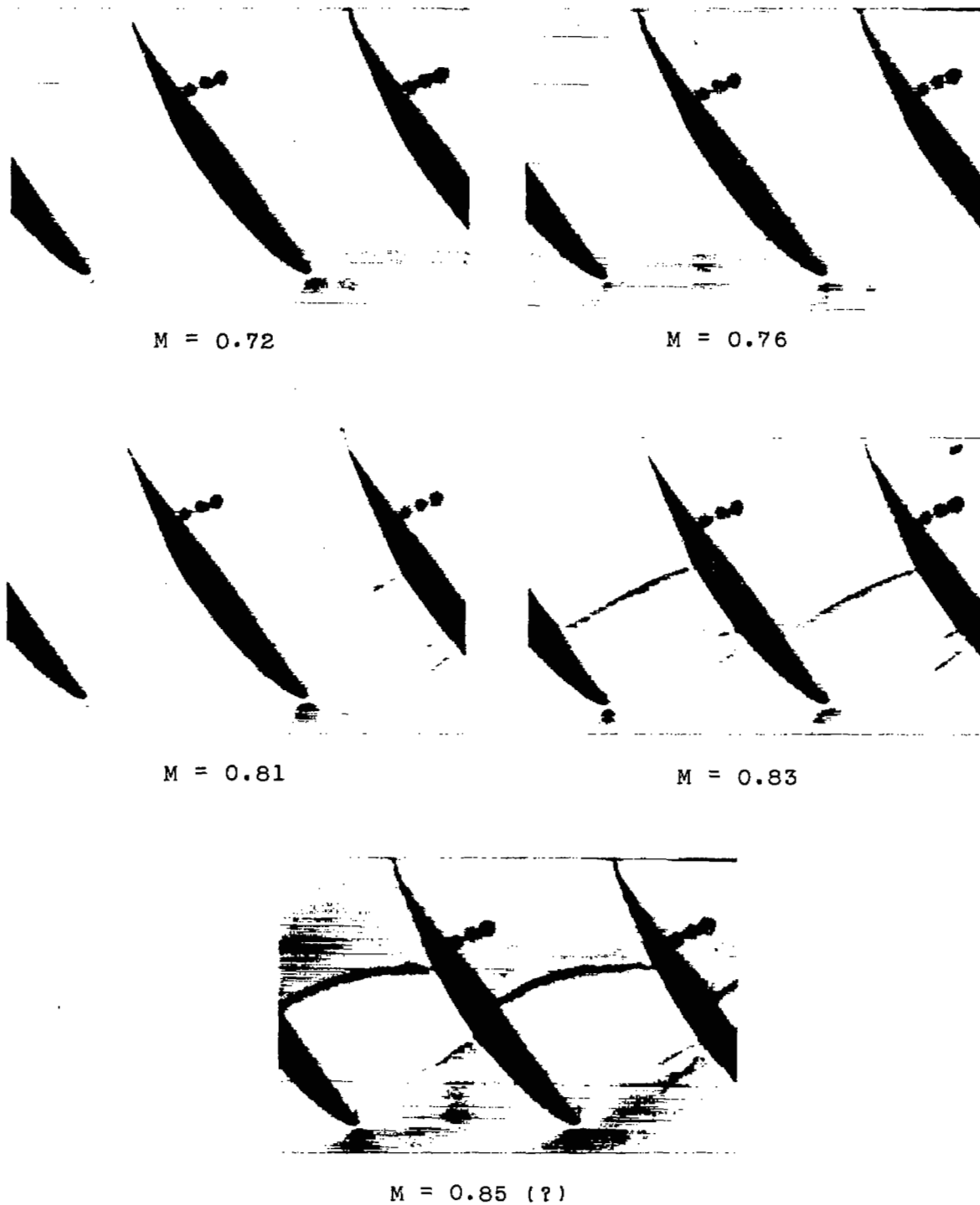


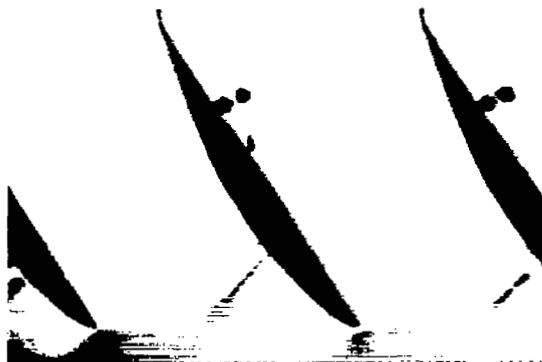
Figure 31.- Schlieren photographs for a range of Mach number. Cascade of NACA 65-810 blower blades:  $\alpha = 10.6^\circ$ ;  $\beta = 45^\circ$ ;  $\sigma = 1.5$ .



$M = 0.73$



$M = 0.78$



$M = 0.85$



$M = 0.88$



$M = 0.89$

Figure 32.- Schlieren photographs for a range of Mach number. Cascade of NACA 65-810 blower blades;  $\alpha = 12.5^\circ$ ;  $\beta = 45^\circ$ ;  $\sigma = 1.5$ .

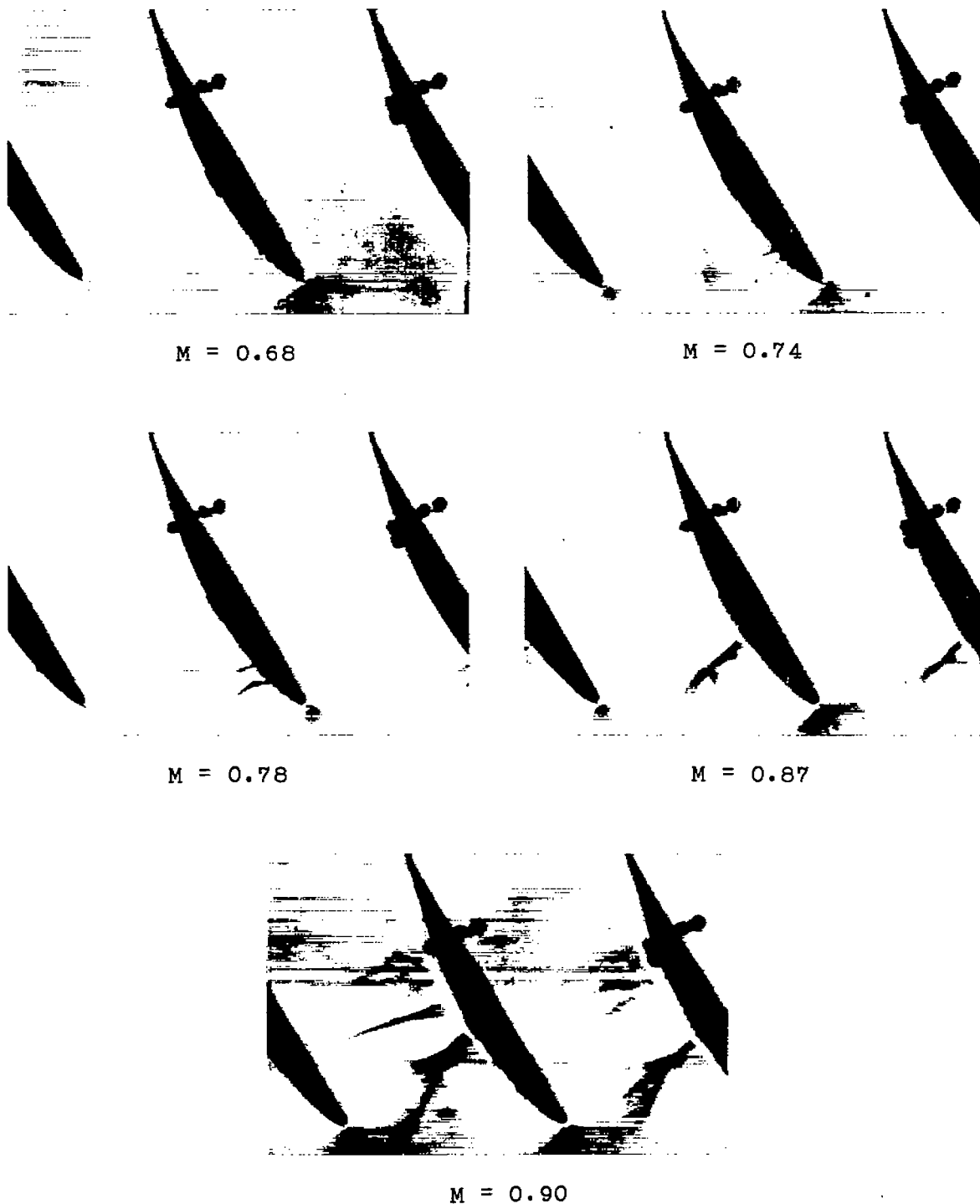


Figure 33.- Schlieren photographs for a range of Mach number. Cascade of NACA 65-810 blower blades;  $\alpha = 15.6^\circ$ ;  $\beta = 45^\circ$ ;  $\sigma = 1.5$ .

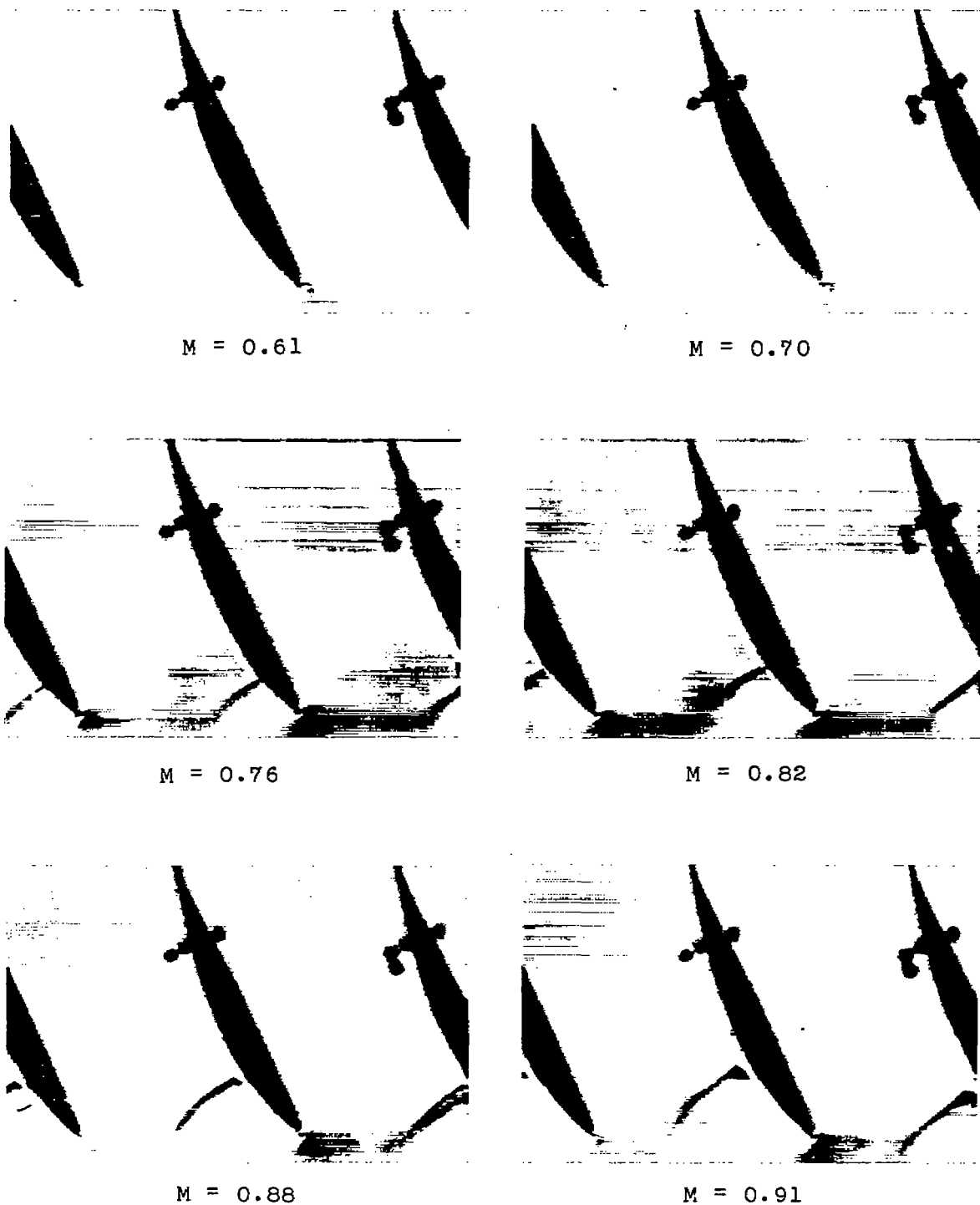


Figure 34.- Schlieren photographs for a range of Mach number. Cascade of NACA 65-810 blower blades;  $\alpha = 20.6^\circ$ ;  $\beta = 45^\circ$ ;  $\sigma = 1.5$ .



M = 0.68



M = 0.71



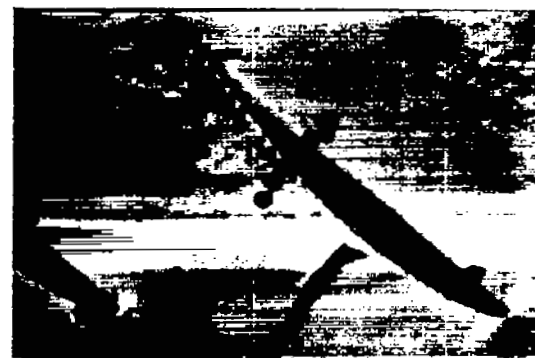
M = 0.78



M = 0.83

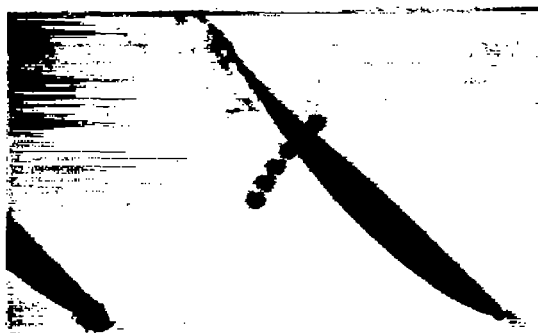


M = 0.88

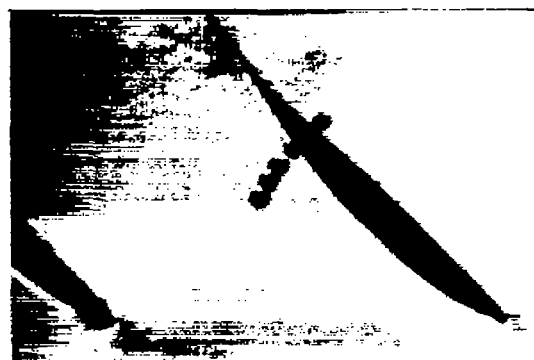


M = 0.91

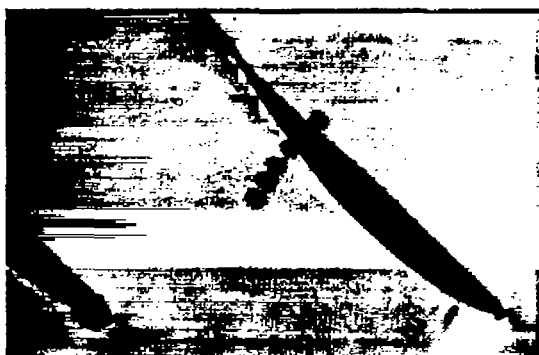
Figure 35.- Schlieren photographs for a range of Mach number. Cascade of NACA 65-810 blower blades;  $\alpha = 10.5^\circ$ ;  $\beta = 60^\circ$ ;  $\sigma = 1.0$ .



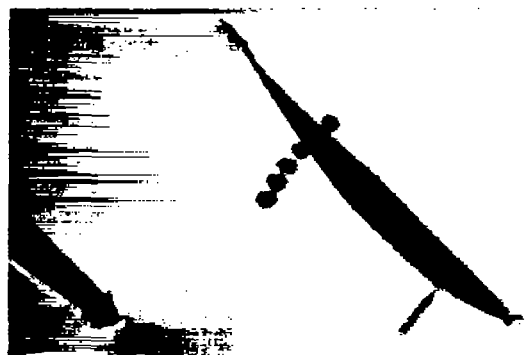
M = 0.58



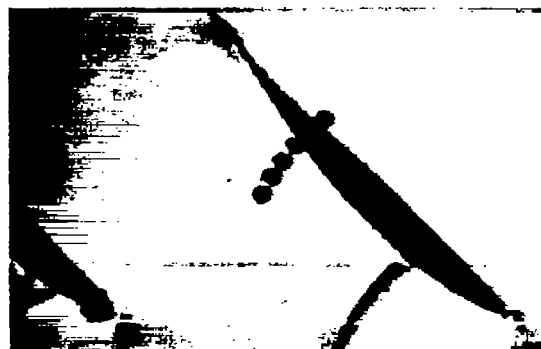
M = 0.63



M = 0.68



M = 0.73



M = 0.78

Figure 36.- Schlieren photographs for a range of Mach number. Cascade of NACA 65-810 blower blades;  $\alpha = 15.5^\circ$ ;  $\beta = 60^\circ$ ;  $\sigma = 1.0$ .

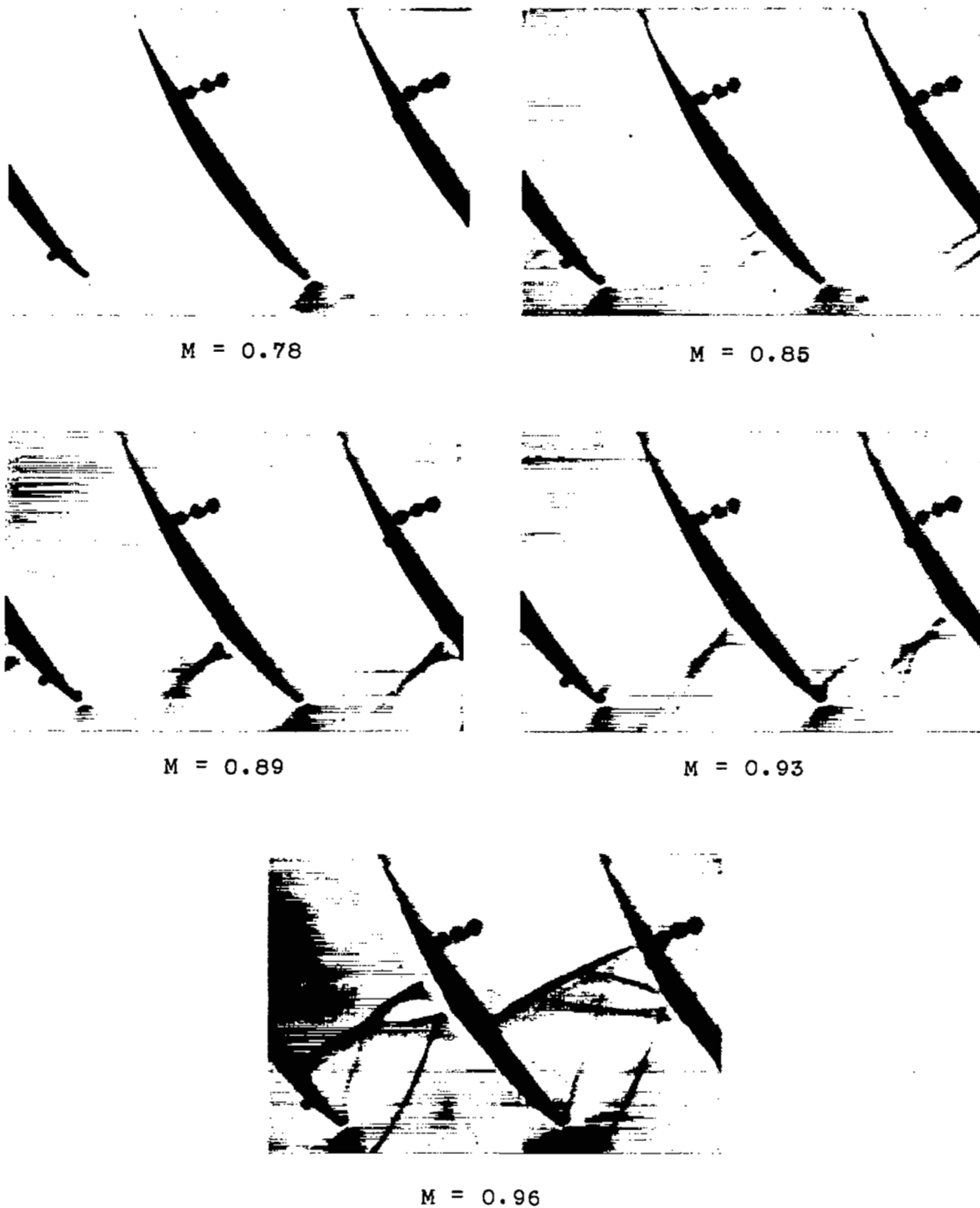


Figure 37.- Schlieren photographs for a range of Mach number. Cascade of NACA 65-806 blower blades;  $\alpha = 11.5^\circ$ ;  $\beta = 45^\circ$ ;  $\sigma = 1.5$ .

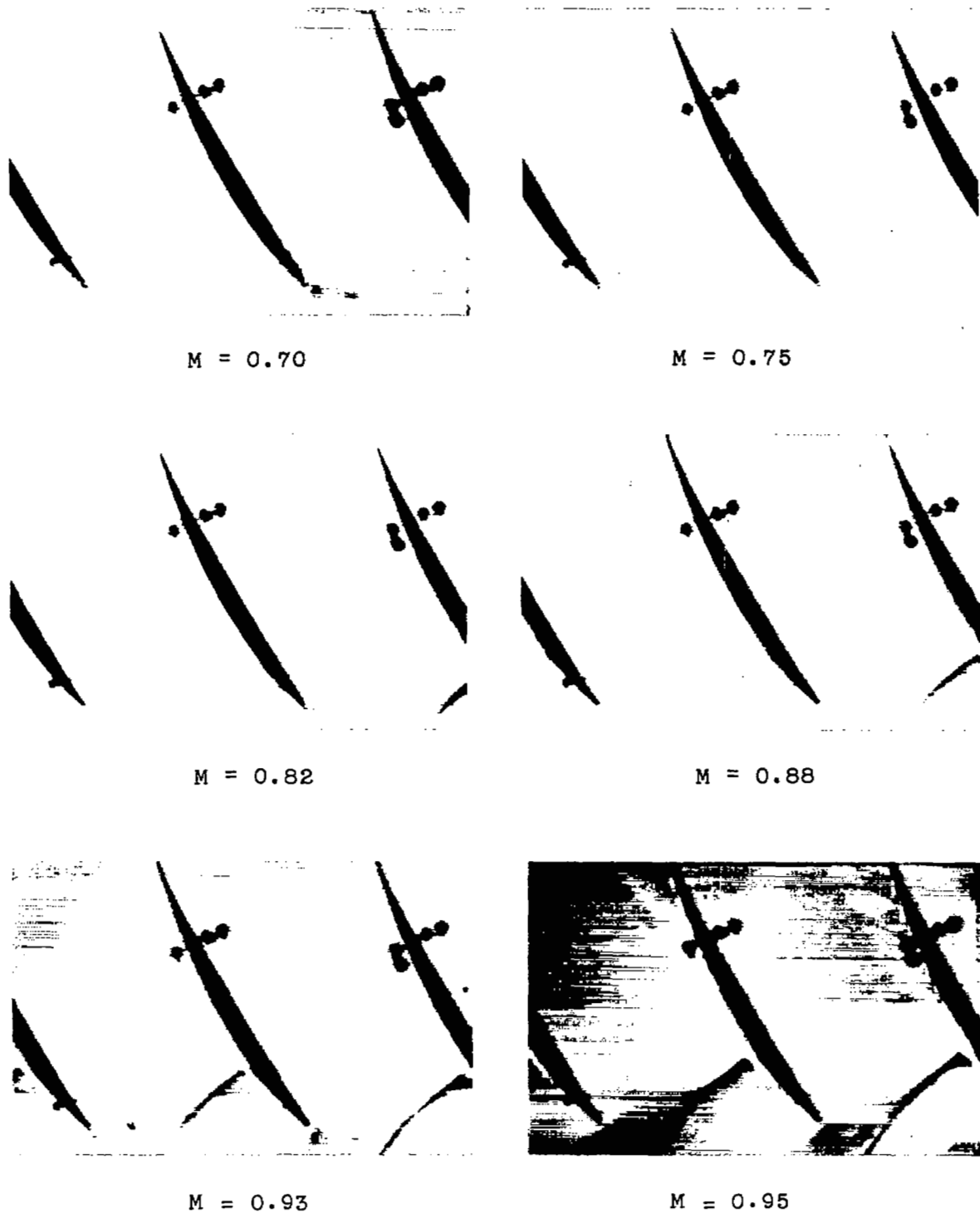


Figure 38.- Schlieren photographs for a range of Mach number. Cascade of NACA 65-806 blower blades;  $\alpha = 16.5^\circ$ ;  $\beta = 45^\circ$ ;  $\sigma = 1.5$ .

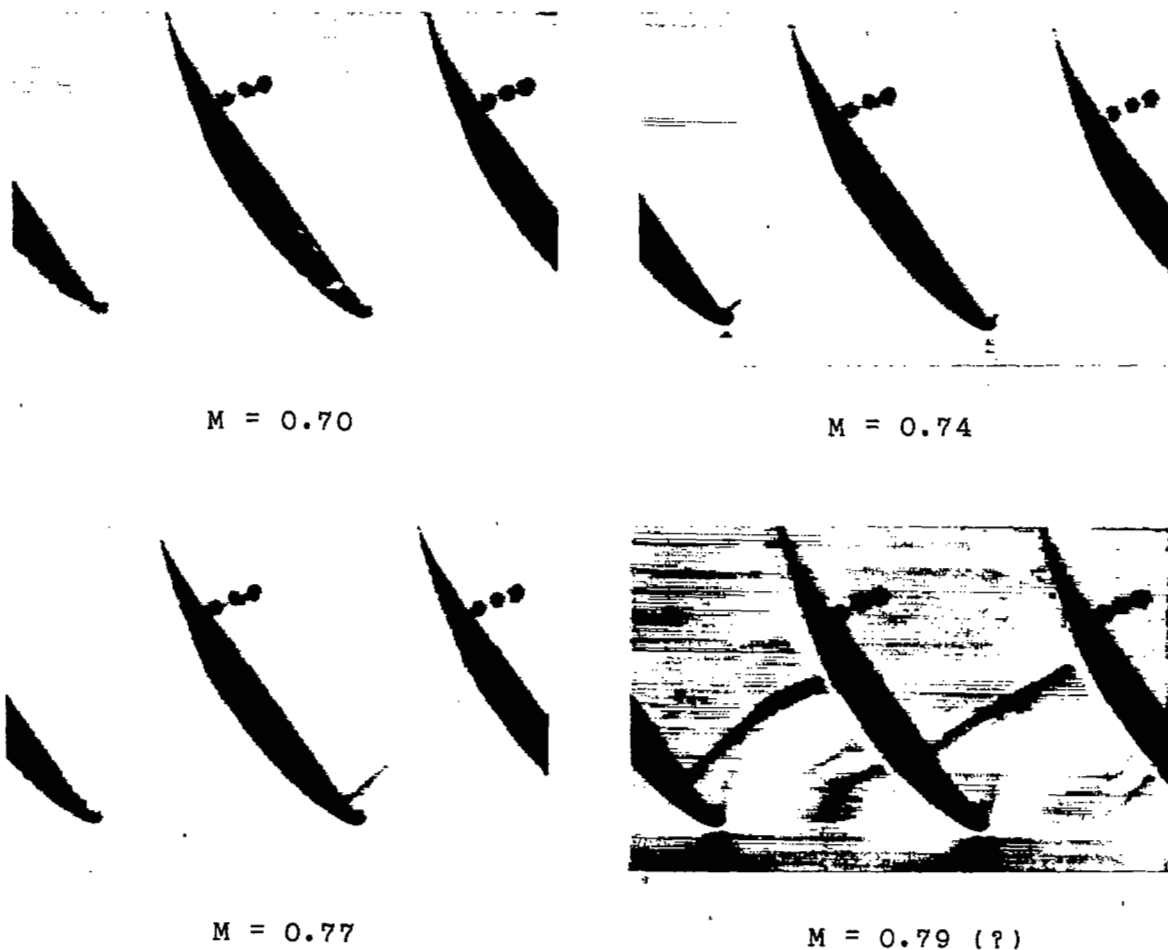


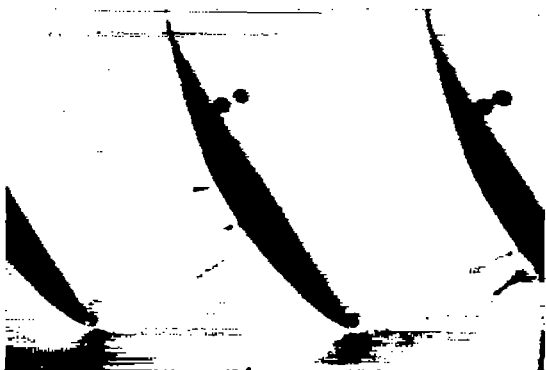
Figure 39.- Schlieren photographs for a range of Mach number. Cascade of NACA 65-(12)10 blower blades;  $\alpha = 12.0^\circ$ ;  $\beta = 45^\circ$ ;  $\sigma = 1.5$ .



M = 0.73



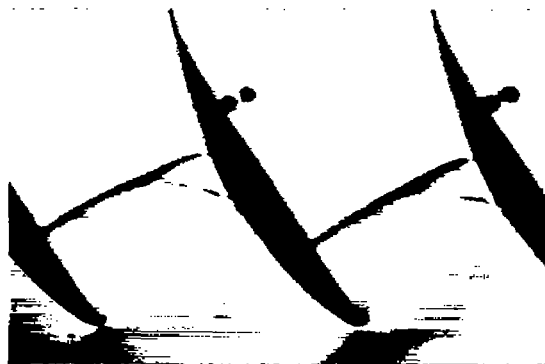
M = 0.79



M = 0.82



M = 0.84

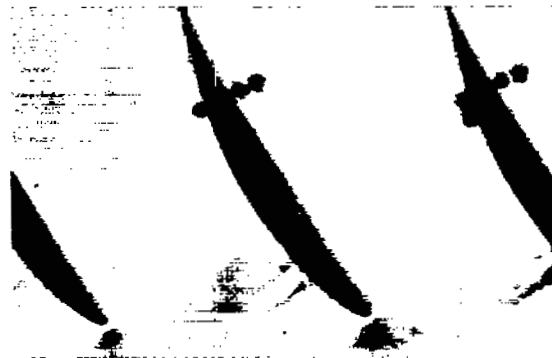


M = 0.87 (?)

Figure 40.- Schlieren photographs for a range of Mach number. Cascade of NACA 65-(12)10 blower blades;  $\alpha = 14.5^\circ$ ;  $\beta = 45^\circ$ ;  $\sigma = 1.5$ .



M = 0.73



M = 0.78



M = 0.85

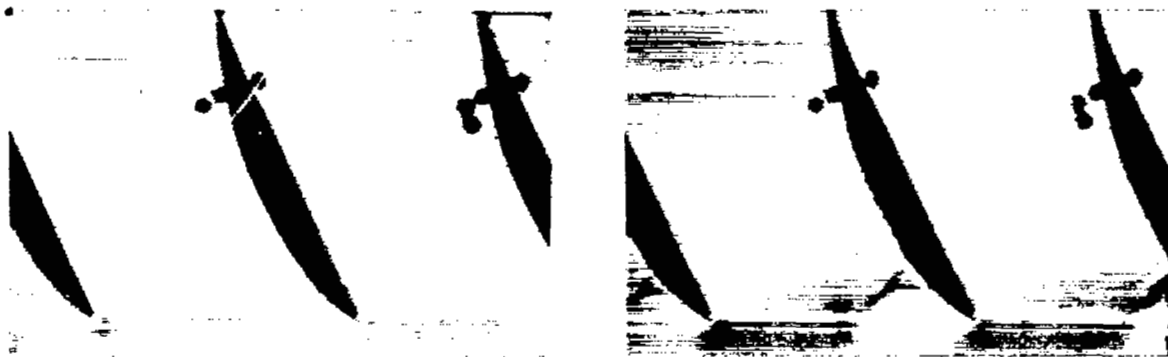


M = 0.87



M = 0.90

Figure 41.- Schlieren photographs for a range of Mach number. Cascade of NACA 65-(12)10 blower blades;  $\alpha = 17.0^\circ$ ;  $\beta = 45^\circ$ ;  $\sigma = 1.5$ .



M = 0.70

M = 0.78



M = 0.82

M = 0.85



M = 0.88

Figure 42.- Schlieren photographs for a range of Mach number. Cascade of NACA 65-(12)10 blower blades;  $\alpha = 22.0^\circ$ ;  $\beta = 45^\circ$ ;  $\sigma = 1.5$ .

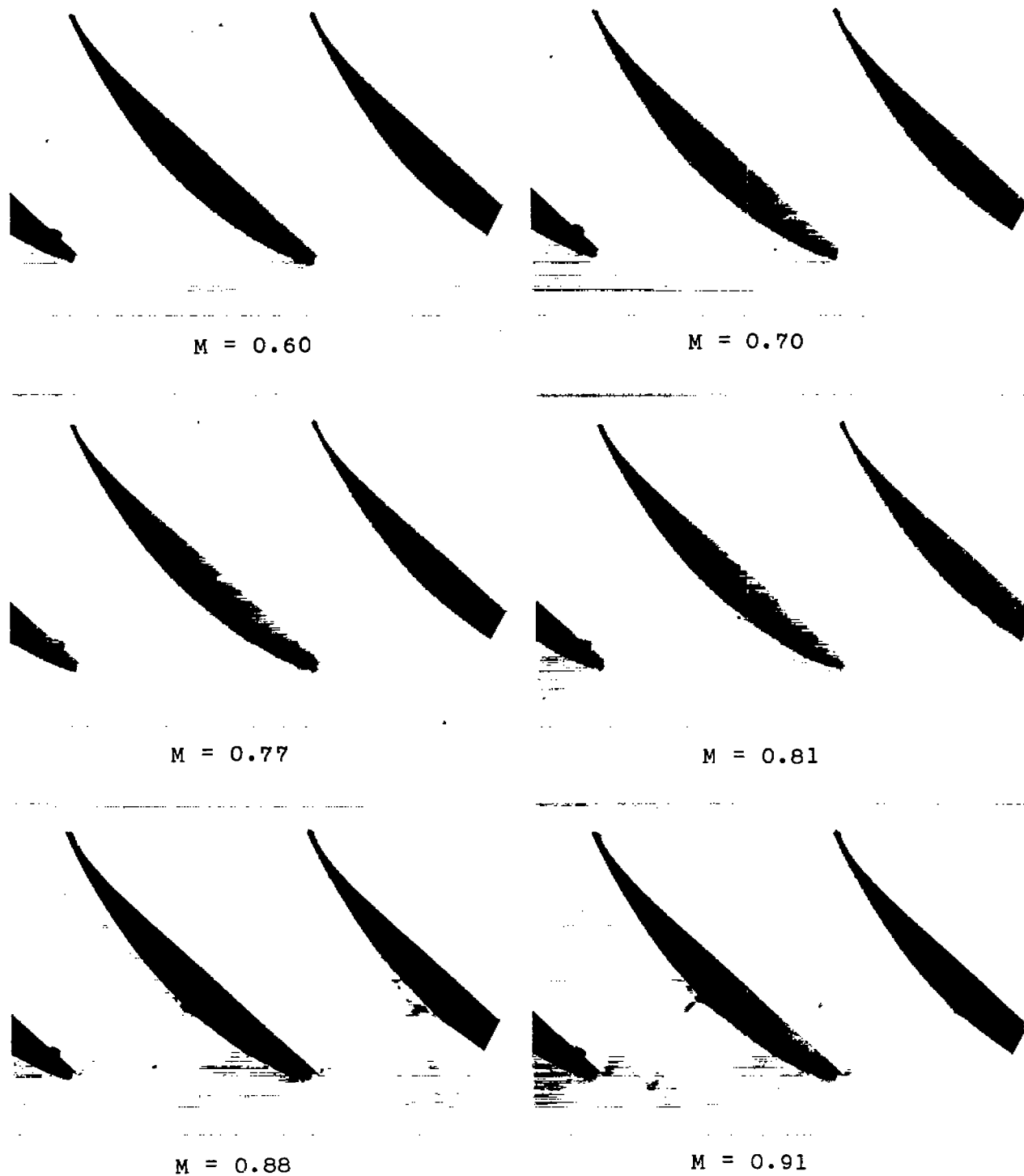


Figure 43.- Schlieren photographs for a range of Mach number. Cascade of NACA 65-(12)10 blower blades;  $\alpha = 15.2^\circ$ ;  $\beta = 60^\circ$ ;  $\sigma = 1.5$ .

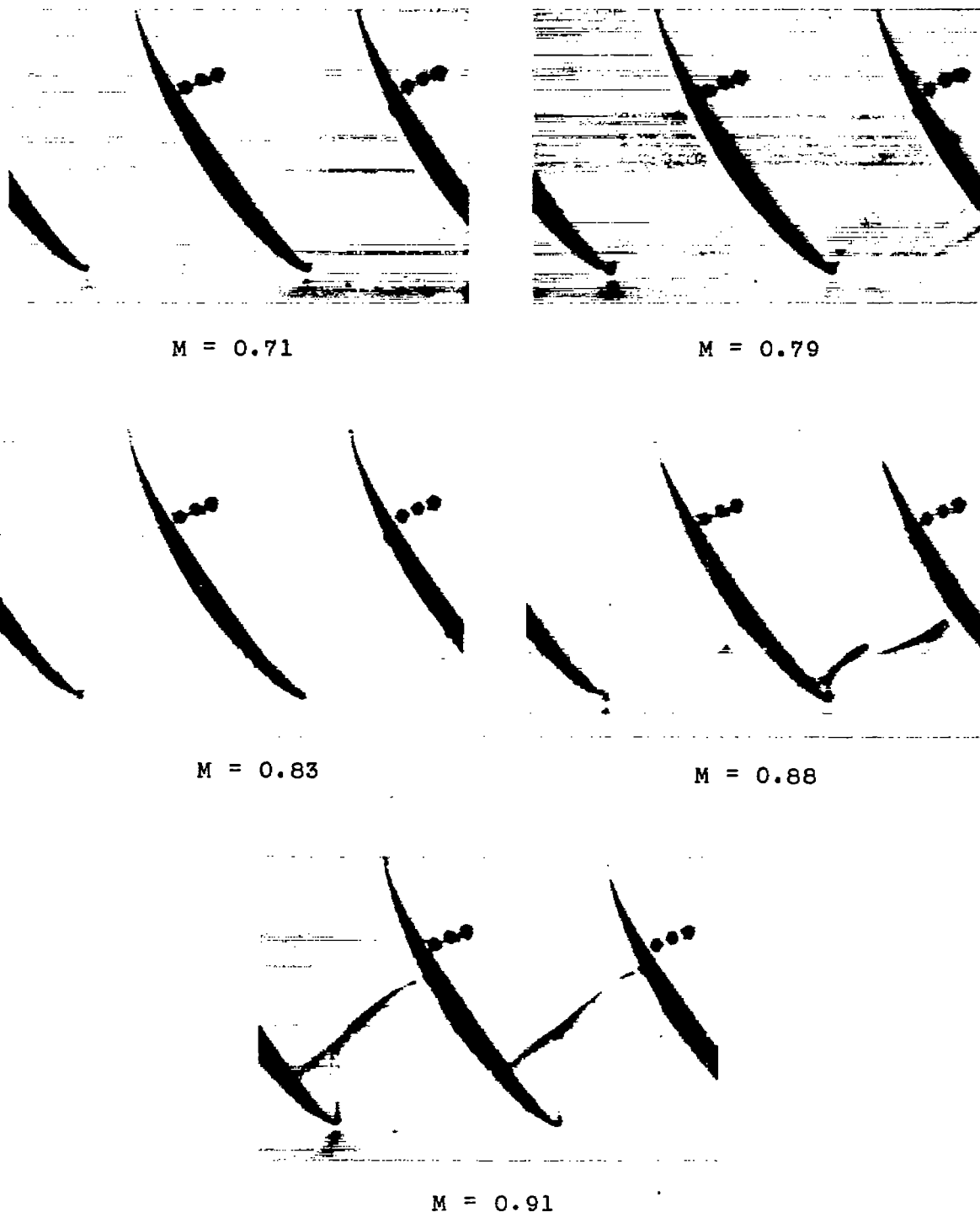


Figure 44.- Schlieren photographs for a range of Mach number. Cascade of NACA 65-(12)06 blower blades;  $\alpha = 12.5^\circ$ ;  $\beta = 45^\circ$ ;  $\sigma = 1.5$ .

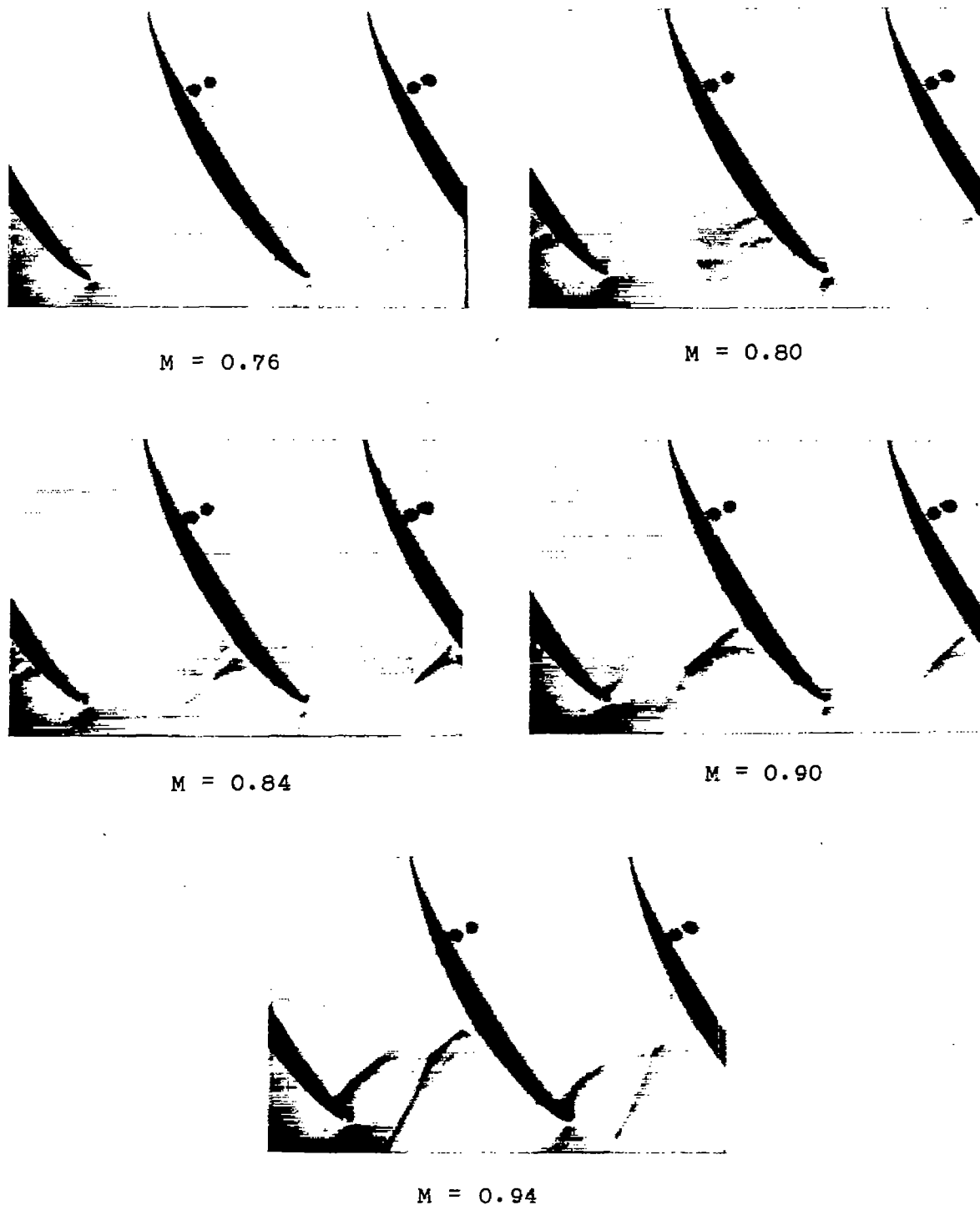
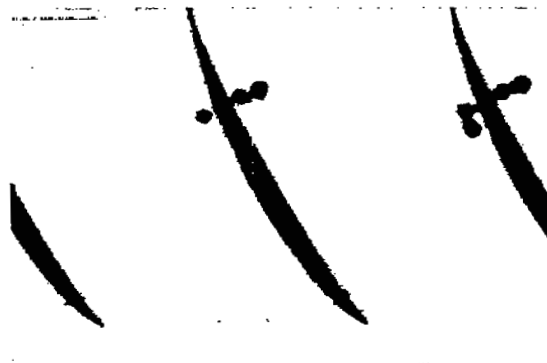


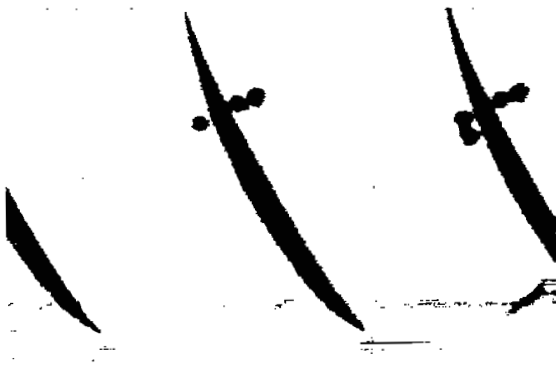
Figure 45.- Schlieren photographs for a range of Mach number. Cascade of NACA 65-(12)06 blower blades;  $\alpha = 15.0^\circ$ ;  $\beta = 45^\circ$ ;  $\sigma = 1.5$ .



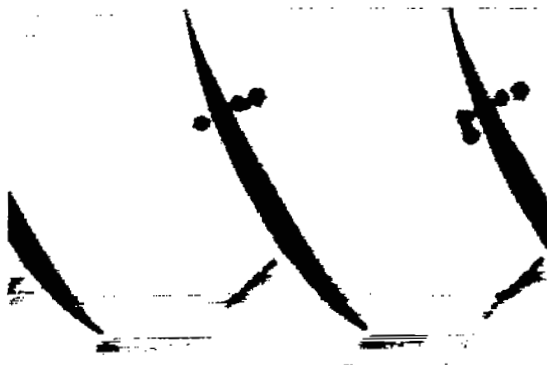
M = 0.70



M = 0.76



M = 0.82



M = 0.89



M = 0.93



M = 0.95

Figure 46.- Schlieren photographs for a range of Mach number. Cascade of NACA 65-(12)06 blower blades;  $\alpha = 17.5^\circ$ ;  $\beta = 45^\circ$ ;  $\sigma = 1.5$ .

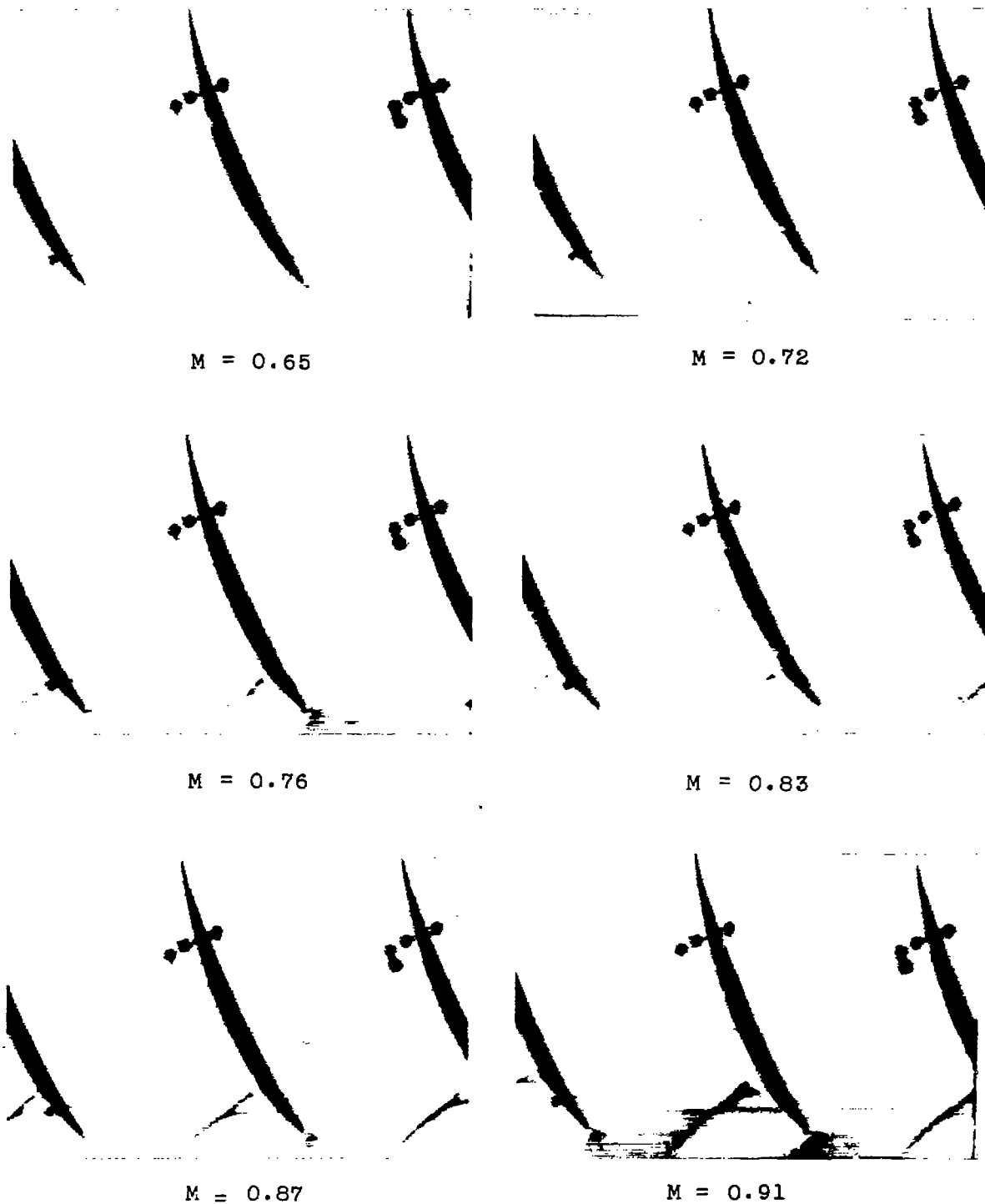


Figure 47.- Schlieren photographs for a range of Mach number. Cascade of NACA 65-(12)06 blower blades;  $\alpha = 22.5^\circ$ ;  $\beta = 45^\circ$ ;  $\sigma = 1.5$ .



M = 0.70



M = 0.72



M = 0.74



M = 0.77



M = 0.79



M = 0.81 (?)

Figure 48.- Schlieren photographs for a range of Mach number. Cascade of NACA 65-(18)10 blower blades;  $\alpha = 18.3^\circ$ ;  $\beta = 45^\circ$ ;  $\sigma = 1.5$ .



M = 0.70



M = 0.73



M = 0.76



M = 0.79



M = 0.83



M = 0.85

Figure 49.- Schlieren photographs for a range of Mach number. Cascade of NACA 65-(18)10 blower blades;  $\alpha = 20.8^\circ$ ;  $\beta = 45^\circ$ ;  $\sigma = 1.5$ .

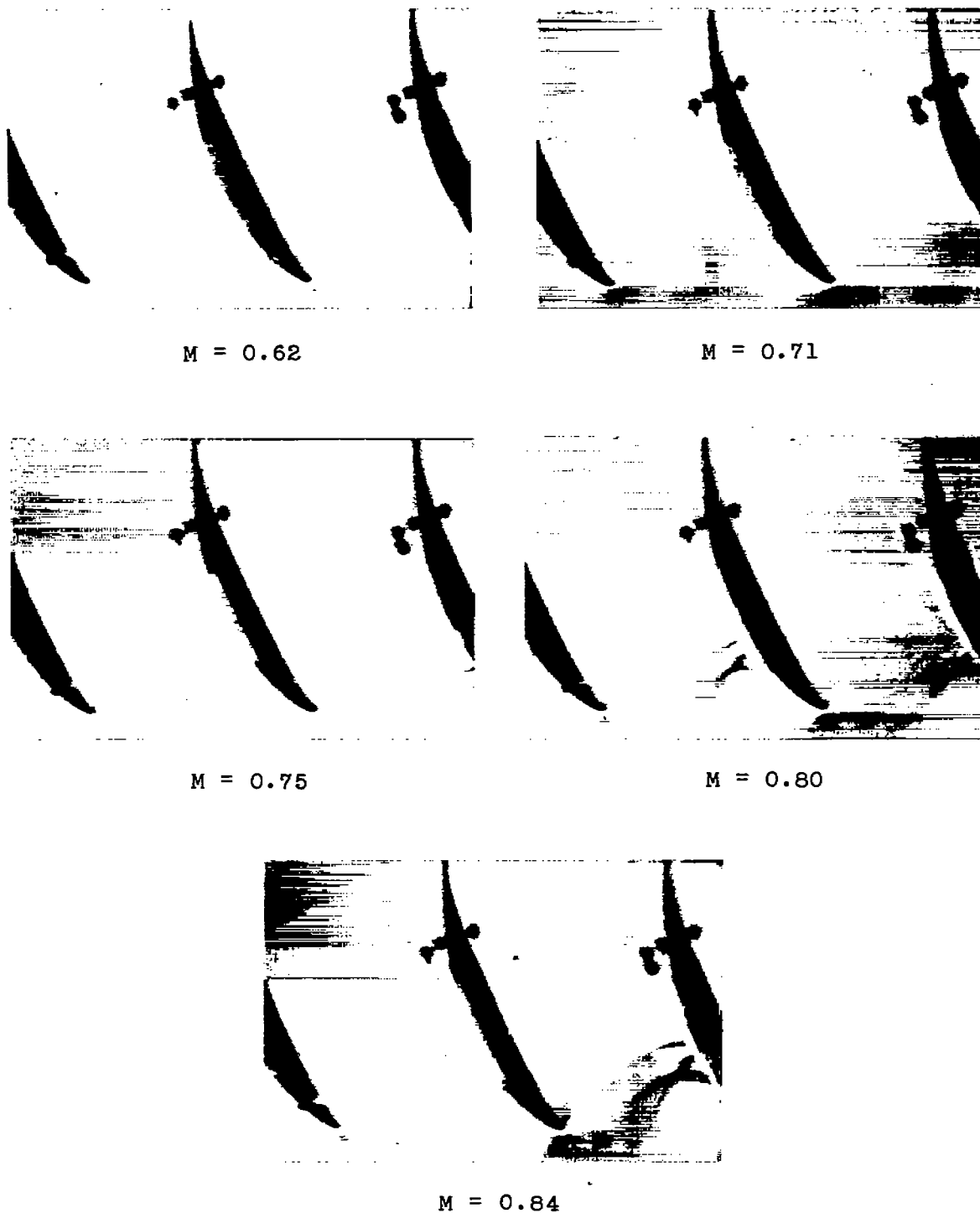


Figure 50.- Schlieren photographs for a range of Mach number. Cascade of NACA 65-(18)10 blower blades;  $\alpha = 23.3^\circ$ ;  $\beta = 45^\circ$ ;  $\sigma = 1.5$ .

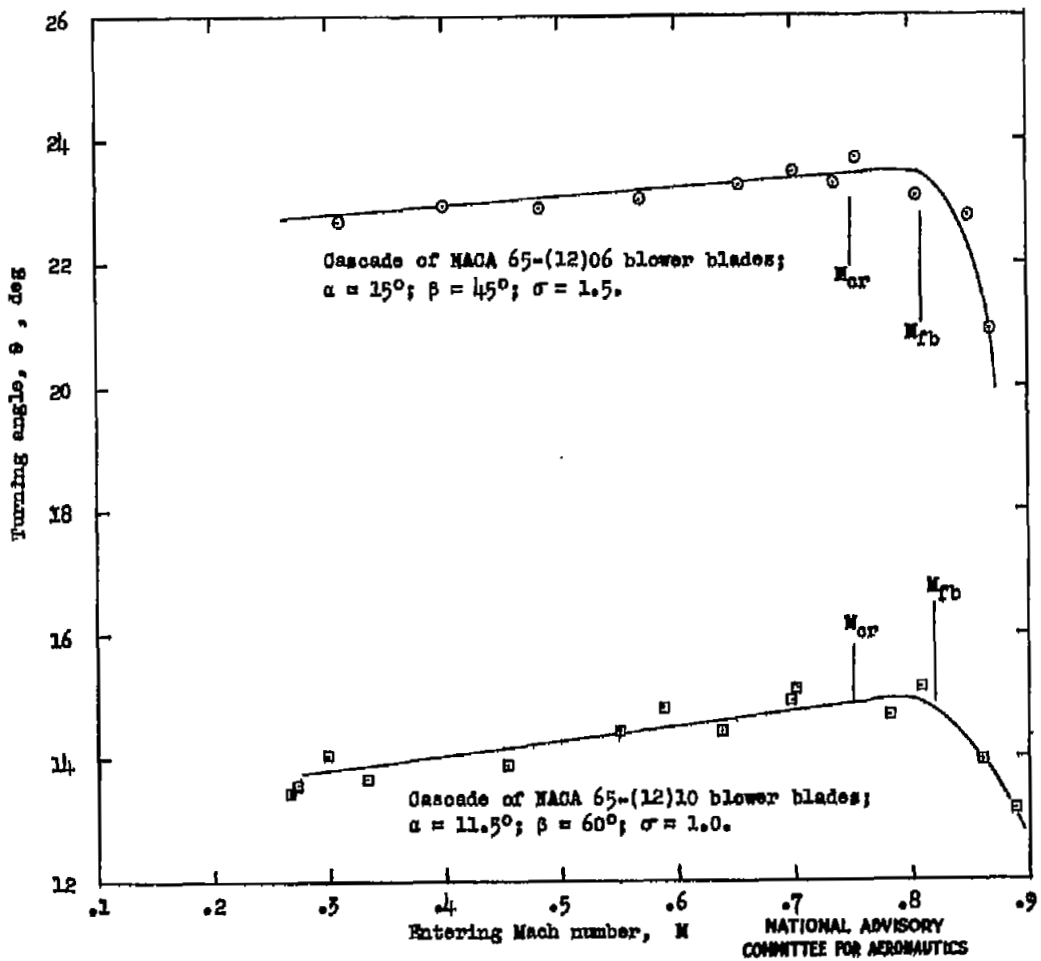


Figure 51.- Variation of turning angle with Mach number for two NACA blower blades.

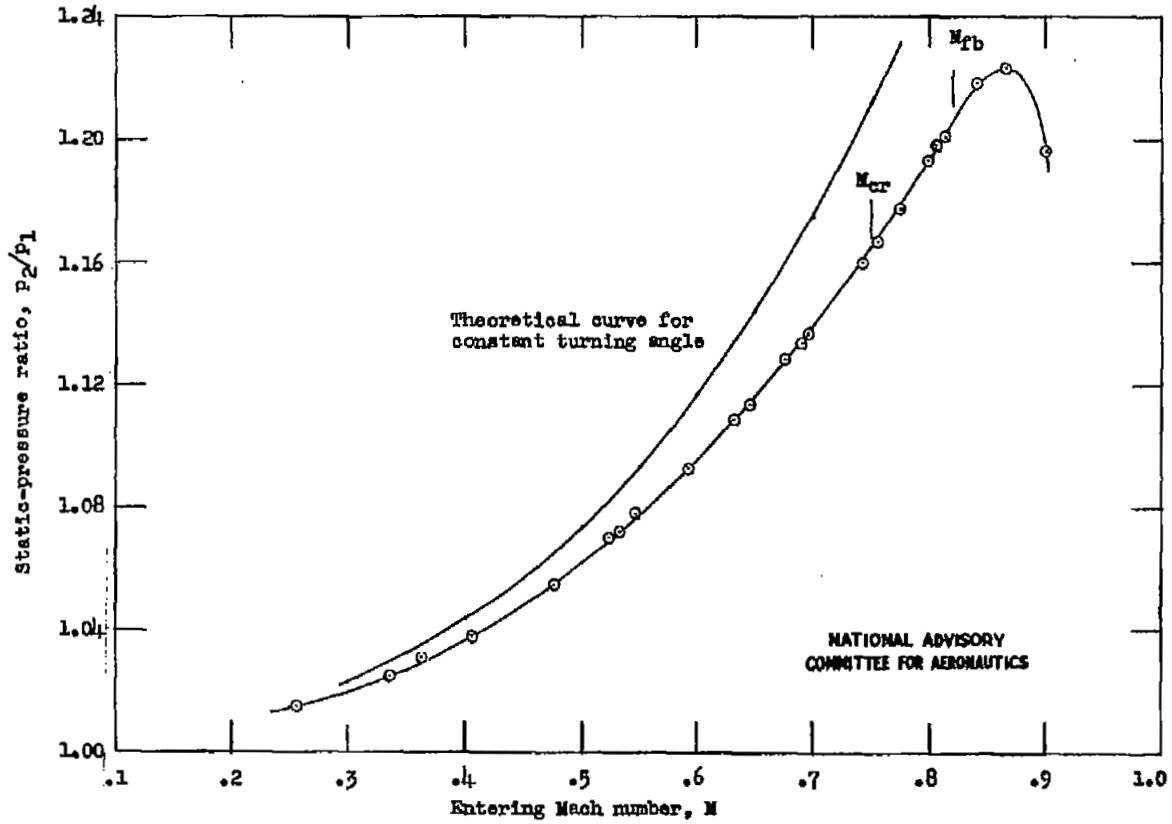


Figure 52.- Variation of static-pressure ratio across cascade with Mach number. NACA 65-810 blower blades;  $\alpha = 11.6^\circ$ ;  $\beta = 45^\circ$ ;  $\sigma = 1.5$ .

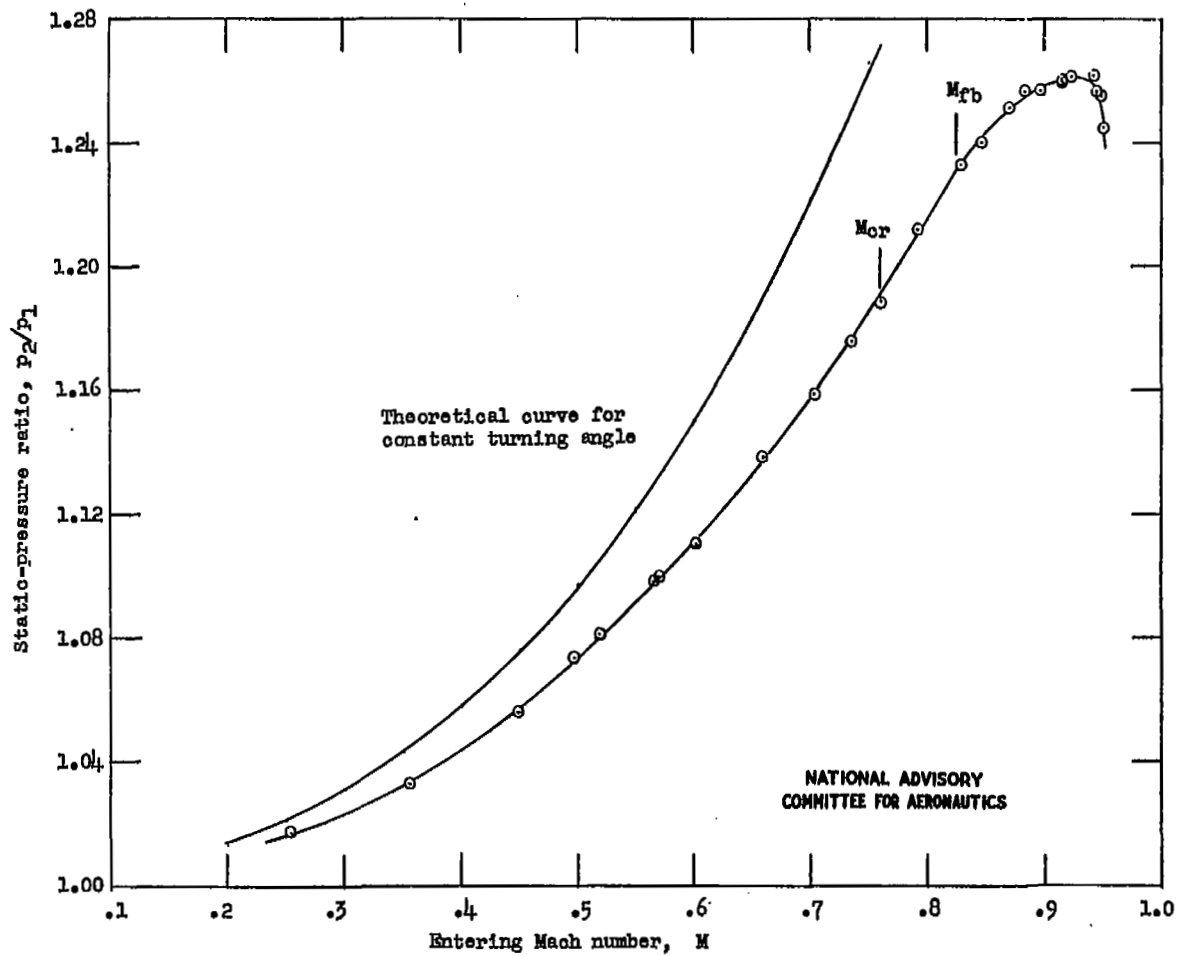


Figure 53.- Variation of static-pressure ratio across cascade with Mach number. NACA 65-810 blower blades;  $\alpha = 10^\circ$ ;  $\beta = 60^\circ$ ;  $\sigma = 1.5$ .

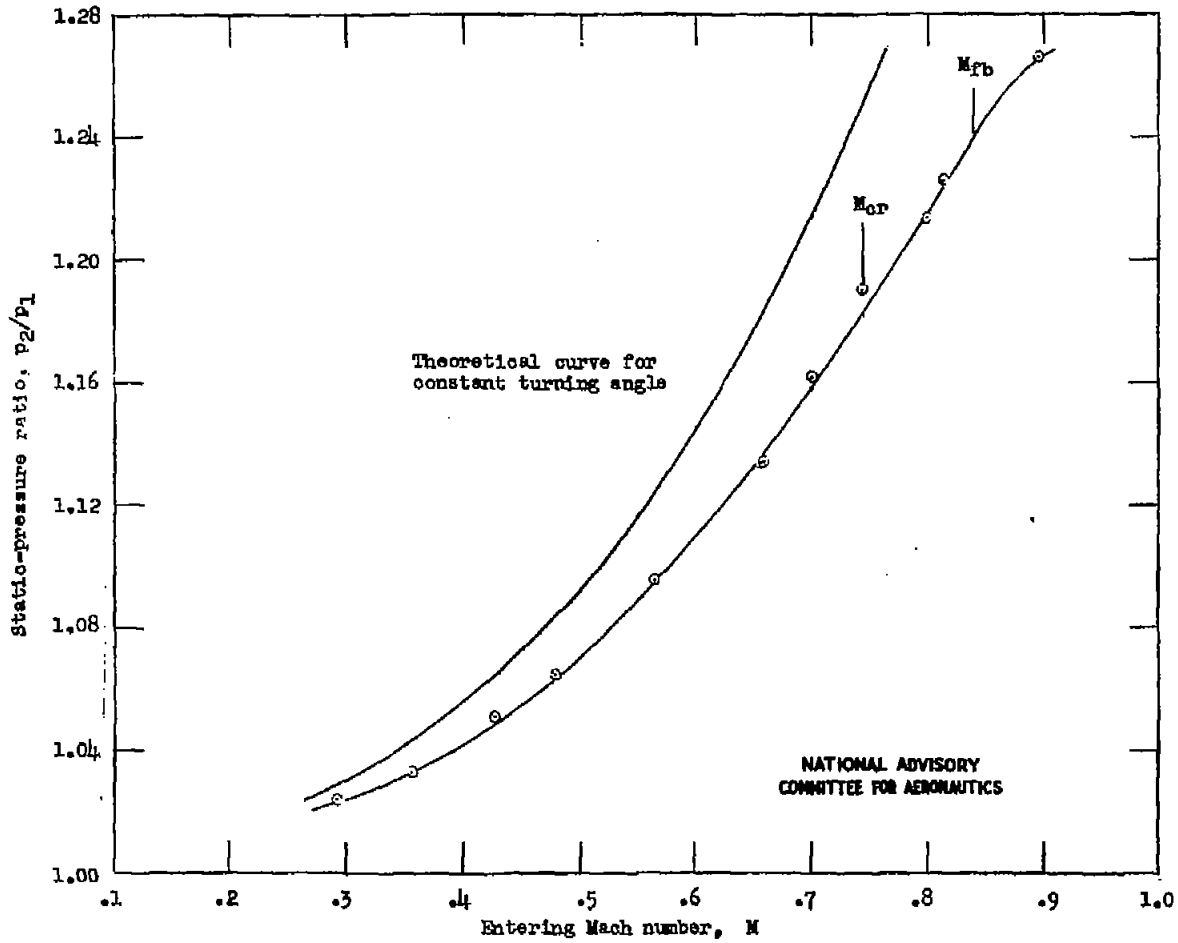


Figure 54.- Variation of static-pressure ratio across cascade with Mach number. NACA 65-810 blower blades;  $\alpha = 10.3^\circ$ ;  $\beta = 60^\circ$ ;  $\sigma = 1.0$ .

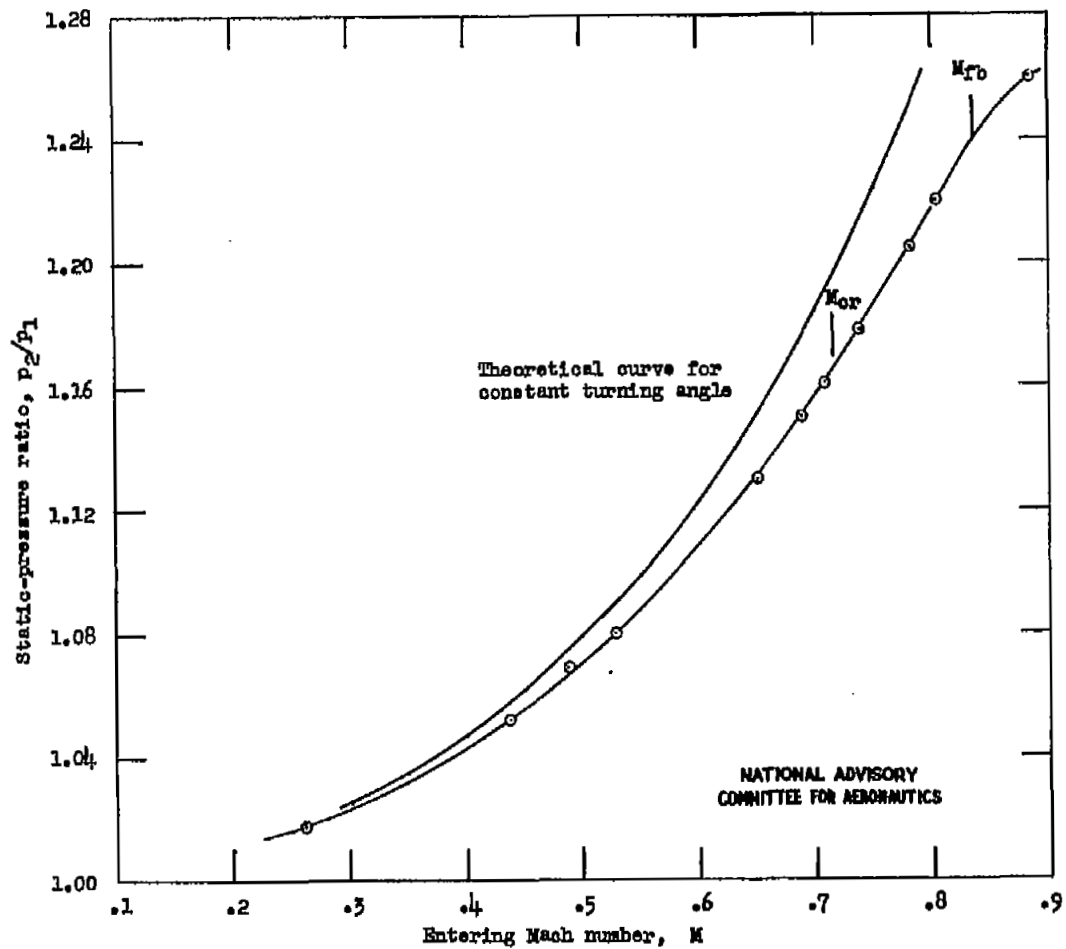


Figure 55.- Variation of static-pressure ratio across cascade with Mach number. NACA 65-806 blower blades;  $\alpha = 13.3^\circ$ ;  $\beta = 45^\circ$ ;  $\sigma = 1.5$ .

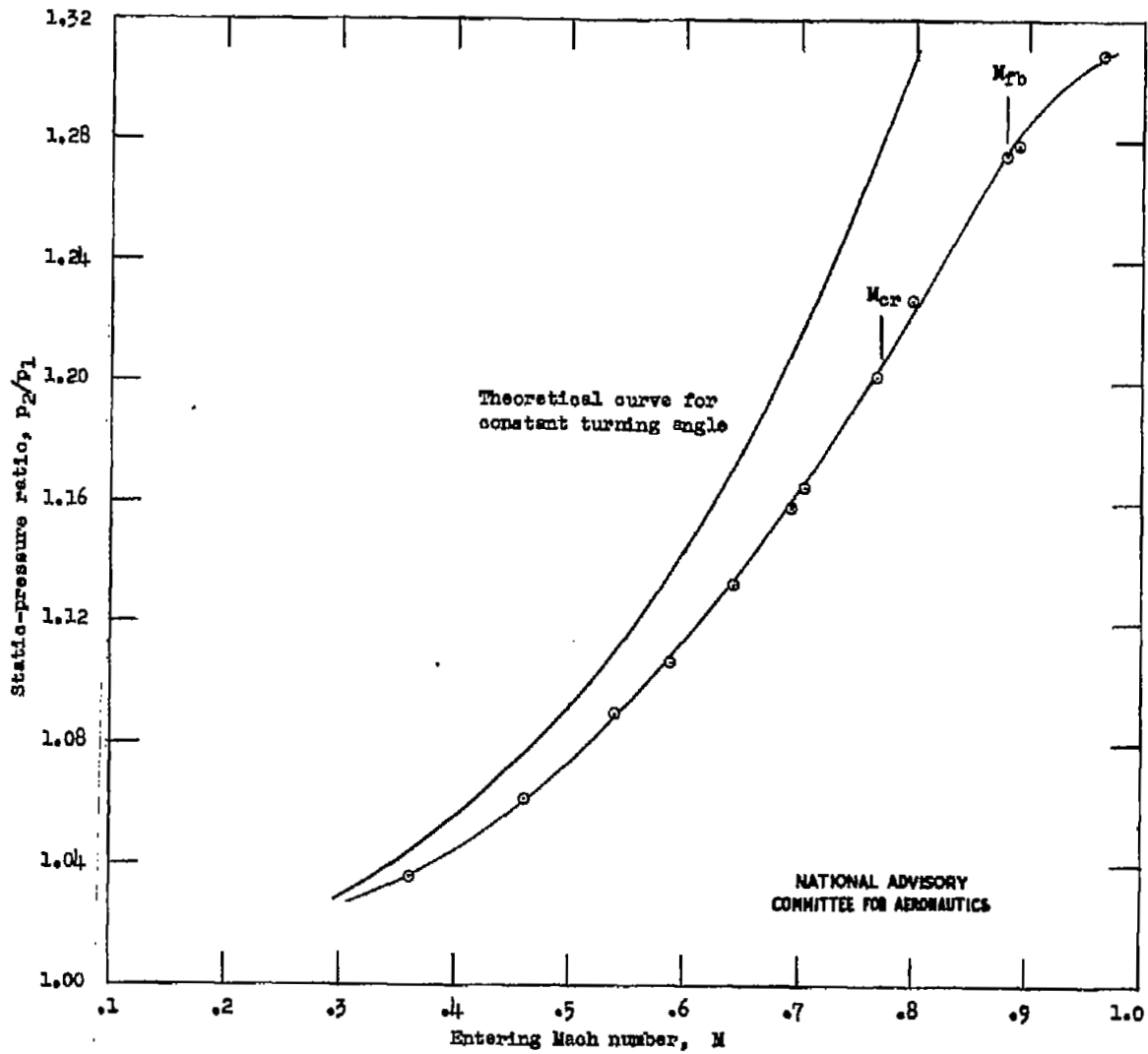


Figure 56.- Variation of static-pressure ratio across cascade with Mach number. NACA 65-806 blower blades;  $\alpha = 10^\circ$ ;  $\beta = 60^\circ$ ;  $\sigma = 1.0$ .

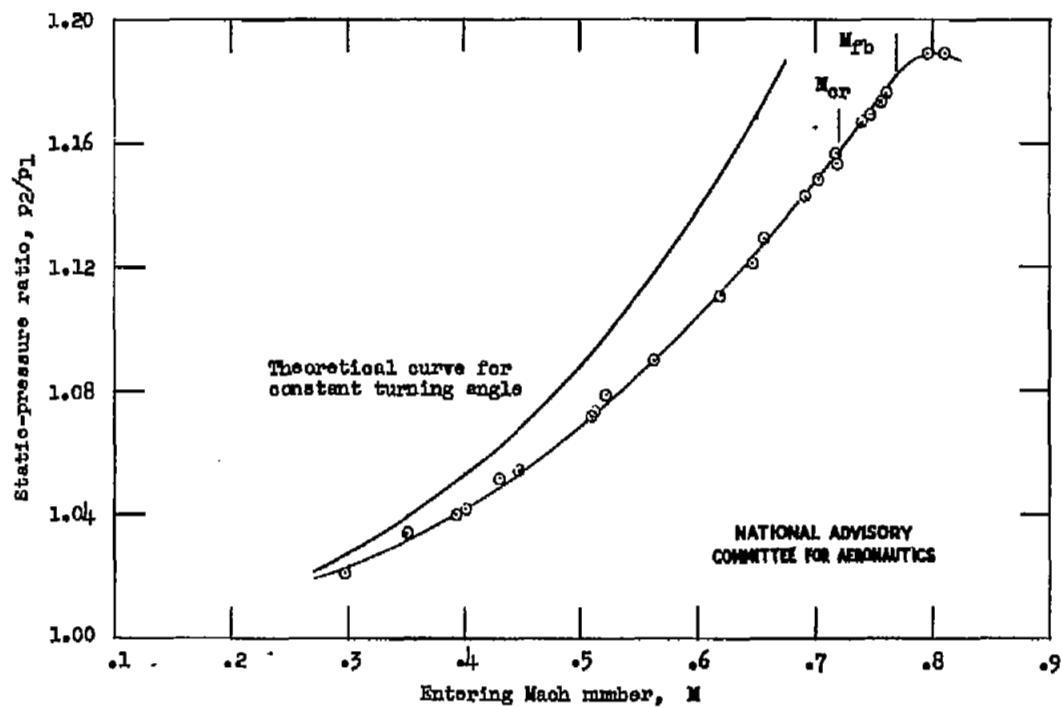


Figure 57.- Variation of static-pressure ratio across cascade with Mach number. NACA 65-(12)10 lower blades;  $\alpha = 14.9^\circ$ ;  $\beta = 45^\circ$ ;  $\sigma = 1.5$ .

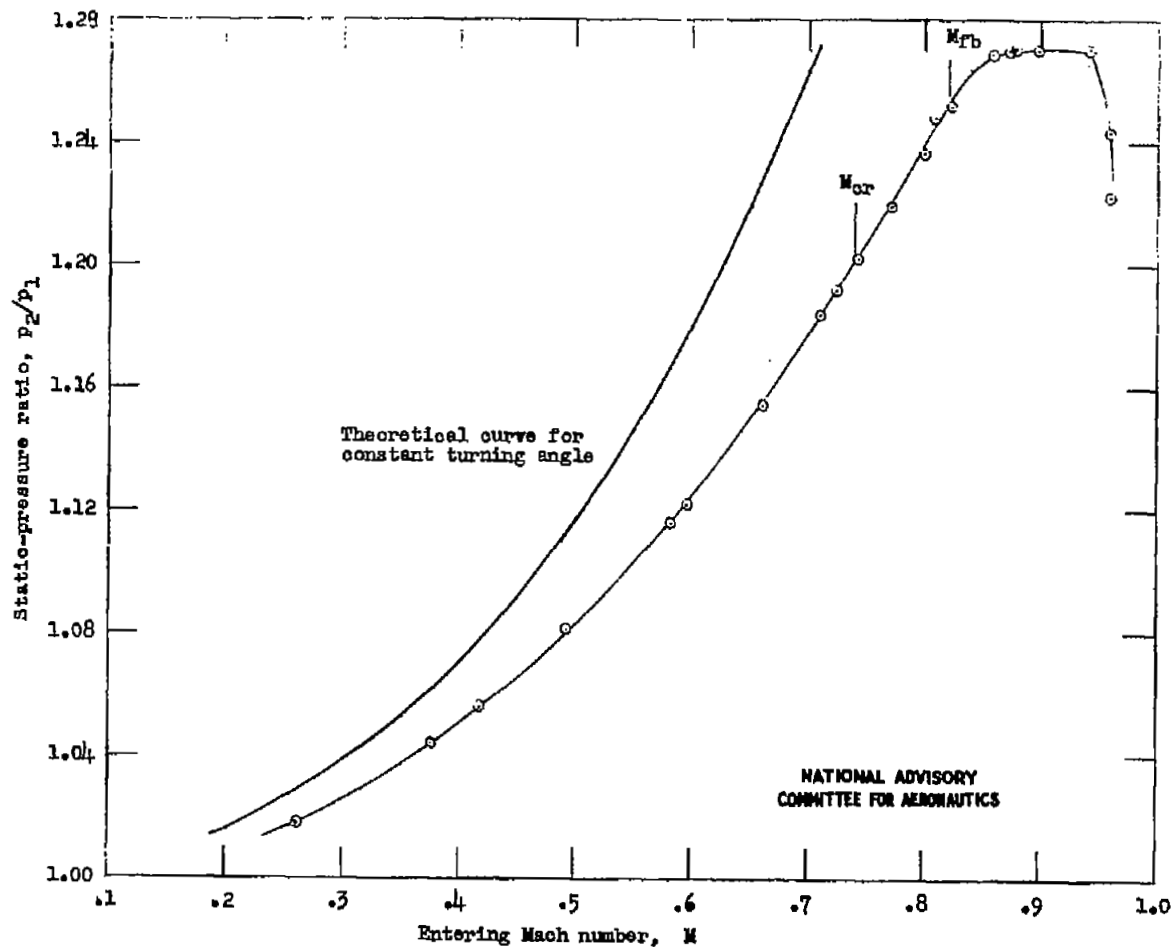


Figure 58.- Variation of static-pressure ratio across cascade with Mach number. NACA 65-(12)10 blower blades;  $\alpha = 14.2^\circ$ ;  $\beta = 60^\circ$ ;  $\sigma = 1.5$ .

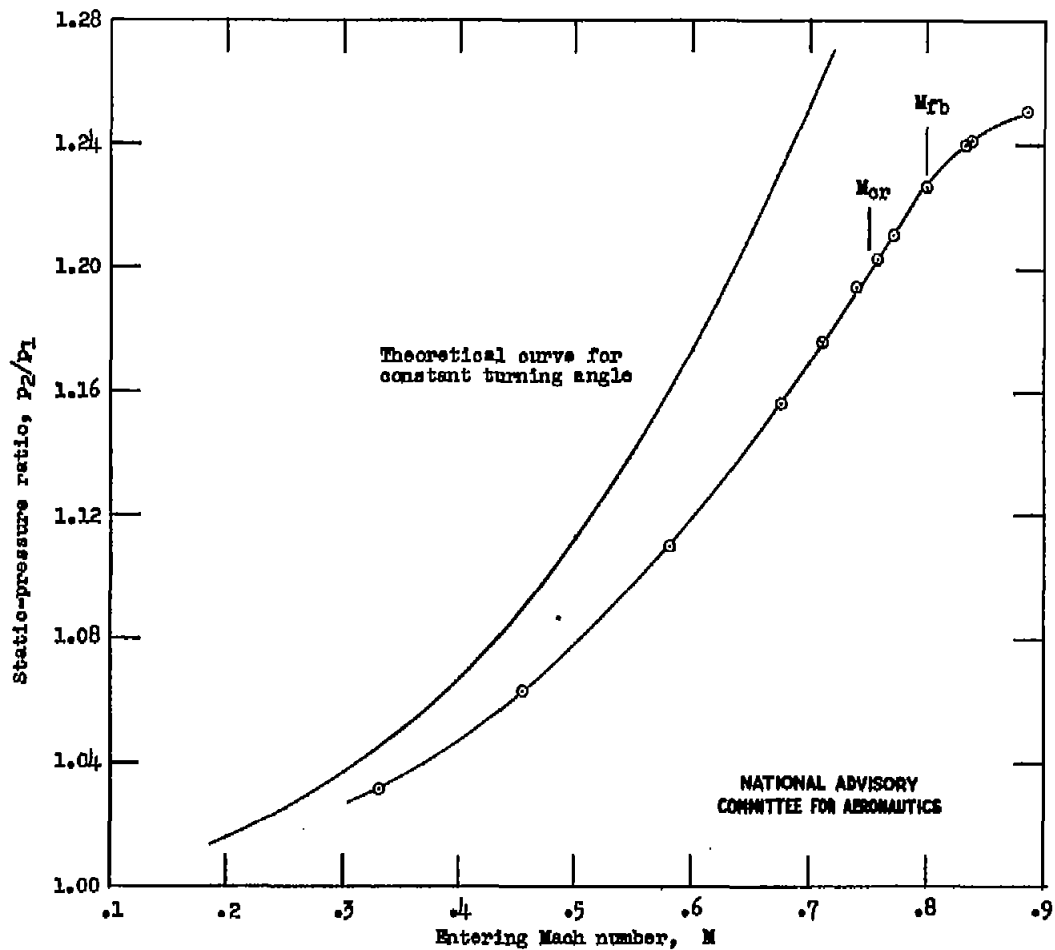


Figure 59.- Variation of static-pressure ratio across cascade with Mach number. NACA 65-(12)10 blower blades;  $\alpha = 14^\circ$ ;  $\beta = 60^\circ$ ;  $\sigma = 1.0$ .

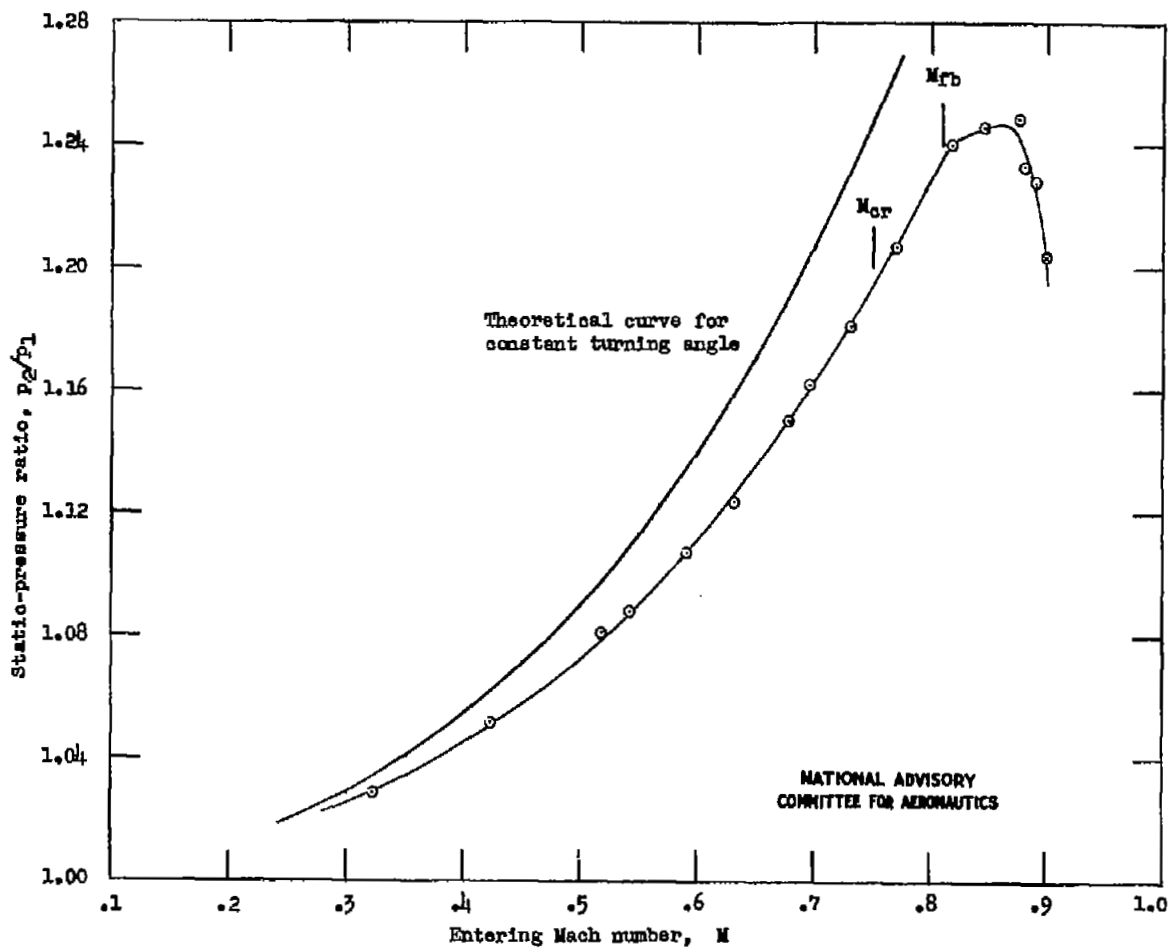


Figure 60.- Variation of static-pressure ratio across cascade with Mach number. NACA 65-(12)06 blower blades;  $\alpha = 15^\circ$ ;  $\beta = 45^\circ$ ;  $\sigma = 1.5$ .

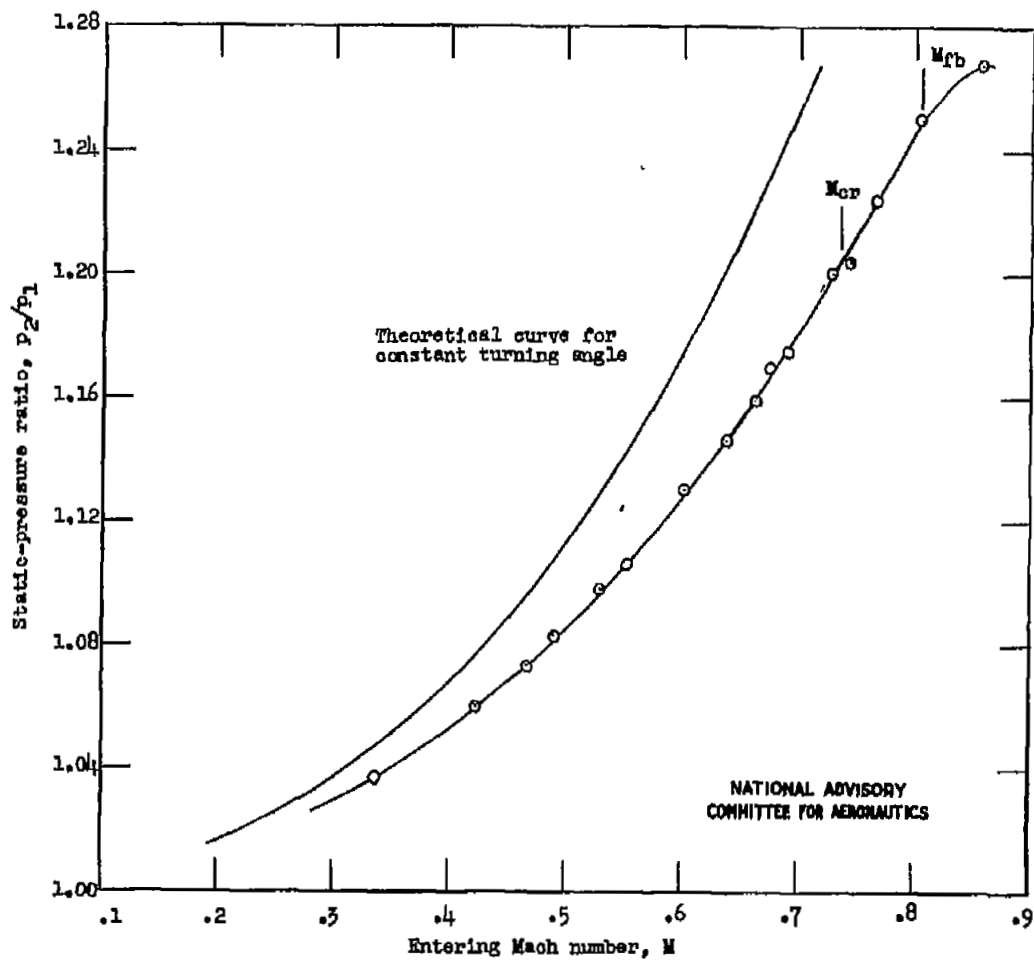


Figure 61.- Variation of static-pressure ratio across cascade with Mach number. NACA 65-(12)06 blower blades;  $\alpha = 14^\circ$ ;  $\beta = 60^\circ$ ;  $\sigma = 1.0$ .

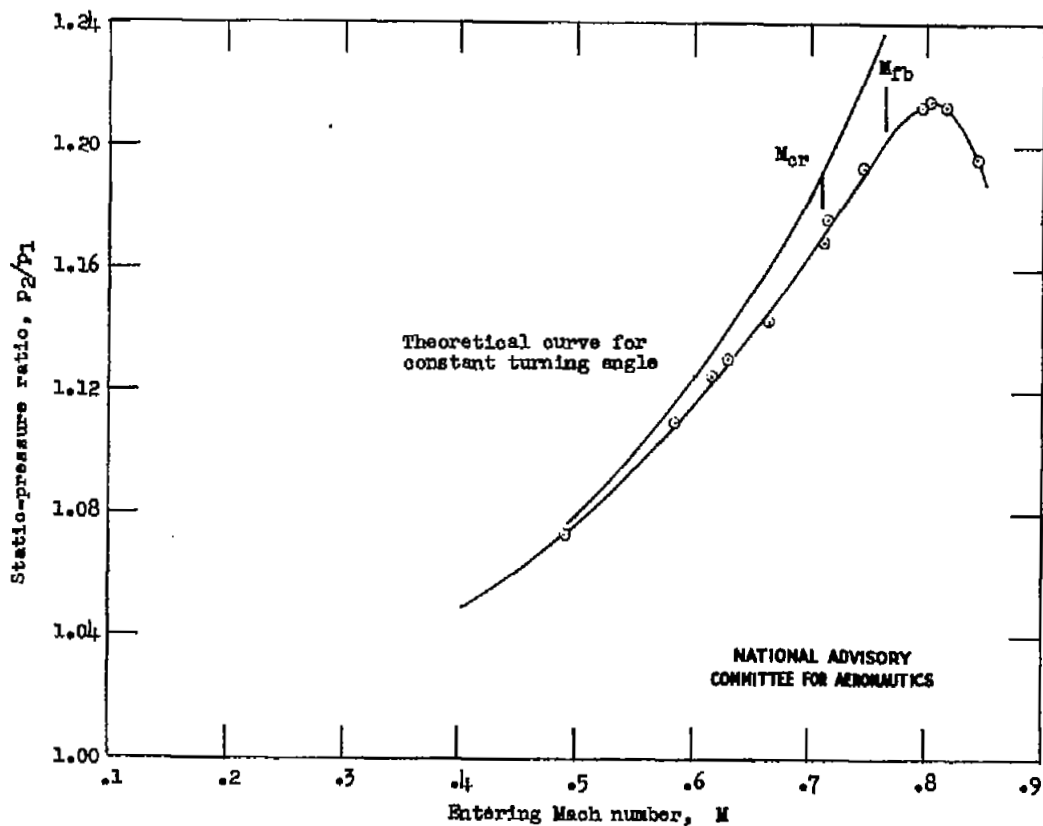


Figure 62.- Variation of static-pressure ratio across cascade with Mach number. NACA 65-(18)10 blower blades;  $\alpha = 23.3^\circ$ ;  $\beta = 45^\circ$ ;  $\sigma = 1.5$ .

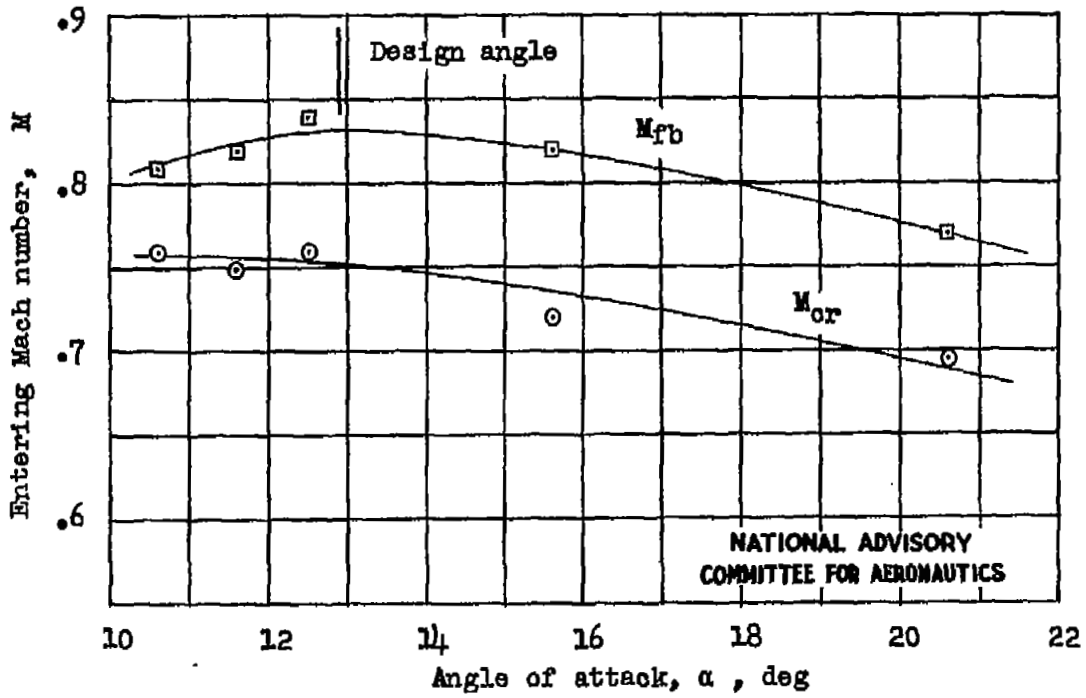


Figure 63.- Variation of  $M_{fb}$  and  $M_{or}$  with angle of attack. Cascade of NACA 65-810 blower blades;  $\beta = 45^\circ$ ;  $\sigma = 1.5$ .

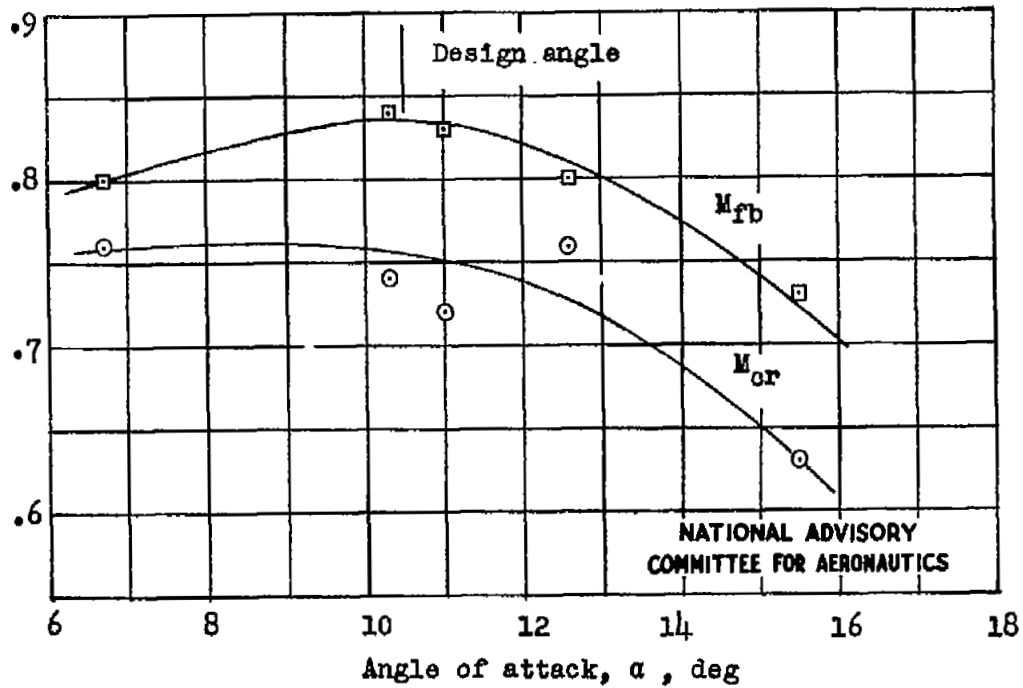


Figure 64.- Variation of  $M_{fb}$  and  $M_{cr}$  with angle of attack. Cascade of NACA 65-810 blower blades;  $\beta = 60^\circ$ ;  $\sigma = 1.0$ .

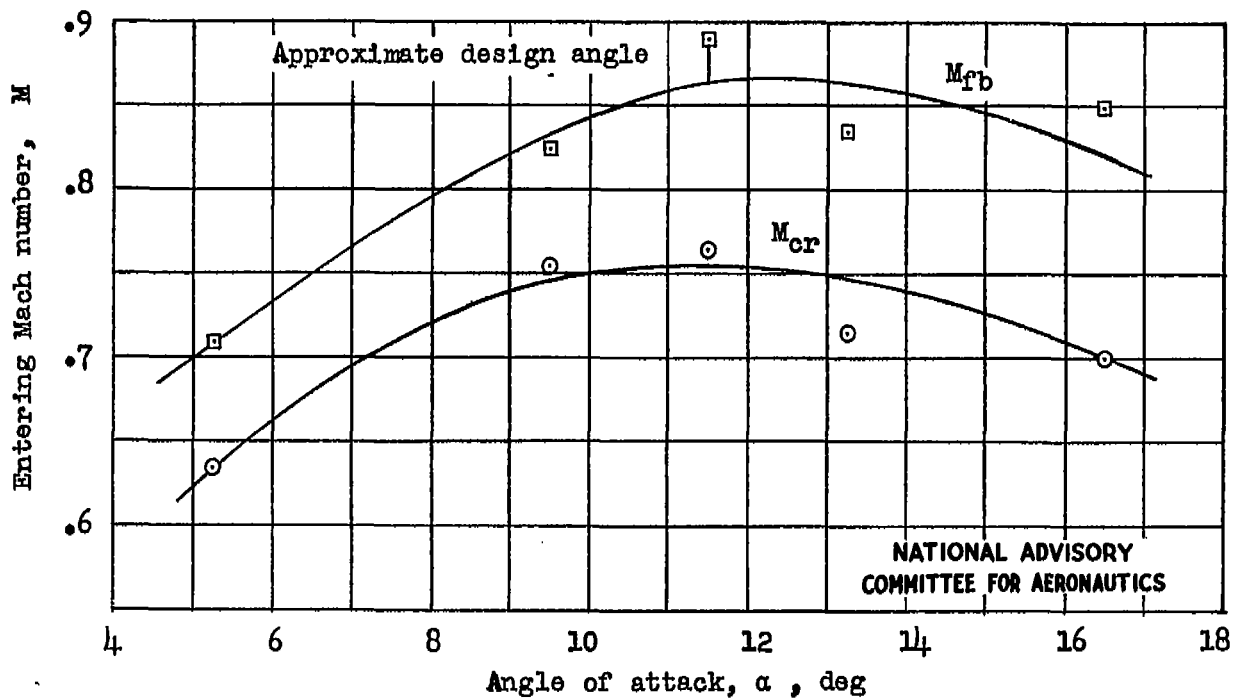


Figure 65.- Variation of  $M_{fb}$  and  $M_{cr}$  with angle of attack. Cascade of NACA 65-806 blower blades;  $\beta = 45^\circ$ ;  $\sigma = 1.5$ .

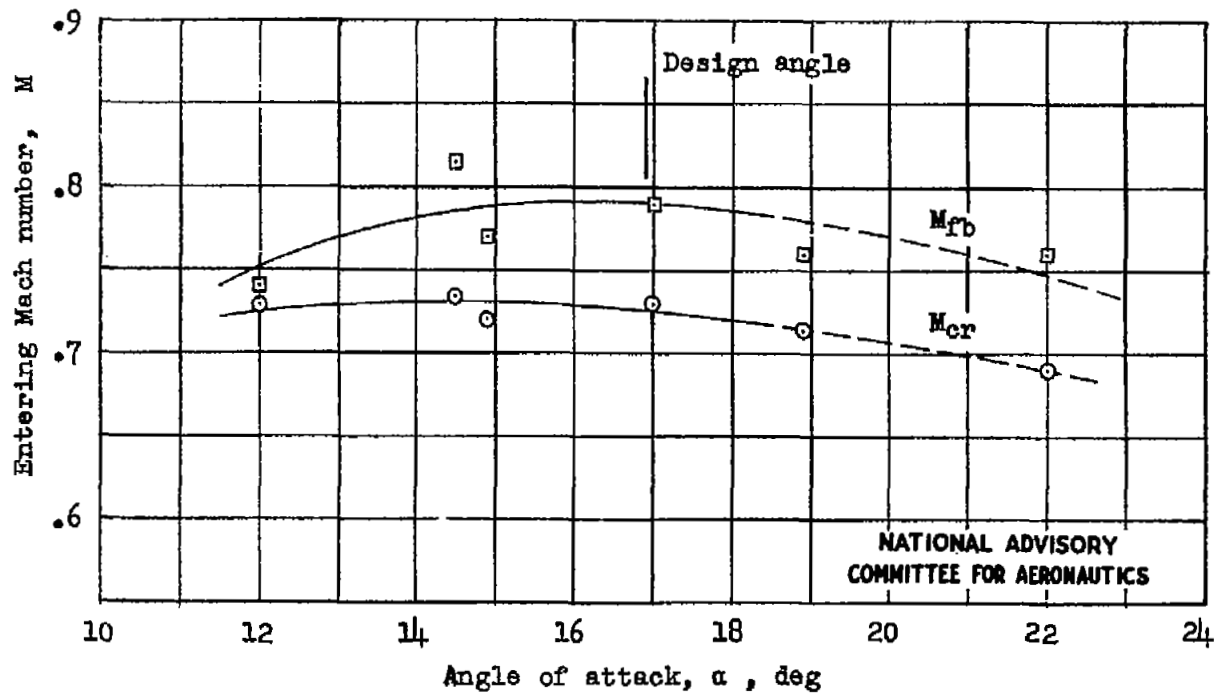


Figure 66.- Variation of  $M_{fb}$  and  $M_{cr}$  with angle of attack. Cascade of NACA 65-(12)10 blower blades;  $\beta = 45^\circ$ ;  $\sigma = 1.5$ .

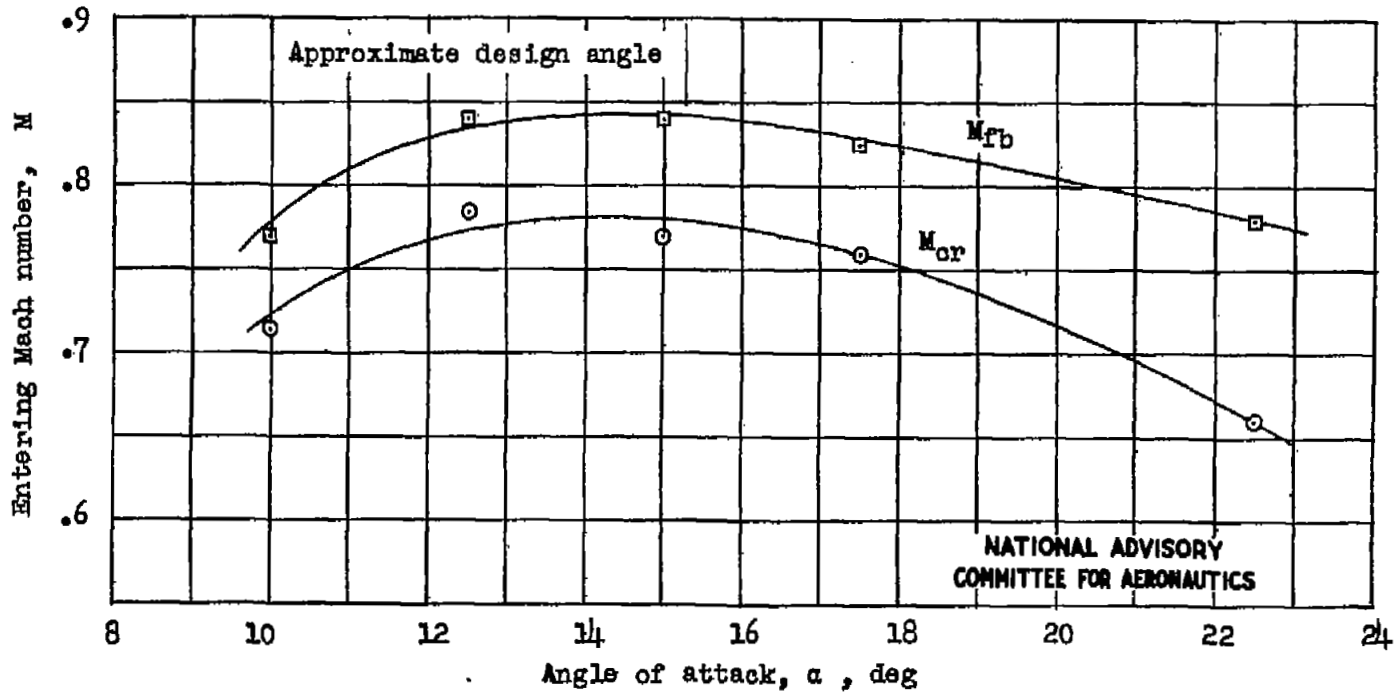


Figure 67.- Variation of  $M_{fb}$  and  $M_{cr}$  with angle of attack, Cascade of NACA 65-(12)06 blower blades;  $\beta = 45^\circ$ ;  $\sigma = 1.5$ .

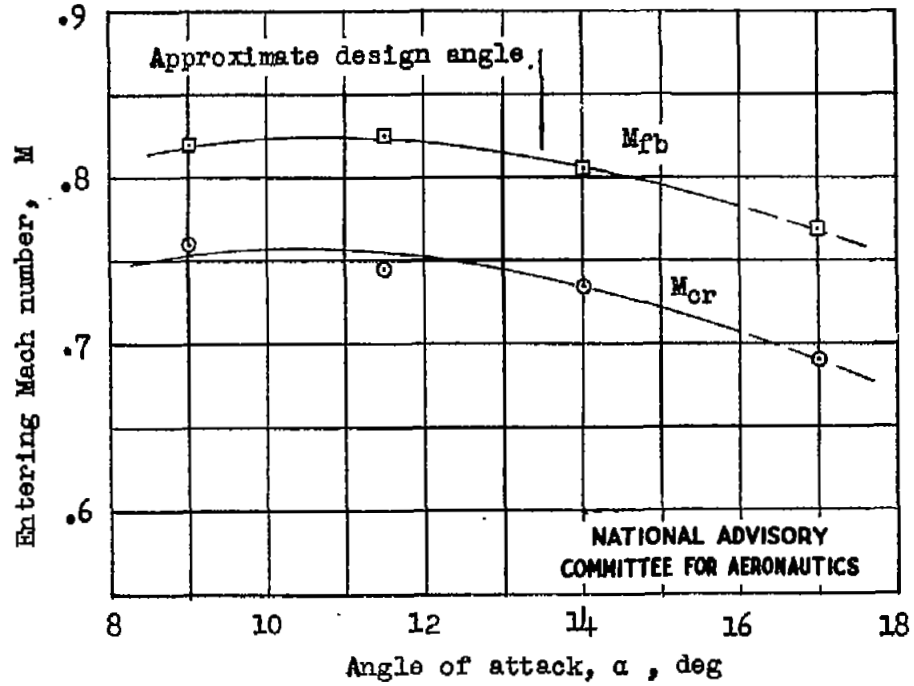


Figure 68.- Variation of  $M_{fb}$  and  $M_{or}$  with angle of attack. Cascade of NACA 65-(12)06 blower blades;  $\beta = 60^\circ$ ;  $\sigma = 1.0$ .

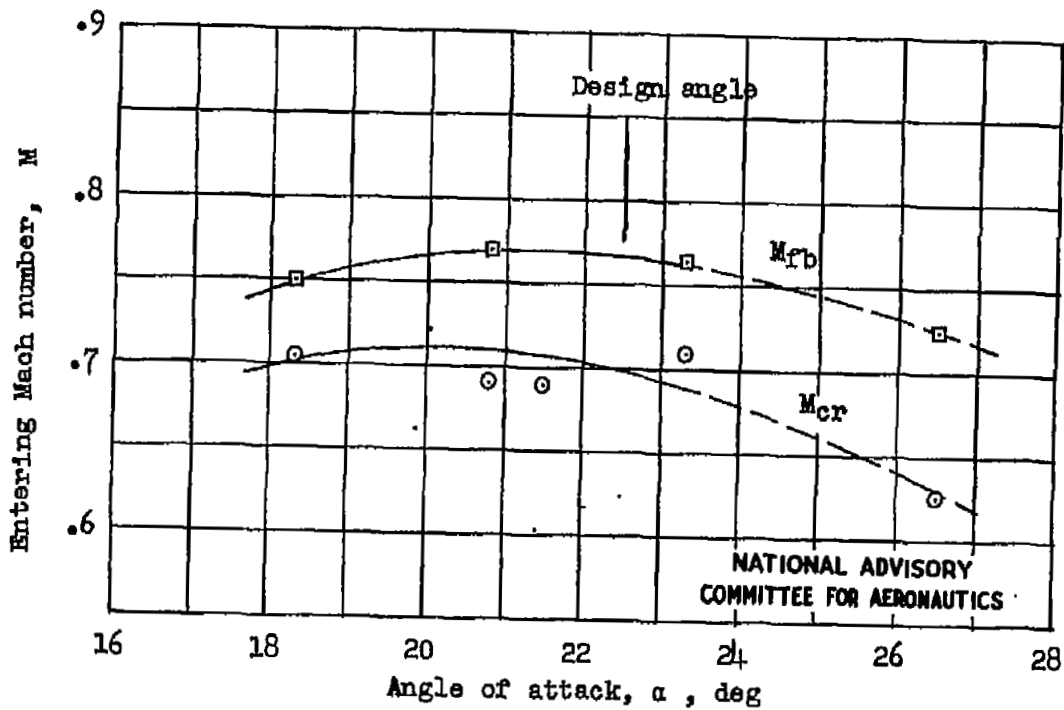


Figure 69.- Variation of  $M_{pb}$  and  $M_{cr}$  with angle of attack. Cascade of NACA 65-(18)10<sup>cr</sup> blower blades;  $\beta = 45^\circ$ ;  $\sigma = 1.5$ .

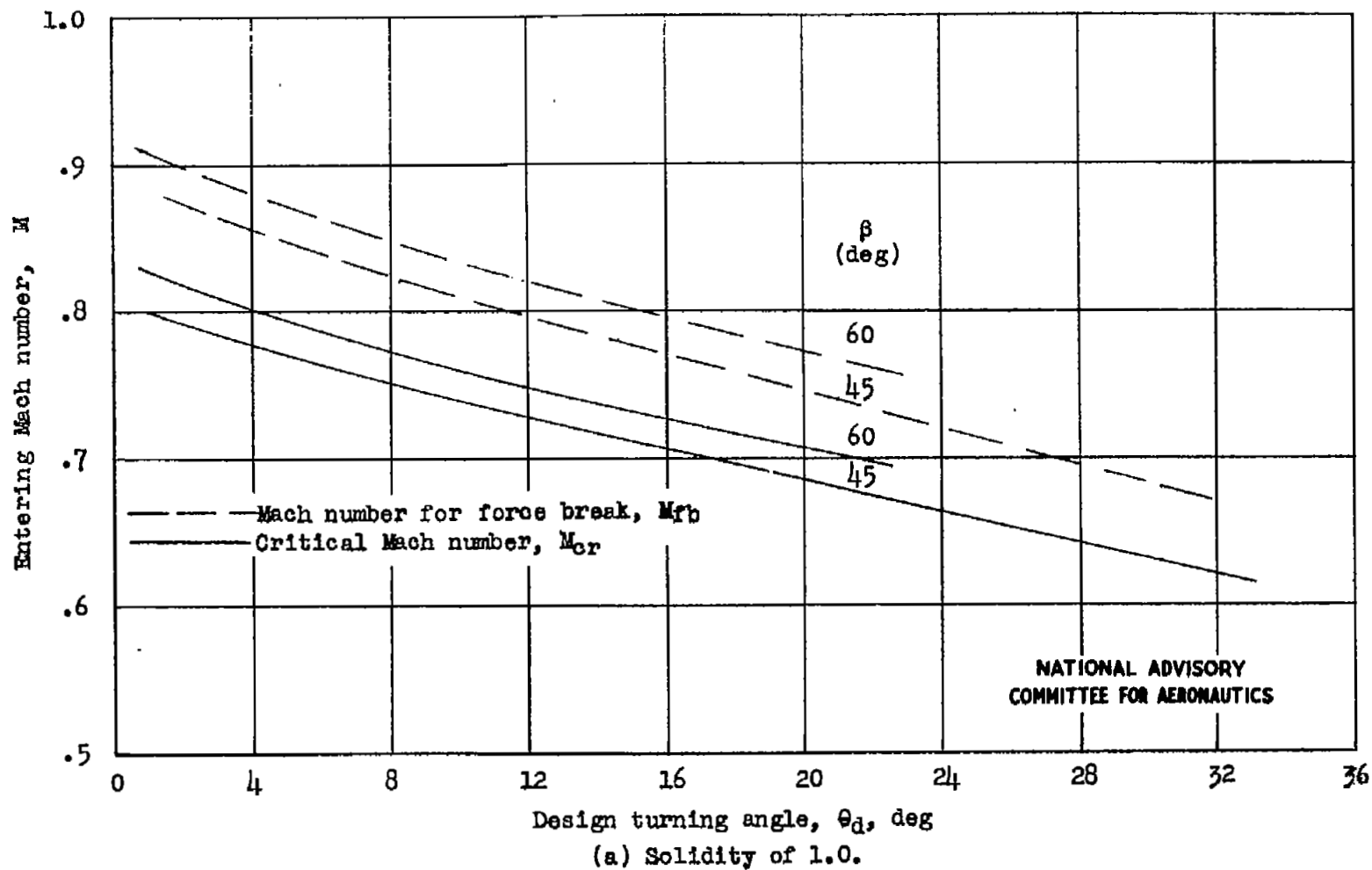


Figure 70.- Variation of predicted  $M_{fb}$  and  $M_{cr}$  with design turning angle. NACA 65-series 10 percent thick blower blades.

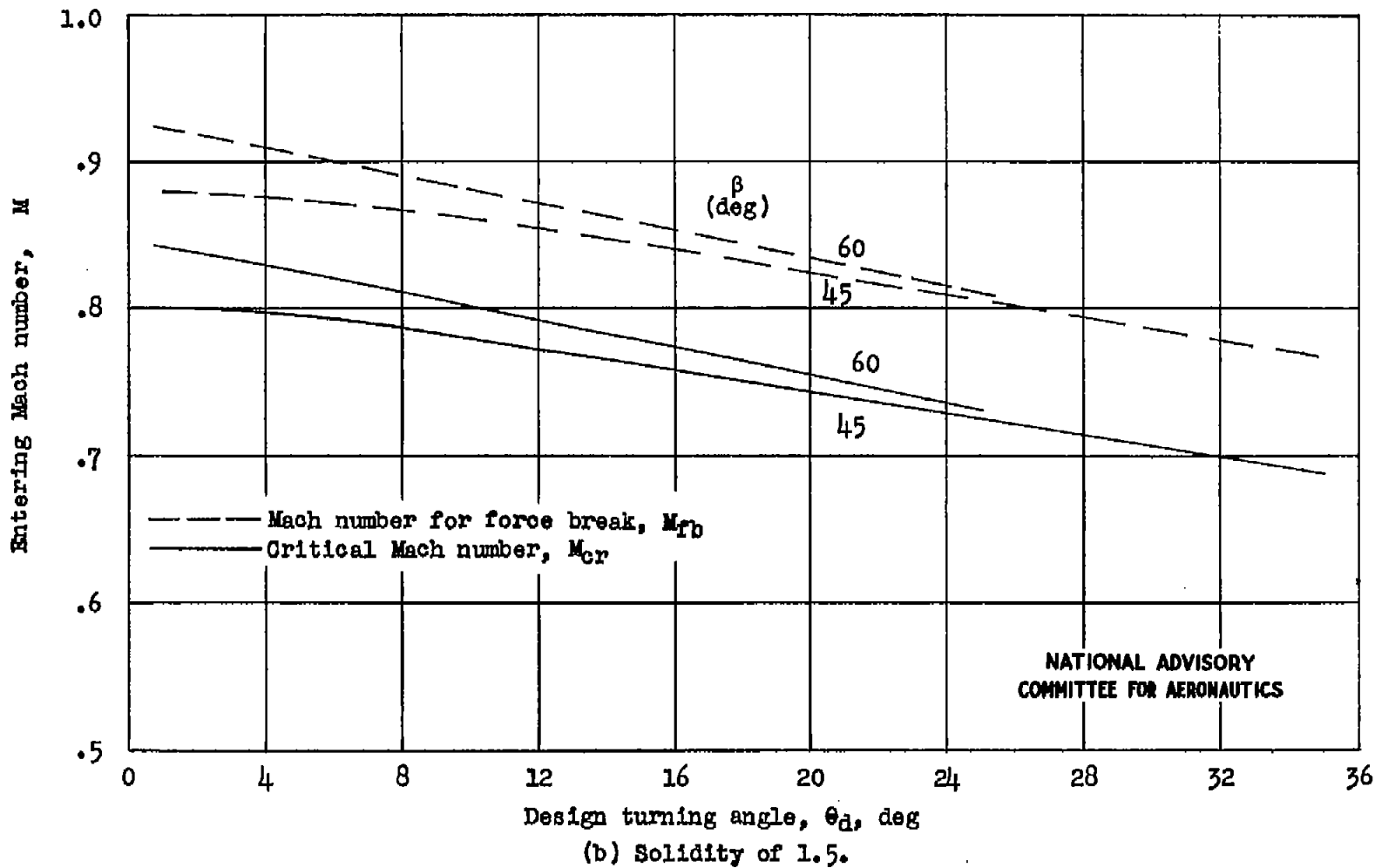


Figure 70.- Concluded.

NASA Technical Library



3 1176 01437 0085